TECHNICAL REPORT STANDARD TITLE PAGE

1. Report No.	2. Government Accession No.	3. Recipient's Catalog No.
FHWA/TX-87/46+437-2		

4. Title and Subtitle	5. Report Date
IN SITU DETERMINATION OF ELASTIC MODULI OF PAVEMENT SYSTEMS BY SPECTRAL-ANALYSIS-OF-SURFACE-WAVES METHOD (THEORETICAL ASPECTS)	November 1986
	6. Performing Organization Code
7. Author(s)	8. Performing Organization Report No.
Soheil Nazarian and Kenneth H. Stokoe, II	Research Report 437-2
9. Performing Organization Name and Address	10. Work Unit No.
Center for Transportation Research The University of Texas at Austin Austin, Texas 78712-1075	11. Contract or Grant No. Research Study 3-8-85-437
	13. Type of Report and Period Covered
12. Sponsoring Agency Name and Address Texas State Department of Highways and Public Transportation; Transportation Planning Division P. O. Box 5051 Austin, Texas 78763-5051	Interim
	14. Sponsoring Agency Code

15. Supplementary Notes

Study conducted in cooperation with the U. S. Department of Transportation, Federal Highway Administration. Research Study Title: "Utilization of Surface Wave System for Measuring Moduli of Pavements"

16. Abstract

The Spectral-Analysis-of-Surface-Waves (SASW) method is an in situ testing method for determining shear wave velocity profiles of soil sites and stiffness profiles of pavement systems. The method is nondestructive and is performed entirely from the pavement or ground surface. Measurements are made at strains below 0.001 percent where elastic properties of the materials are independent of strain amplitude. The key elements in SASW testing are the generation and measurement of surface waves. Transient impacts containing wide ranges of frequencies are transmitted to the pavement surface by means of simple hammers. Surface waves generated by these impacts are captured and recorded by the receivers using a spectral waveform analyzer. The analyzer is used to transform the waveforms into the frequency domain and then to perform spectral analyses on them. The points of interest from this operation are the phase information of the cross power spectrum and the coherence function. By evaluating the coherence function during testing, the range of frequencies which is not contaminated with random background noise can be quickly identified. Phase information from the cross power spectrum is indicative of the relative phase shift of each frequency propagating between the receivers. By knowing the distance between receivers and the phase shift for each frequency, phase velocity and wavelength associated with that frequency are calculated. One of the most important steps in SASW testing is the inversion process which has been the missing link in engineering applications. The theoretical foundation of the SASW method is discussed in detail in this report, with an emphasis placed on the theoretical aspects of the inversion process.

17. Key Words	18. Distribution Statement
Spectral-Analysis-of-Surface-Waves, SASW, theory, shear wave velocity, elastic modulus profiles, pavement sections, soil sites	No restrictions. This document is available to the public through the National Technical Information Service, Springfield, Virginia 22161.

19. Security Classif. (of this report)	20. Security Classif. (of this page)	21. No. of Pages	22. Price
Unclassified	Unclassified	134	

Form DOT F 1700.7 (8-69)

IN SITU DETERMINATION OF ELASTIC MODULI OF PAVEMENT SYSTEMS BY SPECTRAL-ANALYSIS-OF-SURFACE-WAVES METHOD (THEORETICAL ASPECTS)

by

Soheil Nazarian
K. H. Stokoe, II

Research Report Number 437-2

Utilization of Surface Wave System for
Measuring Moduli of Pavements
Research Project 3-8-85-437

conducted for

Texas State Department of Highways
and Public Transportation

in cooperation with the
U.S. Department of Transportation
Federal Highway Administration

by the

CENTER FOR TRANSPORTATION RESEARCH
BUREAU OF ENGINEERING RESEARCH
THE UNIVERSITY OF TEXAS AT AUSTIN

November 1986

The contents of this report reflect the views of the authors, who are responsible for the facts and the accuracy of the data presented herein. The contents do not necessarily reflect the official views or policies of the Federal Highway Administration. This report does not constitute a standard, specification, or regulation.

PREFACE

This report is the second report in a series of three reports on the Spectral-Analysis-of-Surface-Waves (SASW) method. The first report is published under Research Report 368-1F and is a detailed description of the practical aspects of the SASW method. The third report will be published under Research Project 1123 and will consist of a manual for an interactive computer program called INVERT1. This program is essential for determining the stiffnesses of the different layers from the in situ data. In this volume, the theoretical aspects of SASW testing are described. Some practical examples are provided so that a person not familiar with the method can understand it.

The division of the reports on Projects 368, 437 and 1123 was necessary so that readers with different levels of knowledge and interest could easily access the required material. This division of reports also resulted from a natural development of the SASW method. This report has been prepared in a manner that permits the theoretical background of the SASW method to be understood without referring to the other reports.

The authors extend their sincere gratitude to personnel of the Texas Department of Highways and Public Transportation for their continuous support and enthusiasm throughout the course of this study.

Soheil Nazarian
Kenneth H. Stokoe, II

November 1986

LIST OF REPORTS

Report No. 437-1, "Dynamic Interpretation of Dynaflect and Falling Weight Deflectometer Tests" by Ko-Young Shao, J.M. Roesset, and K.H. Stokoe, II, presents the results of analytical studies of the dynamic effects on measurements made with the Dynaflect and Falling Weight Deflectometer methods, based on the consideration of wave propagation including body waves (P-and S-waves) and Rayleigh (surface) waves.

Report No. 437-2, "In Situ Determination of Elastic Moduli of Pavement Systems by Spectral-Analysis-of-Surface-Waves Method (Theoretical Aspects)," by Soheil Nazarian and K.H. Stokoe, II, presents the pertinent theoretical aspects of wave propagation in a layered system (such as a pavement system) as they apply to the SASW method.

Report No. 437-3F, "Investigation of Variables Affecting In Situ Determination of Elastic Moduli of Pavement Systems by Surface Wave Method," by J.C. Sheu, Ignacio Sanchez-Salinero, K.H. Stokoe, II, and J.M. Roesset, presents the results of experimental and analytical studies of variables, such as receiver types, source-receiver configuration, wave reflections and analytical solutions, that effect modulus measurements by the Spectral-Analysis-of-Surface-Wave (SASW) Method.

ABSTRACT

The Spectral-Analysis-of-Surface-Waves (SASW) method is an in situ testing method for determining shear wave velocity profiles of soil sites and stiffness profiles of pavement systems. The method is nondestructive and is performed entirely from the pavement or ground surface. Measurements are made at strains below 0.001 percent where elastic properties of the materials are independent of strain amplitude. The key elements in SASW testing are the generation and measurement of surface waves. Transient impacts containing wide ranges of frequencies are transmitted to the pavement surface by means of simple hammers. Surface waves generated by these impacts are captured and recorded by the receivers using a spectral waveform analyzer. The analyzer is used to transform the waveforms into the frequency domain and then to perform spectral analyses on them. The points of interest from this operation are the phase information of the cross power spectrum and the coherence function. By evaluating the coherence function during testing, the range of frequencies which is not contaminated with random background noise can be quickly identified. Phase information from the cross power spectrum is indicative of the relative phase shift of each frequency propagating between the receivers. By knowing the distance between receivers and the phase shift for each frequency, phase velocity and wavelength associated with that frequency are calculated. A dispersion curve is a plot of phase velocity versus wavelength. By applying an inversion process, an analytical technique for reconstructing the shear wave velocity profile from the dispersion curve, layering and the shear wave velocity and Young's modulus of each layer can be readily obtained. One of the most important steps in SASW testing is the inversion process which has been the missing link in engineering applications. The theoretical foundation of the SASW method is discussed in detail in this report, with an emphasis placed on the theoretical aspects of the inversion process.

SUMMARY

The theoretical aspects of the Spectral-Analysis-of-Surface-Waves (SASW) method are presented herein. The SASW method is used to determine the shear wave velocity and elastic modulus profiles of pavement sections and soil sites. With this method, a transient vertical impulse is applied to the surface, and a group of surface waves with different frequencies are generated in the medium. These waves propagate along the surface with velocities that vary with frequency and the properties of the different layers comprising the medium. Propagation of the waves are monitored with two receivers a known distance apart at the surface. By analysis of the phase information of the cross power spectrum and by knowing the distance between receivers, phase velocity, shear wave velocity and moduli of each layer are determined.

This report contains a comprehensive discussion of the theories used in the in situ testing technique and the in-house data reduction procedure.

IMPLEMENTATION STATEMENT

The Spectral-Analysis-of-Surface-Waves (SASW) method has many applications in material characterization of pavement systems. With this method, elastic moduli and layer thicknesses of pavement systems can be evaluated in situ. The method can be utilized as a tool for quality control during construction and during regular maintenance inspections.

The method can be implemented to evaluate the integrity of flexible and rigid pavements. Reduction of the experimental data collected in the field is fully automated. The inversion process is not automated, as yet. The method has been employed at more than 35 pavement sites to study the precision and reliability of the method. From this study it can be concluded that the thicknesses of different layers are generally within about ten percent of those measured from boreholes and the moduli are, on the average, within 20 percent of moduli measured with other independent methods employing in situ seismic techniques.

TABLE OF CONTENTS

LIST OF TABLES

LIST OF FIGURES

CHAPTER ONE. INTRODUCTION

1.1 PROBLEM STATEMENT

A seismic method for in situ measurement of elastic modulus profiles of pavement systems has been under development for some time at the Center for Transportation Research at The University of Texas at Austin. This method is called the Spectral-Analysis-of Surface-Waves (SASW) method. The SASW method is based on generation and detection of elastic stress waves known as surface waves. Surface waves have a unique characteristic that, if the wavelength is varied, the velocity of propagation of surface waves also varies. This phenomenon is called dispersion. The dispersive characteristic of surface waves can be utilized to determine the layering and modulus profiles of pavement systems quite accurately. Surface waves have been used by investigators in the past but, due to a lack of a theoretical algorithm to determine the modulus profiles, little success was achieved. One of the major contributions of this research is development of such an algorithm. In addition, in situ testing time has been greatly accelerated through employment of the fast Fourier Transform (FFT) and spectral analyses now available with portable waveform analyzers.

To understand the theoretical basis of the SASW method, basic background material pertaining to this study are reviewed in depth herein. This report represents volume two of a three volume series on the SASW method. Volume one (Research Report 386-1F) presents the practical aspects of SASW testing. Volume three (Research Report 1123-1) consists of a manual for a computer program developed for data reduction (inversion).

1.2 ORGANIZATION

The organization of this report is as follows. The theoretical background on the propagation of seismic waves in elastic media is presented in Chapter Two. Both body waves and surface waves are presented, but the emphasis is placed on surface waves as generation and detection of surface waves is the basis of this study. In addition, relationships for determining

propagation velocities and elastic constants of material along with factors affecting elastic moduli of soils (subgrade) and pavement layers are presented.

In Chapter Three the principles of spectral analysis are discussed. Spectral functions from an actual in situ test on subgrade with the SASW method are included for clarity.

Existing in situ methods for determining elastic properties of soil and pavement layers are reviewed in Chapter Four. A literature review of past applications of surface waves is also presented.

Chapter Five contains a review of theoretical aspects concerning the dispersive characteristic of surface waves. The Haskell-Thomson formulation for the propagation of waves in an elastic, layered medium along with its shortcomings and remedies for these problems are discussed. The Haskell-Thomson method is suitable for computer generation of a theoretical dispersion curve for a known stiffness profile. The extension of this work by Dunkin, which eliminates numerical problems at high frequencies contained in the Haskell-Thomson method, is included. Finally, a parametric study of factors affecting the dispersion of surface waves and a discussion of types of waves to be expected in different media, such as soil deposits and pavements, concludes this chapter.

The report then concludes with a short summary presented in Chapter Six.

1.3 OVERVIEW OF SASW METHOD

To allow the reader to understand better the application of the theories introduced in the next chapters, a brief discussion of the SASW method is included herein. All practical aspects of the SASW method are discussed in detail in Nazarian and Stokoe (1985).

1.3.1 General Background

The Spectral-Analysis-of-Surface-Waves (SASW) method is a method of seismic testing which has been developed for determining shear wave velocity and shear modulus profiles at soil sites and Young's modulus profiles at pavement sites (Nazarian, 1984). The SASW method is a nondestructive method in which both the source and receivers are located on the ground surface. The

source is simply a transient vertical impact which generates a group of surface waves of various frequencies that the medium transmits. Two vertical receivers located on the surface monitor the propagation of surface wave energy past them. By analysis of the phase information of the cross power spectrum for each frequency determined between the two receivers, phase velocity, shear wave velocity and finally elastic moduli are determined. The key points in SASW testing are generation and measurement of surface waves (Rayleigh waves). Rayleigh wave velocity, V_R, is constant in a homogeneous half-space and independent of the frequency. Each frequency, f, has a corresponding wavelength, L_R, according to:

$$V_R = f \cdot L_R \tag{1.1}$$

Rayleigh wave and shear wave velocities are related by Poisson's ratio. In an isotropic elastic half-space, the ratio of Rayleigh wave to shear wave velocity increases as Poisson's ratio increases. The change in this ratio is small, and it can be assumed that the ratio is approximately equal to 0.90 without introducing an error larger than five percent. (This point is discussed in Section 2.3.)

If the stiffness of a site varies with depth, then the velocity of the Rayleigh wave (R-wave) will vary with frequency. The variation of R-wave velocity with frequency (wavelength) is called dispersion, and a plot of surface wave velocity versus wavelength is called a dispersion curve. The dispersion curve is developed from phase information of the cross power spectrum. This information provides the relative phase between two signals (two-channel recorder) at each frequency in the range of frequencies excited in the SASW test. For a travel time equal to one period of the wave, the phase difference is 360 degrees. Thus, for each frequency the travel time between receivers can be calculated by:

$$t(f) = \phi(f)/(360 \cdot f) \tag{1.2}$$

where:

f = frequency,
$t(f)$ = travel time for a given frequency, and
$\phi(f)$ = phase difference in degrees for a given frequency.

The distance between the receivers, X, is a known parameter. Therefore, R-wave velocity at a given frequency, $V_R(f)$, is simply calculated by:

$$V_R(f) = X/t(f) \tag{1.3}$$

and the corresponding wavelength of the R-wave is equal to:

$$L_R(f) = V_R(f)/f \tag{1.4}$$

By repeating the procedure outlined by Eqs. 1.2 through 1.4 for every frequency, the R-wave velocity corresponding to each wavelength is evaluated, and the dispersion curve is determined.

On the basis of studies at several soil sites, Heisey et al (1981) suggested that the distance between the receivers, X, should be less than two wavelengths and greater than one-third of a wavelength. This relationship can be expressed as:

$$L_R/3 < X < 2L_R \tag{1.5}$$

As the velocities of different layers are unknown before testing, it is difficult to know if these limits are satisfied. Practically speaking, it is more appropriate to test with various distances between the receivers in the field and then evaluate the range of wavelengths over which reliable measurements were made. The relationship between receiver spacing and wavelength is then better expressed as:

$$X/2 < L_R < 3X \tag{1.6}$$

The procedure is to select a spacing between receivers, perform the test, and reduce the data to determine the wavelengths and velocities. The next step is to eliminate the points that do not satisfy Eq. 1.6.

Rayleigh wave velocities determined by this method are not actual velocities of the layer but are apparent R-wave velocities (known as phase velocities). Existence of a layer with high or low velocity at the surface of the medium affects measurement of the velocities of the underlying layers. Therefore, a method for evaluation of shear wave velocities from phase velocities is necessary in SASW testing.

Inversion of the dispersion curve, or (in short) inversion, is the procedure of determining the shear wave velocity profile from the dispersion curve. Inversion consists of determination of the depth of each layer and the actual shear wave velocity of each layer from the apparent R-wave velocity versus wavelength information.

The inversion process used herein is based upon a modified version of Thomson's (1950) and Haskell's (1953) matrix solution for elastic surface waves in a layered solid media. To simplify the process of inversion, some assumptions were made. These assumptions include: 1) the layers are horizontal, 2) the velocity of each layer is constant, and 3) the layers are homogeneous and linearly elastic.

The inversion process is an iterative process in which a shear wave velocity profile is assumed and a theoretical dispersion curve is constructed. The experimental and theoretical dispersion curves are compared and necessary changes are made in the assumed shear wave velocity profile until the two curves (experimental and theoretical dispersion curves) match within a reasonable tolerance.

Once the shear wave velocities are determined, the following formulae are used to calculate shear and Young's moduli:

$$G = \rho \cdot V_s^2 \tag{1.7}$$

and

$$E = 2G(1 + \nu) \tag{1.8}$$

where:

G = shear modulus,
E = Young's modulus,
ρ = mass density (total unit weight divided by the acceleration of gravity), and
ν = Poisson's ratio.

1.3.2 Field Procedure

The general configuration of the source, receivers, and recording equipment is shown in Fig. 1.1. Accelerometers are used as receivers for close receiver spacings (4 ft and less), and geophones are used as receivers for greater spacings. This is done to optimize recording of the wave passage.

The common receivers midpoint (CRMP) geometry (Nazarian et al, 1983) is used for testing. With this geometry the two receivers are moved away from an imaginary centerline midway between the receivers at an equal pace, and the source was moved so that the distance between the source and near receiver is equal to or greater than the distance between the two receivers. In addition, the location of the source is reversed for each receiver spacing so that forward and reverse profiles are run. This testing sequence is illustrated in Fig. 1.2. Typically, distances between receivers of 0.5, 1, 2, 4, and 8 ft are used at each pavement site.

Different sources are used. For close receiver spacings, a 4-oz hammer is used. For greater distances, 2.5- and 5-lb sledge hammers are employed.

The recording device is a Fourier spectral analyzer. A Fourier analyzer is a digital oscilloscope that by means of a micro-processor attached to it has the ability to perform directly in either the time or frequency domain. Fourier analysis is a power tool in decomposition of complicated waveforms, and testing cannot be performed without such an analysis.

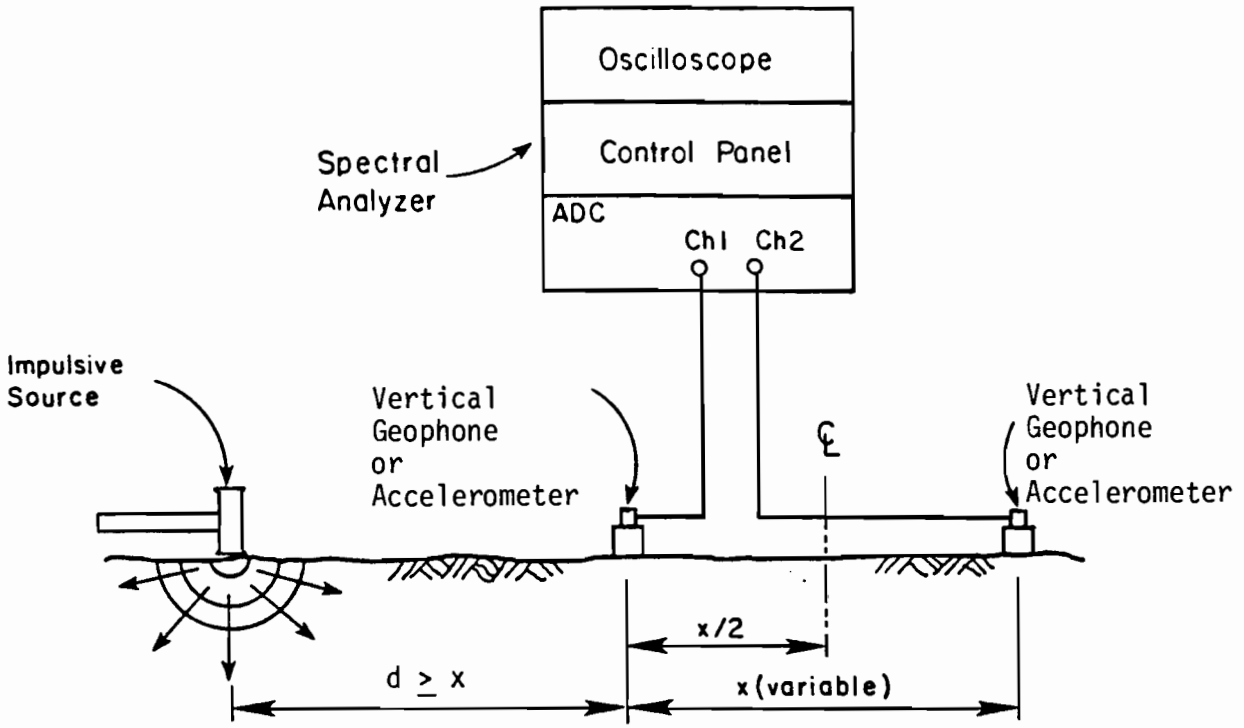

Fig. 1.1. General Configuration of SASW Testing.

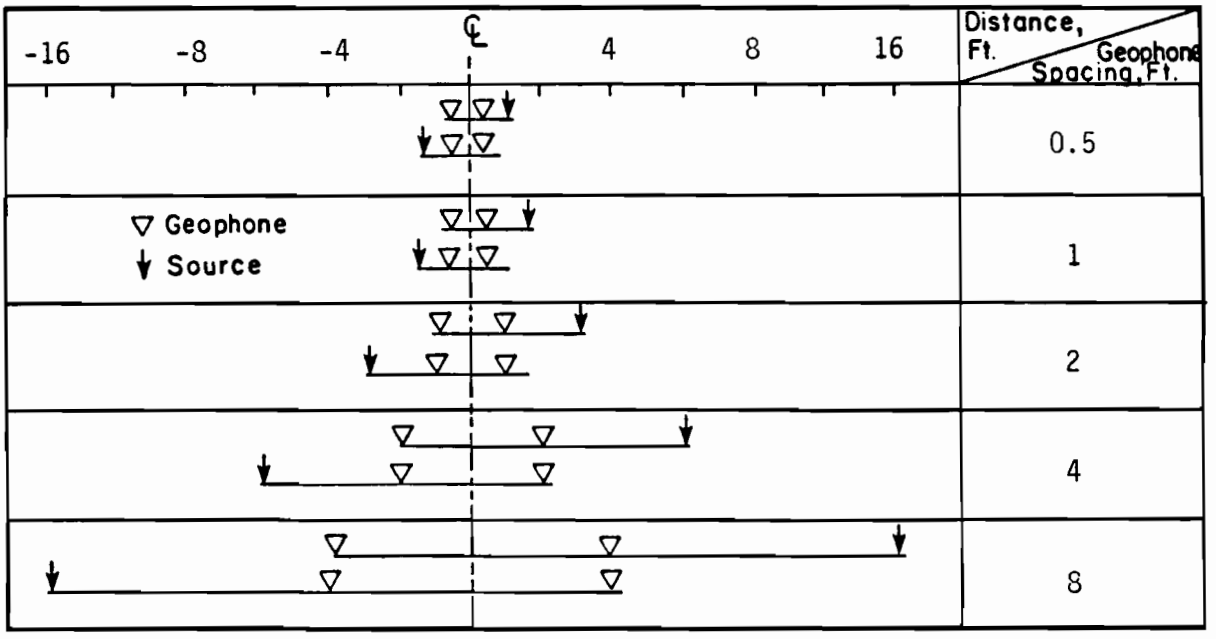

Fig. 1.2. Schematic of Typical Experimental Arrangement for SASW Testing at Pavement Sites.

CHAPTER TWO. WAVE PROPAGATION IN A LAYERED HALF-SPACE

2.1 INTRODUCTION

An overview of wave propagation theory in a layered medium and the theory of elasticity pertaining to this study are presented in this chapter. The relationship between the stiffnesses of different materials, which is expressed in terms of elastic moduli, and wave velocities is also briefly discussed. In the last section, factors affecting the stiffness of materials are presented.

For engineering purposes, many soil and most pavement sites can be approximated by a layered half-space with reasonable accuracy; especially over the short distances (on the order of tens of feet) used in SASW testing. With this approximation, the profiles are assumed to be homogeneous and to extend to infinity in two horizontal directions while being heterogeneous in the vertical direction. This heterogeneity is often modelled by a number of layers with constant properties within each layer. In addition, it is assumed that the material in each layer is elastic and isotropic. The waves are assumed to be plane. Propagation of plane waves in a medium is independent of the properties of one direction, so that the solution of the wave equations reduces to a two-dimensional problem. The coordinate system used in this study consists of a Cartesian system with the x-axis horizontal and positive to the right, and the z-axis vertical and positive downward. The y-axis is ignored due to the assumption of plane waves. A medium characterized by these assumptions is called an ideal medium, hereafter.

2.2 SEISMIC WAVES

2.2.1 Body Waves

Wave motion created by a disturbance within an ideal whole space can be described by two kinds of waves: compression waves and shear waves. These waves are collectively called body waves as they travel within the body of the medium. Compression and shear waves can be distinguished by the direction of particle motion relative to the direction of wave propagation.

Compression waves (also called dilatational waves, primary waves, or P-waves) exhibit a push-pull motion. As a result, wave propagation and particle motion are in the same direction, as shown in Fig. 2.1a. Compression waves travel faster than the other types of waves; hence, appear first in a direct travel time record.

Shear waves (also called distortional waves, secondary waves or S-waves) generate a shearing motion, which causes particle motion to occur perpendicularly to the direction of wave propagation as shown in Fig. 2.1b. Shear waves can be polarized. If the directions of propagation and particle motion are contained in a vertical plane, the wave is said to be vertically polarized and is called an SV-wave. However, if the direction of particle motion is perpendicular to a vertical plane containing the direction of propagation, the wave is said to be horizontally polarized and is termed an SH-wave. Shear waves travel slower than P-waves and thus appear as the second major wave type in a direct travel time record.

2.2.2 Surface Waves

In a half-space, other types of waves occur in addition to body waves. These waves are called surface waves. Many different types of surface waves have been identified and described. The two major types are Rayleigh waves and Love waves.

Surface waves propagate near the surface of the half-space. Rayleigh waves (R-waves) propagate at a speed of approximately 90 percent of S-waves. Particle motion associated with R-waves is composed of both vertical and horizontal components, which, when combined, form a retrograde ellipse close to the surface (see Fig. 2.1d). However, as depth increases, R-wave particle motion changes to pure vertical and finally to a prograde ellipse as illustrated in Fig. 2.2. One can infer from Fig. 2.2 that the amplitude of motion attenuates quite rapidly with depth. At a depth equal to about 1.5 times the wavelength, the vertical component of the amplitude is approximately equal to ten percent of the original amplitude at the ground surface.

Particle motion associated with Love waves is confined to a horizontal plane and is perpendicular to the direction of wave propagation as shown in Fig. 2.1c. This type of surface wave can only exist when low-velocity layers are underlain by higher-velocity layers because the waves are generated by

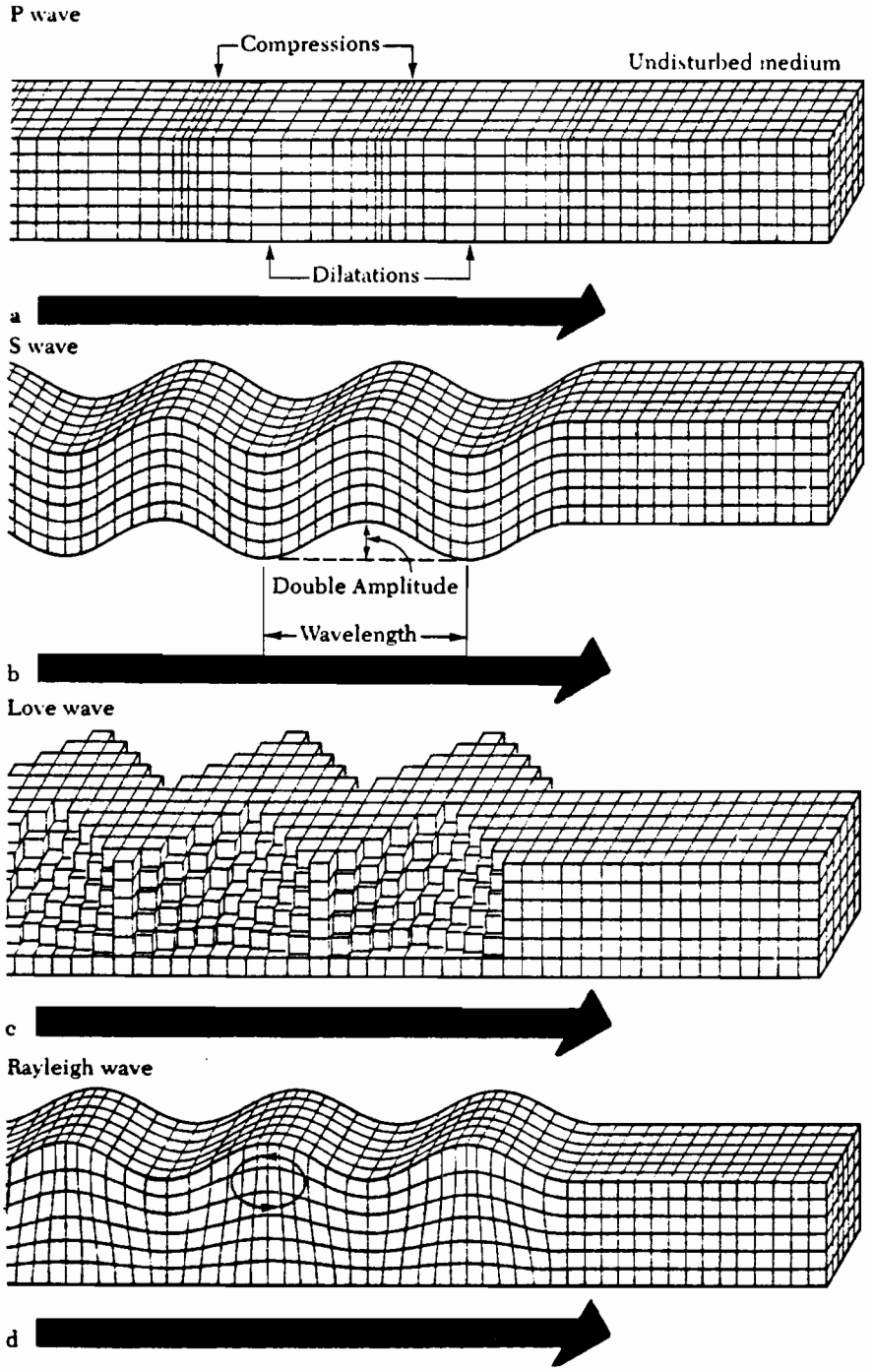

Fig. 2.1. Characteristic Motion of Seismic Waves (from Bolt, 1976).

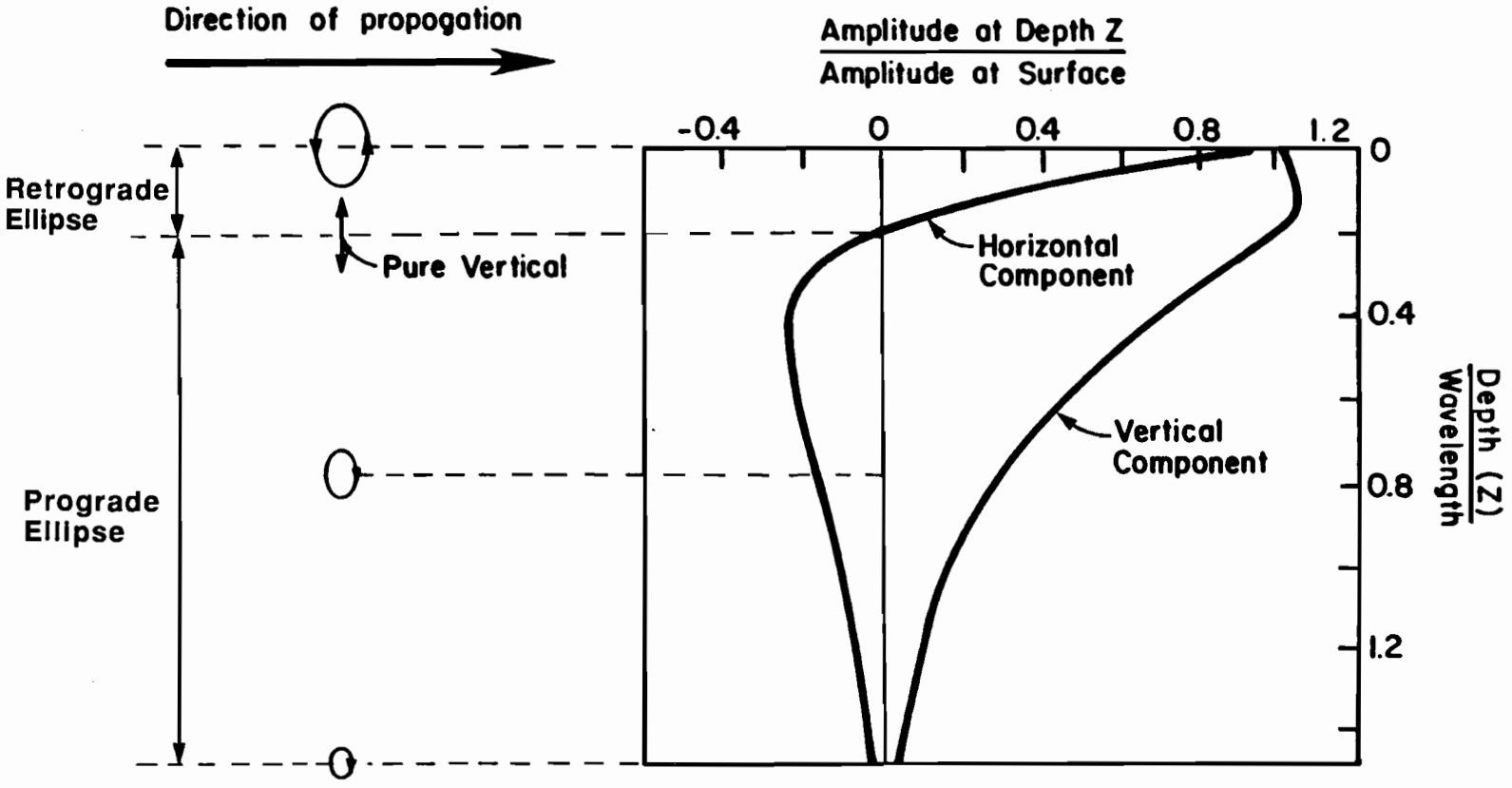

Fig. 2.2. Amplitude and Particle Motion Distribution with Depth for Rayleigh Waves.

total multiple reflections between the top and bottom surfaces of the low-velocity layer.

Other types of surface waves, such as Stonely waves which exist at the boundary of a liquid and solid, are of less significance and are not discussed herein.

The propagation of body waves (shear and compression waves) and surface waves (Rayleigh waves) away from a vertically vibrating circular source at the surface of a homogeneous, isotropic, elastic half-space is shown in Fig. 2.3. Miller and Pursey (1955) found that for the situation shown in Fig. 2.3, approximately 67 percent of the input energy propagates in the form of R-waves while shear and compression waves carry 26 and 7 percent of the energy, respectively. Compression and shear waves propagate radially outward from the source, but R-waves propagate along a cylindrical wavefront near the surface. Although, body waves travel faster than surface waves, body waves attenuate much faster at the surface than R-waves, due to geometrical damping. At the surface of an elastic half-space, body waves attenuate in proportion to r^{-2}, where r is the distance from the source; whereas, surface wave amplitude decreases in proportion to $r^{-0.5}$.

2.3 SEISMIC WAVE VELOCITIES

Seismic wave velocity is defined as the speed that a wave advances in the medium. Wave velocity is a direct indication of the stiffness of the material; higher wave velocities are associated with higher stiffnesses. By employing elastic theory, compression wave velocity can be defined as:

$$V_p = \sqrt{(\lambda + 2G) / \rho} \qquad (2.1)$$

where,

V_p = compression wave velocity,
λ = Lame's constant,
G = shear modulus, and
ρ = mass density.

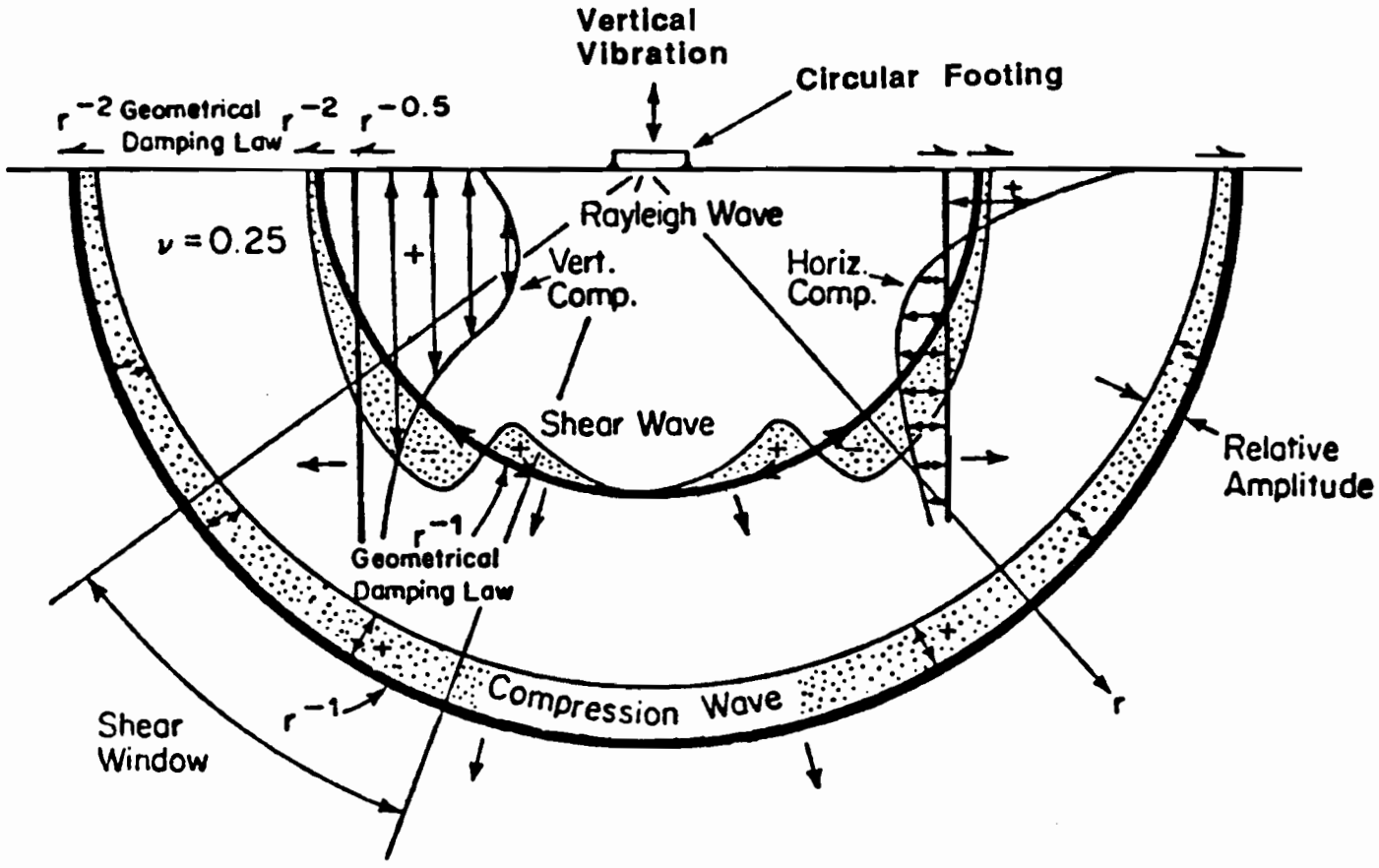

Fig. 2.3. Distribution of Rayleigh, Shear and Compression Wave Displacements from a Circular Footing on a Homogeneous, Isotropic, Elastic Half-Space (from Richart, et al, 1970).

Shear wave velocity, V_s, is equal to:

$$V_s = \sqrt{G / \rho} \tag{2.2}$$

For an isotropic and homogeneous material, compression and shear wave velocities are theoretically interrelated by Poisson's ratio. The relation can be expressed as:

$$(V_p/V_s) = [(1-\nu) /(0.5-\nu)]^{0.5} \tag{2.3}$$

where ν is the Poisson's ratio. A graphic illustration of Eq. 2.3 is shown in Fig. 2.4. From this figure it can be seen that, for a constant shear wave velocity, compression wave velocity increases with an increase in Poisson's ratio. For a value of Poisson's ratio of zero, the ratio of V_p to V_s is equal to $\sqrt{2}$, and for ν = 0.5 (an incompressible material), this ratio is equal to infinity.

Equation 2.3 can be rewritten as:

$$\nu = [0.5(V_p/V_s)^2 - 1)] / [V_p/V_s)^2 - 1] \tag{2.4}$$

This equation can be used in the calculation of Poisson's ratio once V_s and V_p are known.

For an isotropic layer with constant properties, R-wave velocity and shear wave velocity are related by Poisson's ratio as well. Although, the ratio of R-wave to S-wave velocities increases as Poisson's ratio increases, the change in this ratio is not significant as shown in Fig. 2.5. For Poisson's ratio of zero and 0.5, this ratio changes from approximately 0.86 to 0.95, respectively, and it can be assumed that the ratio is equal to 0.90 without introducing an error larger than about five percent.

2.4 ELASTIC CONSTANTS

Propagation velocities per se have limited use in engineering applications. In geotechnical earthquake engineering and soil dynamics, shear modulus and its variation with strain is of interest. In transportation

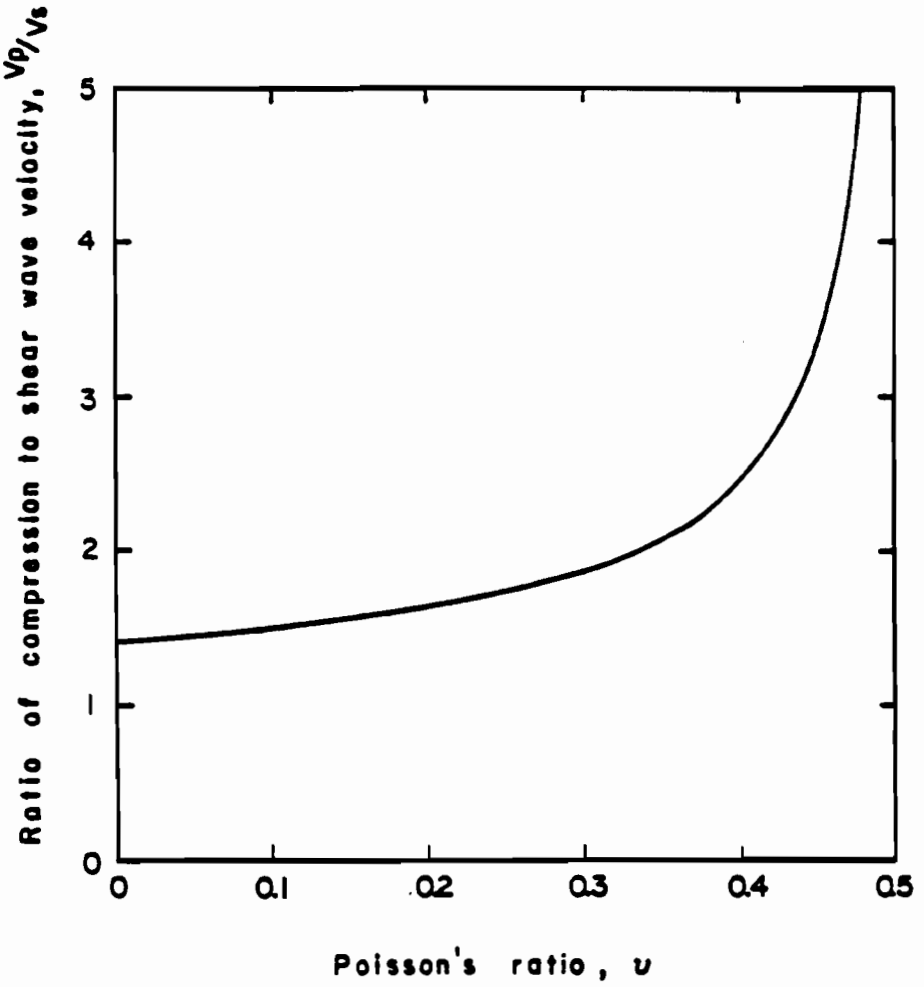

Fig. 2.4. Theoretical Elastic Relationship Between Poisson's Ratio and the Ratio of Compression to Shear Wave Velocity.

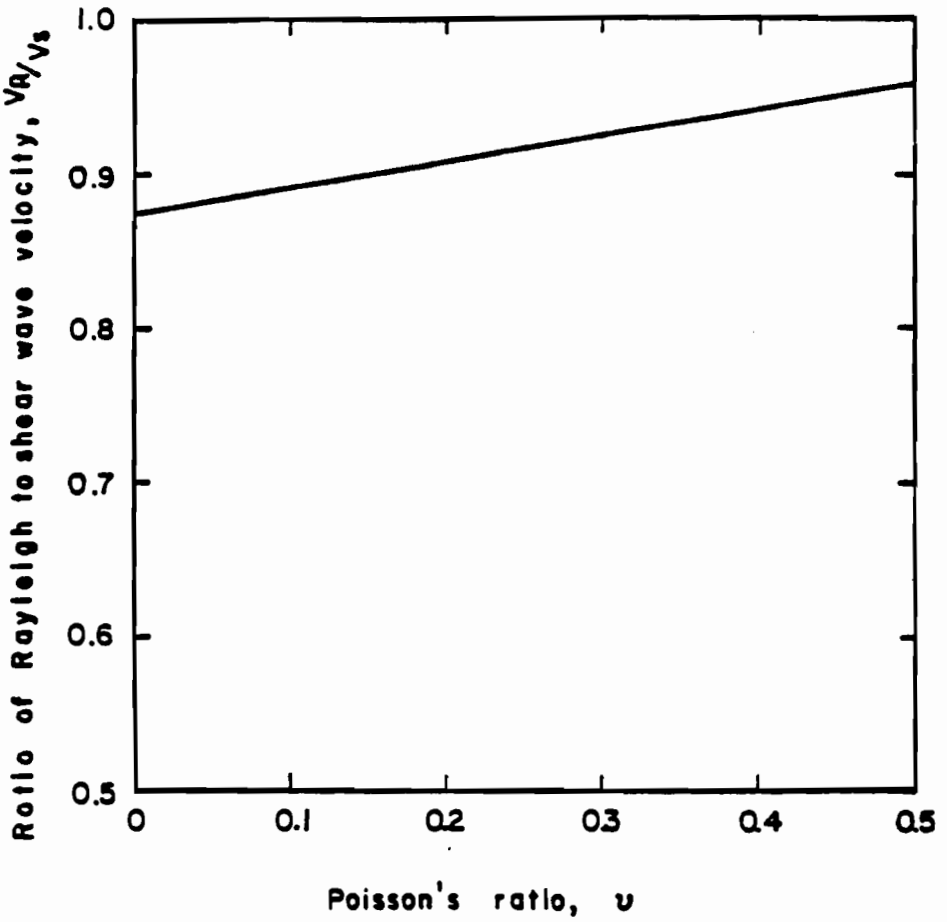

Fig. 2.5. Theoretical Elastic Relationship Between Poisson's Ratio and the Ratio of Rayleigh to Shear Wave Velocity.

engineering for material characterization and the design of overlays, Young's moduli of the different layers should be measured. Calculation of elastic moduli from propagation velocities is, thus, important.

Shear wave velocity, V_s, is used to calculate shear modulus, G, by:

$$G = \rho \cdot V_s^2 \tag{2.5}$$

in which ρ is the mass density. Mass density is equal to, γ_t/g, where γ_t is total unit weight of the material and g is gravitational acceleration. If Poisson's ratio (or compression wave velocity) is known, other moduli can be calculated for a given V_s. For an isotropic, homogeneous material, Young's and shear moduli are related by:

$$E = 2G\ (1 + \nu) \tag{2.6}$$

or,

$$E = 2\rho V_s^2\ (1 + \nu) \tag{2.7}$$

In a medium where the material is restricted from deformation in two lateral directions, the ratio of axial stress to axial strain is called constrained modulus. Constrained modulus, M, is defined as:

$$M = \rho \cdot V_p^2 \tag{2.8}$$

or in terms of Young's modulus and Poisson's ratio:

$$M = (1 - \nu)\ E\ /\ [(1 + \nu)(1 - 2\nu)] \tag{2.9}$$

Bulk modulus, B, is the ratio of hydrostatic stress to volumetric strain and can be determined by:

$$B = M - 4/3\ G \tag{2.10}$$

2.5 FACTORS AFFECTING ELASTIC MODULI

2.5.1 Soil (or Subgrade)

Based upon numerous laboratory tests, Hardin and Drnevich (1972) proposed many parameters that affect shear moduli of soils. These parameters, along with their degree of importance in affecting shear moduli, are tabulated in Table 2.1. Hardin and Drnevich suggested that state of stress, void ratio, and strain amplitude are the main parameters affecting moduli measured in the laboratory. However, for this study dealing with in situ measurement of moduli at small strains, the main factors affecting the elastic moduli and wave velocities are void ratio and state of stress (confining stress).

Strain amplitude has essentially no effect on the in situ tests because the measurements are performed at very low strains. Up to a shearing strain amplitude of about 0.01 percent, shear moduli are nearly constant, with a slight decrease in the strain range from 0.001 to 0.01 percent. This constant modulus is called the elastic modulus or maximum modulus. Above a strain level of 0.01 percent, moduli decrease significantly.

In Eqs. 2.6, it was shown that Young's modulus and shear modulus are interrelated with Poisson's ratio. By means of Mohr circles, it can be shown that normal strain and shear strain are also related. For uniaxial loading, this relationship can be written as:

$$\gamma = \varepsilon (1 + \nu) \tag{2.11}$$

where γ and ε are shear and normal strains, respectively. Therefore, it is common to assume a similar strain dependency between Young's modulus and axial strain as has been found for shear modulus and shearing strain.

A typical example of the variation in Young's modulus, E, with normal strain, ε, for a stiff clay is shown in Figs. 2.6 and 2.7. An undisturbed sample of stiff clay from San Antonio, Texas was tested using the resonant column method (Richart et al, 1970). The variation of E with log ε at several confining pressures is shown in Fig. 2.6. As the confining stress increases, the low-amplitude modulus increases, as shown in this figure. Also, it is evident that below strain levels of 0.001, E is constant and independent of strain at each pressure.

TABLE 2.1. PARAMETERS AFFECTING SHEAR MODULUS (FROM HARDIN AND DRNEVICH, 1972).

Parameter	Importance[a]	
	Clean Sands	Cohesive Soils
Strain Amplitude	V	V
Effective Mean Principle Stress	V	V
Void Ratio	V	V
Number of Cycles of Loading	R[b]	R
Degree of Saturation	R	V
Overconsolidation Ratio	R	L
Effective Strength Envelope	L	L
Octahedral Shear Stress	L	L
Frequency of Loading	R	R
Other Time Effects (Thixotropy)	R	L
Grain Characteristics	R	R
Soil Structure	R	R
Volume Change Due to Shear Strain	V	R

a) V means Very Important, L means Less Important, R means Relatively Unimportant, and U means relative importance is not known at the time.

b) Except for saturated clean sand where the number of cycles of loading is a less Important Parameter.

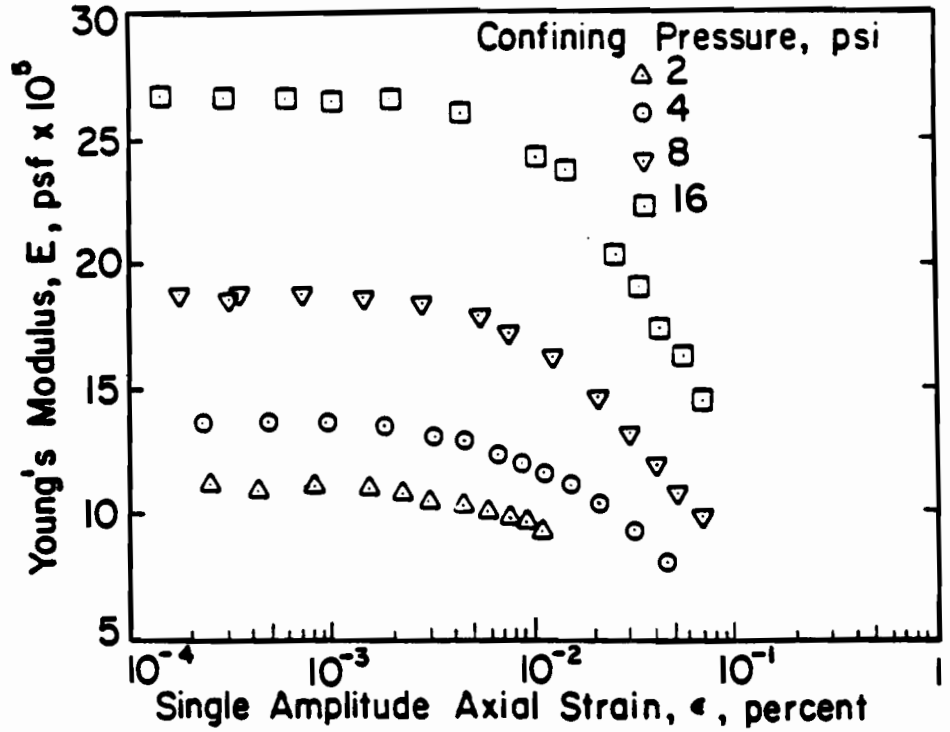

Fig. 2.6. Variation in Young's Modulus with Strain Amplitude at Different Confining Pressures of an Unsaturated Clay Subgrade.

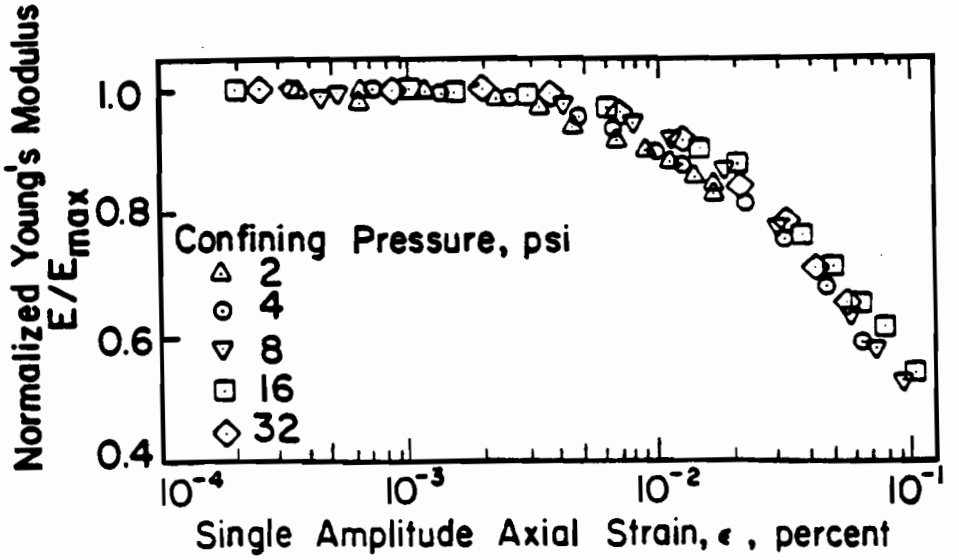

Fig. 2.7. Variation in Normalized Young's Modulus with Strain Amplitude of an Unsaturated Clay Subgrade.

The effect of strain on modulus is easily seen by plotting the variation of normalized modulus, E/E_{max}, versus log ε as shown in Fig. 2.7. In this figure, E_{max} is taken as the maximum value of Young's modulus at each confining pres sure. It can be seen that normalized modulus is constant below a strain of about 0.001 percent and is equal to E_{max}. Also all the modulus-strain curves are nearly independent of confining pressure once they are normalized. If a normalized modulus-strain curve such as that shown in Fig. 2.7 is available for the material, then moduli at higher strains can be determined once E_{max} has been measured. This idea is a very important concept in using in situ small-strain measurements to estimate nonlinear moduli.

Similar modulus-strain trends also occur with shear moduli as shown in Fig. 2.8 for a soft clay from the San Francisco Bay area.

Several studies performed on Poisson's ratios of different soils show that they are strain dependent. Chen (1948) reported Poisson's ratio as low as 0.1 for small-strain measurements on sand. Krizek (1977) reported the variation of Poisson's ratio with strain based upon measurements in unconfined compression tests. His data are shown in Fig. 2.9. The range of Poisson's ratio in this figure is from 0.10 for near zero strain to 0.50 for 10 percent strain. Hardin (1978) recommends using values for Poisson's ratio between zero and 0.20 for low-strain tests on soil, with a mean value of 0.12.

2.5.2 Base and Subbase

Two types of base and subbase materials are usually used, granular or treated materials. Granular base and subbase materials demonstrate the same characteristic as natural soil deposits. The base or subbase material are sometimes treated by additives such as cement, bitumen, or lime. In this situation, the moduli of the layer depends on additional factors such as type of aggregate and percentage of additive. Typical values of Young's moduli for granular and treated layers are in the range of 15 to 110 ksi (100 to 750 MPa) and 50 to 2000 ksi (350 to 14000 MPa), respectively. Poisson's ratios of these materials are on the order of 0.20 to 0.45 (Yoder and Witczak, 1975).

Nazarian and Stokoe (1986b) recently performed SASW tests at nine sites at the pavement test facility of Texas A&M University pavement test facility. Properties of different materials are given in Table 2.2. It can be seen that the moduli of untreated materials such as sandy gravel, sandy clay, and

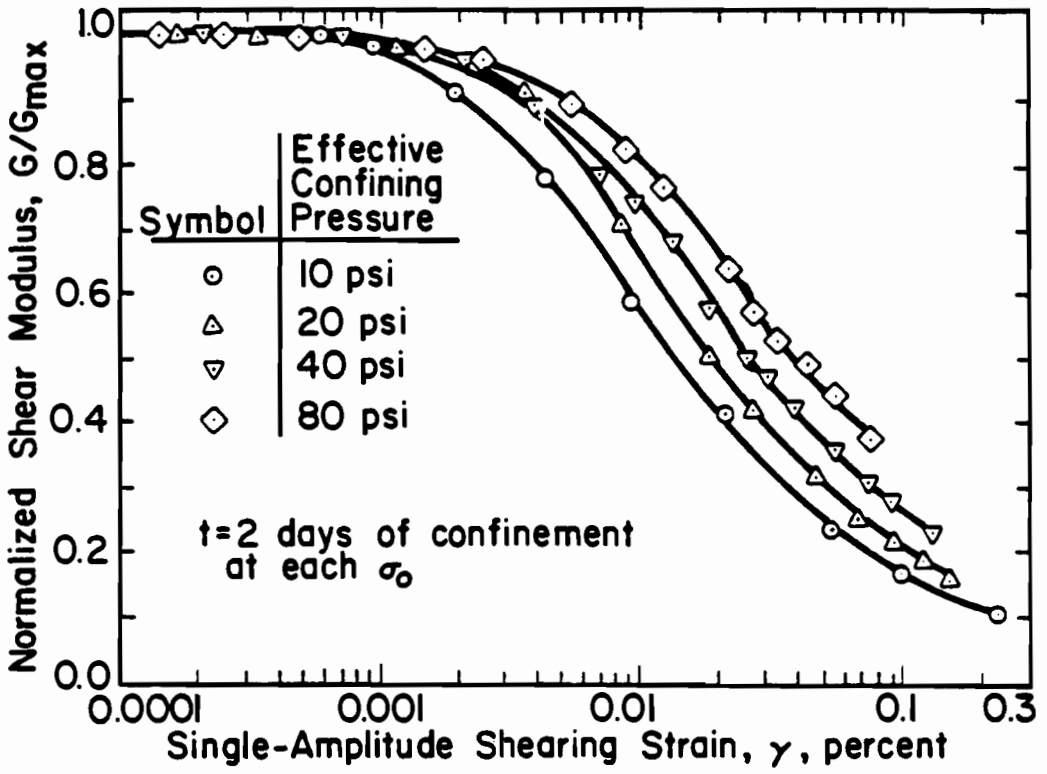

Fig. 2.8. Variation in Normalized Shear Modulus with Shearing Strain and Confining Pressure (from Stokoe and Lodde, 1978).

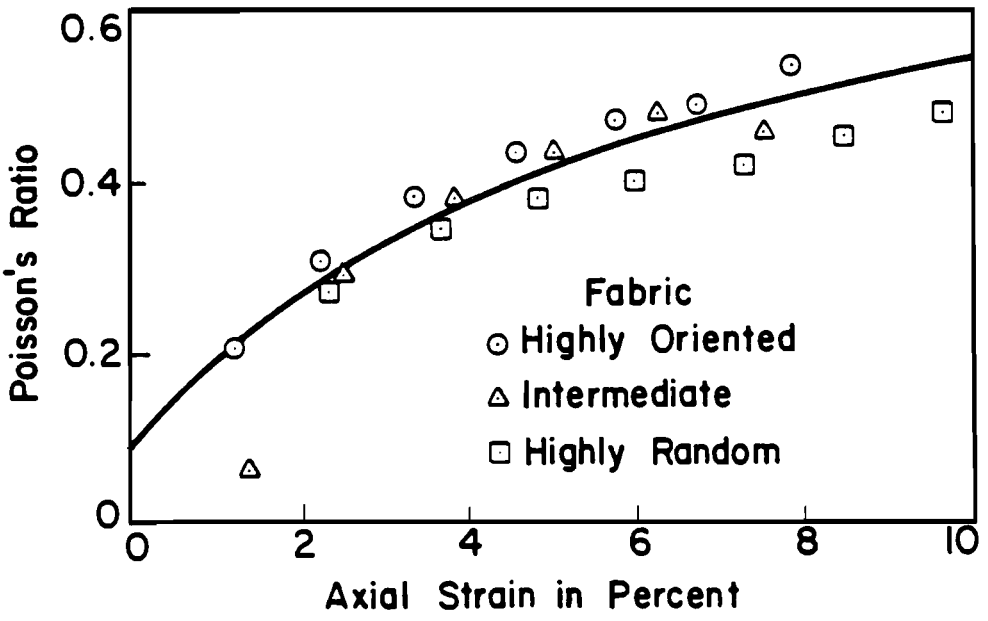

Fig. 2.9. Variation of Poisson's Ratio with Strain for Sedimented Kaolinite Tested in Unconfined Compression (from Krizek, 1977).

TABLE 2.2. SUMMARY OF AVERAGE MODULUS VALUES OF MATERIALS DETERMINED FROM SASW TESTS PERFORMED AT THE PAVEMENT TEST FACILITY OF THE TEXAS TRANSPORTATION INSTITUTE (FROM NAZARIAN AND STOKOE, 1986b).

Site	Average Modulus of Each Material, ksi						
	AC*	LS	LS+C	LS+L	GR	SC	PC
2	409	545	2500	--	--	--	34
4	338	509	3390	--	--	--	33
7	338	362	2727	--	--	--	17
9	314	977	--	--	29	--	--
10	500	60	--	--	25	--	--
11	605	32	--	--	25	--	--
16	371	--	2700	--	33	--	--
17	395	--	--	1340	--	51	--
18	395	--	--	1200	--	50	--

*AC: Hot Mix Asphalt Concrete
LS: Crushed Limestone
LS+C: Crushed Limestone + 4% Cement
LS+L: Crushed Limestone + 2% Lime
GR: Sandy Gravel
SC: Sandy Clay
PC: Plastic Clay

plastic clay is close to the lower limit reported by Yoder and Witczak (1975). The modulus of crushed limestone varies from 30 to 1000 ksi. Exposure to moisture and the effects of time have probably caused such a wide range of variation in this modulus. The lime-treated materials exhibit variations closer to the upper bound of values of treated materials reported by Yoder and Witczak. However, the cement-stabilized layers represent moduli higher than those reported by Yoder and Witczak (1975).

2.5.3 Asphalt-Cement Concrete

The main factor that affects the moduli of asphaltic materials, besides the mixture properties, is temperature. Typical variation of elastic moduli with temperature is shown in Fig. 2.10 for a bitumenous sample. As the temperature in creases the material behaves more viscously resulting in a decrease in the modulus (Van der Poel, 1954). The age of the material affects the modulus; with time, asphaltic materials become stiffer. The other factor that has some effect on the asphaltic material is the level of strain (or stress). The variation of modulus with strain level is similar to the effect of temperature; that is, the modulus de creases with increase in strain level. Unfortunately, no figure indicating the trend of this variation could be found in the literature, but it seems that the asphaltic material should behave somewhat like the soil samples shown in Fig. 2.7 and 2.8. Typical values of Young's modulus and Poisson's ratio of asphaltic material are in the range of 200 to 1100 ksi (1400 to 7700 MPa) and 0.25 to 0.40, respectively. Total unit weight of this material is on the order of 125 to 145 pcf (19 to 23 kN/m^3).

Modulus values obtained by Nazarian and Stokoe (1986b) at the Texas Transportation Institute's pavement test facility is in the range reported above (see Table 2.2, column 2).

2.5.4 Portland-Cement Concrete

The factor that affects the modulus of concrete, ignoring the method of preparation and curing, are type of aggregate and water-cement ratio. The concrete used in overlay of roads and runways are of high quality and are very stiff, and it is expected to behave elastically under most of the loads imposed by vehicular traffic. The elastic modulus of concrete as reported by Yoder and Witczak (1975) ranges from 3000 to 6000 ksi (21 to 42 GPa) and

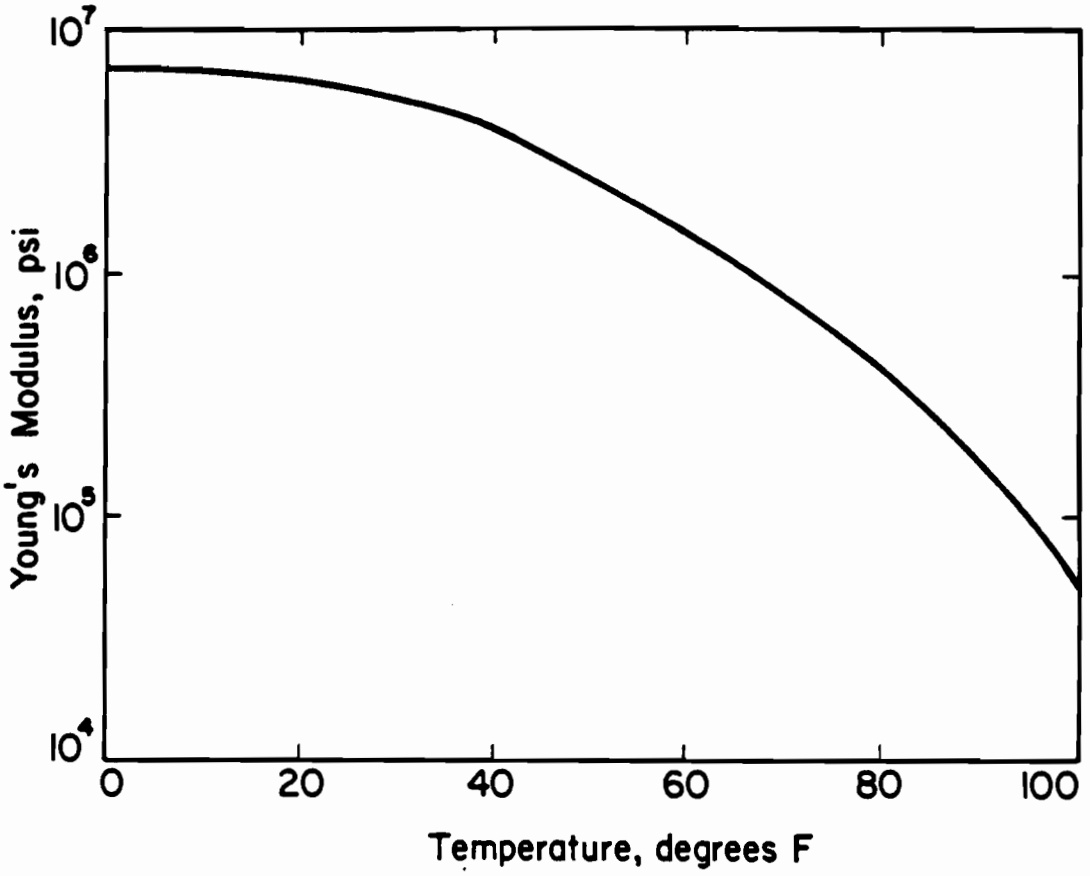

Fig. 2.10. Effect of Temperature on Young's Modulus of Asphaltic Concrete Material (inferred from Van der Poel, 1954).

Poisson's ratio varies from 0.10 to 0.25. The unit weight of concrete is typically 140 to 150 pcf (21 to 23 kN/m^3). Values of compression wave velocity for concrete range from 10,000 to 14,000 fps (3000 to 4300 m/sec), where the upper limit corresponds to competent concrete and the lower limit (below 11,000 fps) usually represents poor concrete.

2.6 SUMMARY

In this chapter, the different types of waves that propagate in a layered medium are presented. Waves of most importance to this study are compression, shear and Rayleigh waves. The propagation velocities of these waves are defined, and the relationship of material stiffness to propagation velocities are presented. Also, factors that affect the stiffness of different types of materials such as soil, asphalt-cement concrete, and portland-cement concrete are discussed. In soils, strain amplitude has the most effect on elastic moduli, but it can be neglected in this study as testing is being performed in the low-strain range where moduli are independent of strain (strains less than about 0.001 percent). Therefore, the major parameters that affect moduli of soils are void ratio and state of stress. Temperature and age are parameters that affect moduli the most for asphalt concrete, while for portland-cement concrete, type of aggregate, water-cement ratio and curing are the significant factors.

CHAPTER THREE. FREQUENCY DOMAIN ANALYSES APPLIED TO FIELD MEASUREMENTS

3.1 INTRODUCTION

Analyses in the frequency domain have been employed for many years as a helpful analytical tool in studying linear systems. However, even with significant computer capabilities, algorithms based upon the Fourier transform are not efficient enough to be applied in the field to actual engineering problems because of the prohibitive amount of time required for computation (even on main-frame computers). With the development of the fast Fourier transform, many aspects of engineering dealing with vibration theory and dynamic systems were revolutionized, and new areas could be explored economically and efficiently. The fast Fourier transform and spectral analyses are now widely used in field and laboratory testing. These frequency domain analyses form one of the key components of SASW testing and therefore are discussed briefly, herein.

3.2 FOURIER TRANSFORM

The Fourier transform is employed to decompose an arbitrary function in the time domain into a group of harmonic waves. Each waveform is defined by its frequency, amplitude and phase lead or lag. If the Fourier transform is properly performed, no information is lost or added; but it is possible to extract additional information from the data which was obscured in the time domain. As one example, a signal in the time domain is shown in Fig. 3.1a, and its Fourier transform is shown in Fig. 3.1b. Although a periodicity can be detected from the time domain record (Fig. 3.1a), it is very difficult, if not impossible, to measure the amplitude and frequency of the waves contained in this waveform. However, this information can be easily obtained from Fig. 3.1b.

3.2.1 Theory of the Fourier Transform

A waveform in the time domain, h(t), can be written in terms of a group of harmonic waves by:

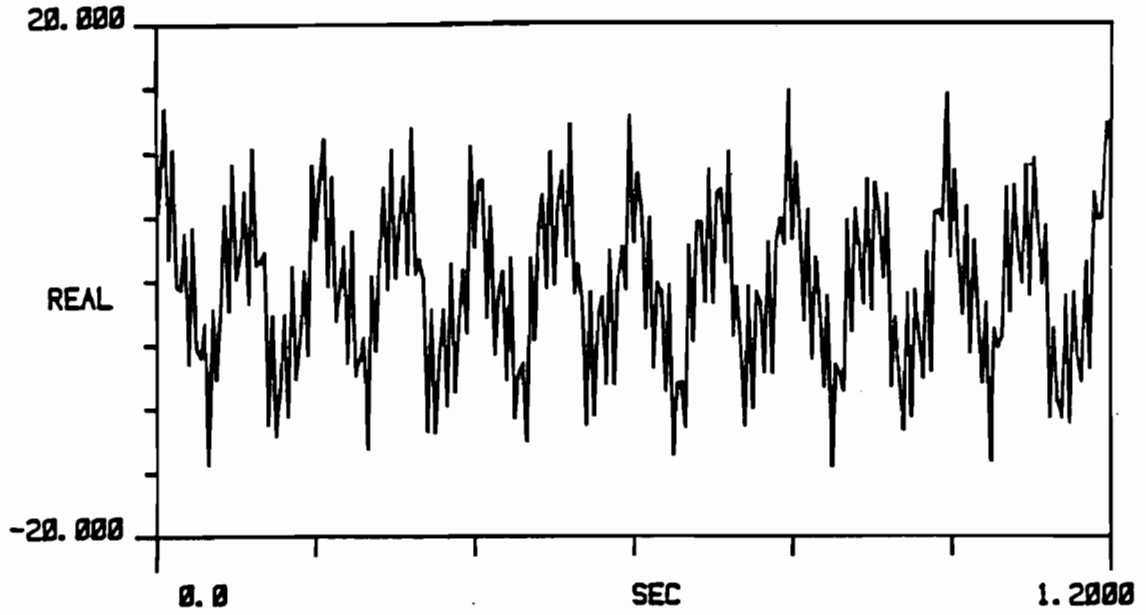

a. Signal in the Time Domain.

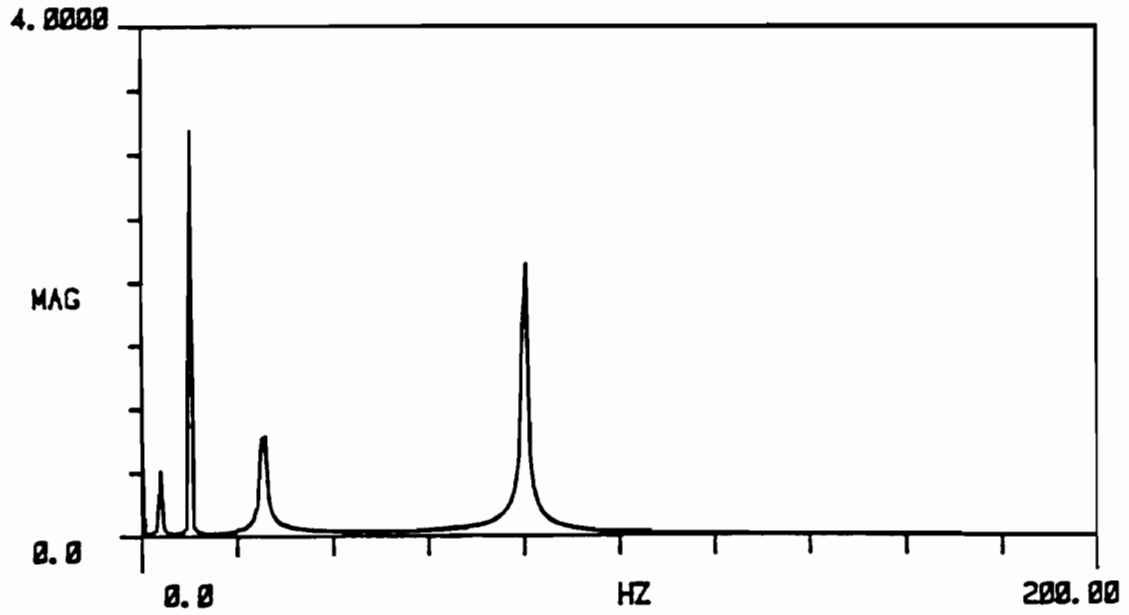

b. Signal in the Frequency Domain.

Fig. 3.1. Representation of a Time Domain Signal and Its Fourier Transform (from Heisey, et al, 1982).

$$h(t) = a_o/2 + \sum_{n=1}^{\infty} [a_n \cos(n\omega_o t) + b_n \sin(n\omega_o t)] \tag{3.1}$$

where coefficients a_n and b_n are called the Fourier coefficients and ω_o is called the fundamental frequency. Coefficient a_o represents the average value of the function h(t) over one period (and is analogous to a DC offset). Parameters a_n and b_n can be written as:

$$a_n = \frac{2}{T_o} \int_{\tau}^{\tau+To} h(t) \cos(n\omega_o t)dt \tag{3.2}$$

$$b_n = \frac{2}{T_o} \int_{\tau}^{\tau+To} h(t) \sin(n\omega_o t)dt \tag{3.3}$$

where T_o $(= 2\pi/\omega_o)$ is the fundamental period.

Alternatively, Eq. 3.1 can be written in terms of one trigonometrical function.

$$h(t) = A_o/2 + \sum_{n=1}^{\infty} A_n \sin(n\omega_o t + \phi_n) \tag{3.4}$$

in which

$$A_n = \sqrt{a_n^2 + b_n^2} \tag{3.5}$$

and

$$\phi_n = \tan^{-1} (b_n/a_n) \tag{3.6}$$

In terms of complex functions, Eq. 3.4 can be written using Euler's identity as:

$$h(t) = \sum_{n=-\infty}^{\infty} C_n \exp(jn\omega_o t) \tag{3.7}$$

where

$$C_n = 1/2 \ (a_n - jb_n) \tag{3.8}$$

and j is $\sqrt{-1}$ as normally used in mathematical representations.
Substituting Eqs. 3.2 and 3.3 into Eq. 3.8 results in:

$$C_n = \frac{1}{T_o} \int_o^{T_o} h(t) \exp(-jn\omega_o t)dt \tag{3.9}$$

To clarify Eqs. 3.4 through 3.9 in more physical terms, the principle of rotating phasors can be utilized. The representation of Fourier coefficients by a phasor for Eqs. 3.4 through 3.6 is shown in Fig. 3.2 while the phasor for Eqs. 3.7 through 3.9 is shown in Fig. 3.3.

The Fourier integral transform of a signal is defined as:

$$H(f) = \int_{-\infty}^{\infty} h(t) \exp(-j2\pi ft)dt \tag{3.10}$$

where, H(f) is the frequency domain representation of function h(t). Similarly, the inverse transform can be written as:

$$h(f) = \int_{-\infty}^{\infty} H(t) \exp(j2\pi ft)dt \tag{3.11}$$

The negative frequencies are introduced for mathematical convenience.

3.2.2 Discrete Finite Transform (DFT)

To incorporate the theory discussed in the last section into a computer algorithm, the Fourier transform should be done digitally. In other words, the integrals introduced in Eqs. 3.10 and 3.11 should be performed numerically. This matter will cause three distinct problems.

First, although the desired result is a continuous function, its value at discrete points can be calculated.
As such, Eq. 3.10 can be written as:

$$H_d(m \cdot \Delta f) = \Delta t \int_{-\infty}^{\infty} h(t) \exp(-j2\pi m \cdot \Delta f \cdot t)dt \tag{3.12}$$

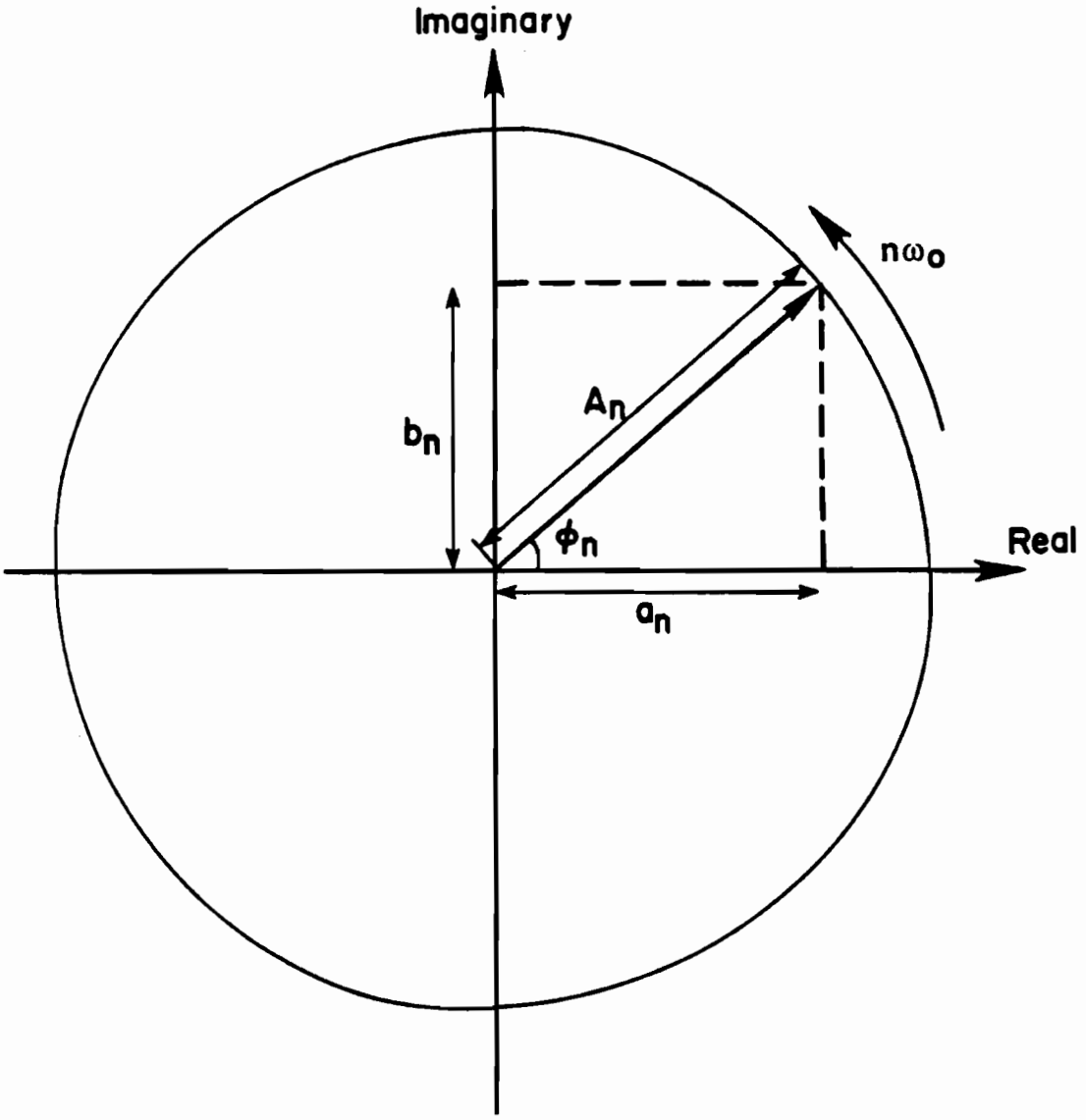

Fig. 3.2. Representation of Fourier Coefficients by a Rotating Phasor in the Complex Plane for Eqs. 3.4 to 3.6.

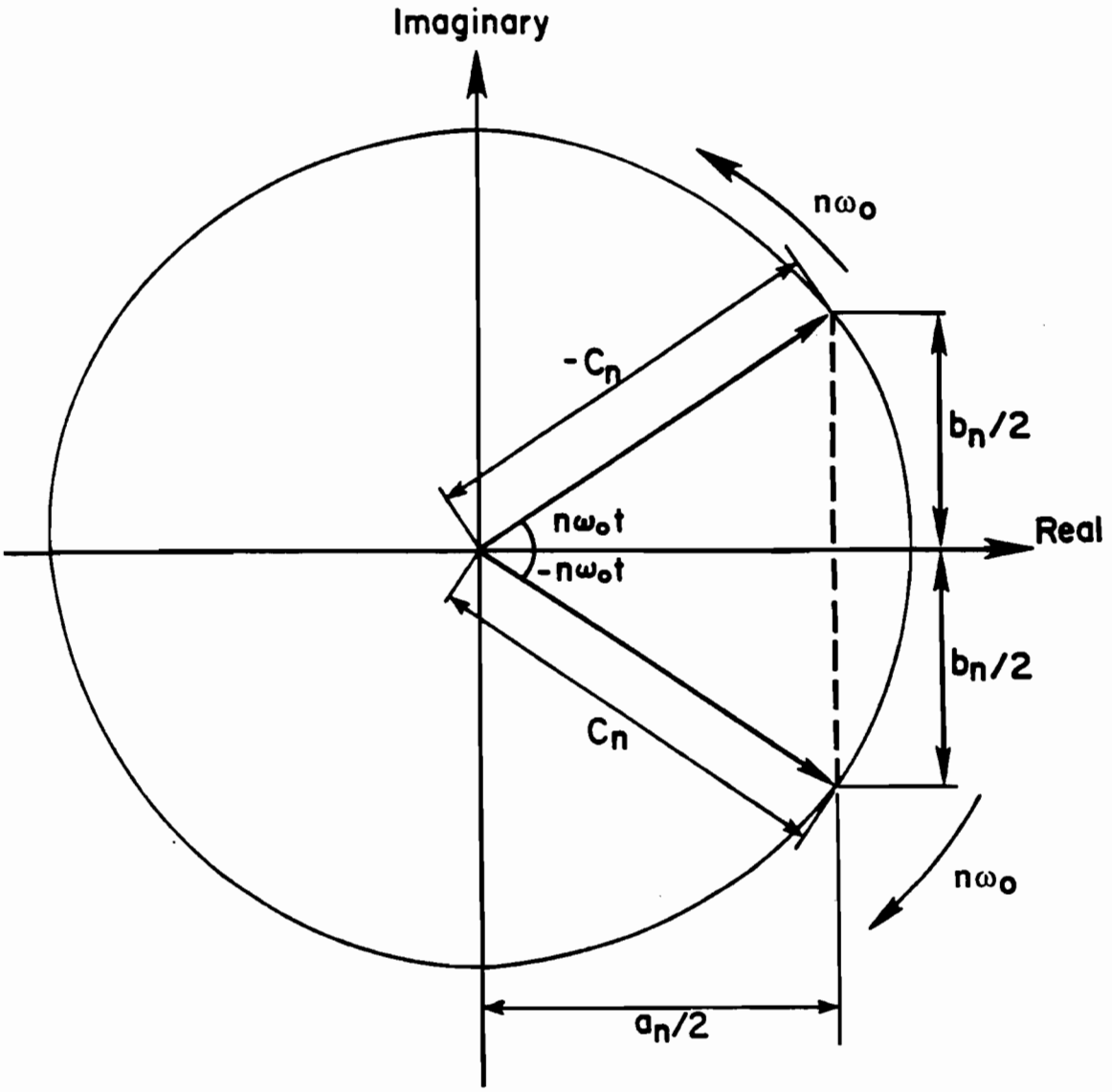

Fig. 3.3. Representation of Fourier Coefficients by a Rotating Phasor in the Complex Plane for Eqs. 3.7 to 3.9.

where m is an integer number representing each data point being discretized and Δf is the increment of frequency between each two discretized points. Function $H_d(m \cdot \Delta f)$ represents the digitized form of the continuous function H(f).

Secondly, an integral, which corresponds to computing the area under a curve, must be evaluated as shown in Fig 3.4. Equation 3.12 can be written as:

$$H_d(m \cdot \Delta f) = \Delta t \sum_{n=-\infty}^{\infty} [h_d(n \cdot \Delta t) \exp(-j2\pi m \Delta f n \Delta t)] \qquad (3.13)$$

where Δt is the time interval between samples.

Finally, as it is impossible to sample over a time period of infinity, the transform must be limited to a finite time interval. Thus, the final outcome is in the form of:

$$H_d(m \cdot \Delta f) = \Delta t \sum_{n=0}^{N-1} [h_d(n - \Delta t) \exp(-j2\pi m \Delta f n \Delta t)] \qquad (3.14)$$

It can be shown that (Hewlett Packard, 1981) Δt and Δf are related by:

$$\Delta f \cdot \Delta t \cdot N = 1 \qquad (3.15)$$

where N is the number of digitized points on the record. Therefore,

$$H_d(m \cdot \Delta f) = \Delta t \sum_{n=0}^{N-1} [h_d(n \cdot \Delta t) \exp(-j2\pi mn/N)] \qquad (3.16)$$

This is the formula being used in the discrete Fourier transform, DFT.

3.2.3 Fast Fourier Transform (FFT)

The fast Fourier transform (FFT) is an algorithm for per forming a discrete finite transform more efficiently. By assuming that the number of data points is a multiple of two, the computation time will be reduced substantially. This assumption allows certain symmetries to occur which reduces the number of operations. In Fig. 3.5 the number of operations for the DFT and FFT are compared. For the number of data points, N, equal to 1024, the reduction in number of multiplications is more than 200 times.

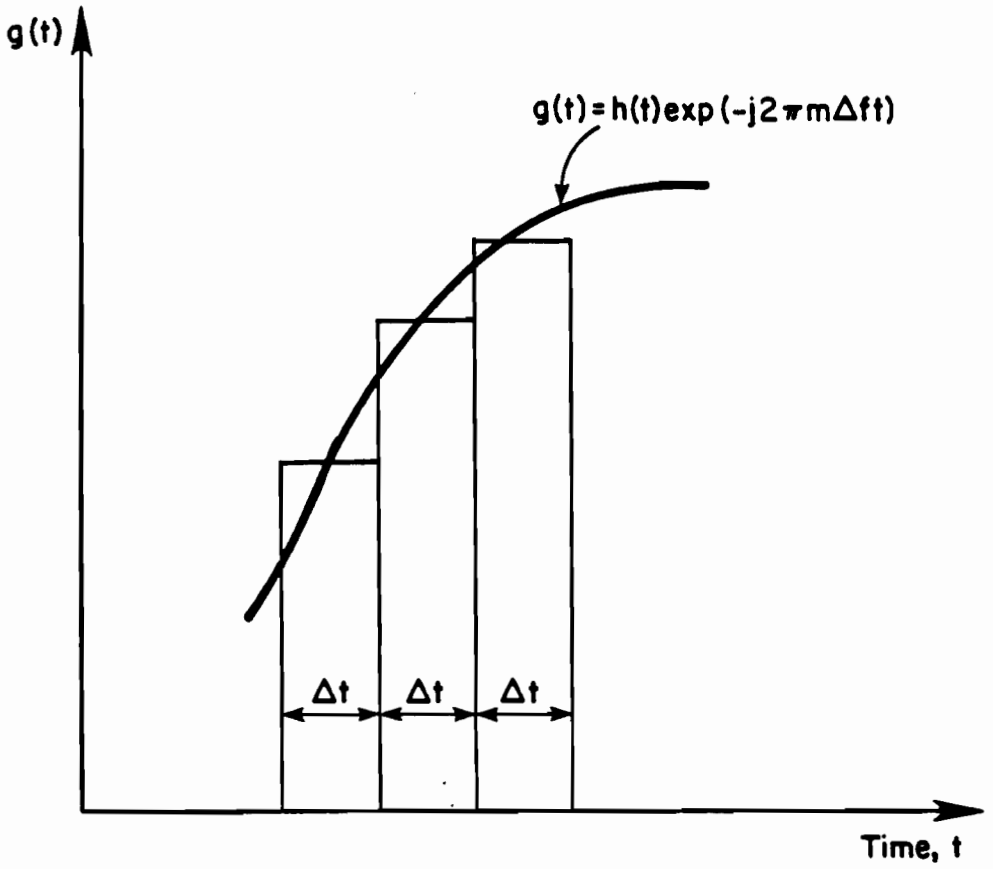

Fig. 3.4. Schematic of Numerical Integration in Discrete Finite Transform.

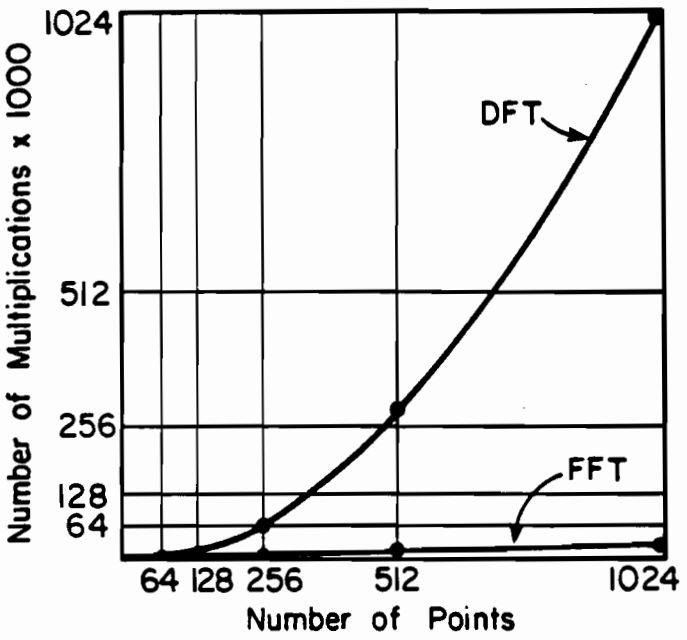

Fig. 3.5. Comparison of Number of Operations in Computing the Fast Fourier Transform and Discrete Finite Transform (after Brigham, 1974).

3.3 SPECTRAL ANALYSES

Several types of measurements can be made in the frequency domain once the signals are Fourier transformed. Spectral analyses are basically statistical operations on one or two signals in the frequency domain.

Measurements are often made on two channels of data. The first channel is usually named the "input" and the second one is termed the "output". Spectral analyses are either the correlation of the input or of the output with itself, or correlation of these two, considering that the object being tested is a linear system. The idealized and actual models being used in spectral analyses are shown in Fig. 3.6. In the idealized model, Fig. 3.6a, it is assumed that the output, y(t), results from the input, x(t), that goes through the linear system. But in actuality, the input, x(t), is contaminated with background noise, shown as n(t), and the output after going through the system consists of a response due to x(t) and n(t) and also is distorted by additional background noise, named m(t), after going through the system.

The advantage of spectral analyses, other than identifying the amplitude and phase of each frequency component in the waveform, is that relationships between two signals can be easily identified. Ease of operation in the frequency do main is another advantage of spectral analyses. For example, an integration in the time domain is equivalent to a simple multiplication in the frequency domain. Also, in most measurements in the frequency domain, triggering does not have to be synchronized. Therefore, it is quite simple to average signals which results in enhancing the records being measured. If the background noise is random and the actual signals are repeatable, the averaging of several records will be (theoretically) free of undesirable noise. The average value of a random process tends toward zero, whereas the average of a repeatable signal is presumably representative of the "true" value of the actual signal. In other words by averaging signals one is able to get outcomes which are represented more closely by an idealized model as shown in Fig. 3.6a rather than the actual model.

In the remainder of this section, the functions used in frequency domain measurements in SASW testing are discussed. For each function, the outcomes for the two time records shown in Fig. 3.7 are presented for more clarity.

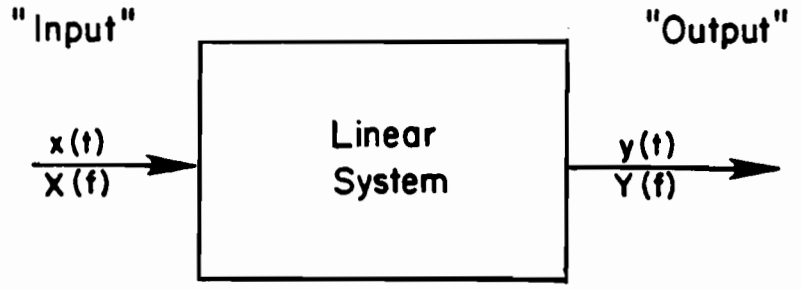

a. Idealized System

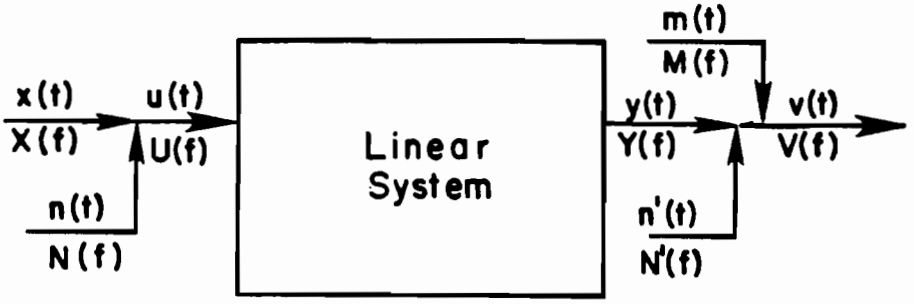

b. Actual System

Note:

x(t) = Input due to Experiment,
y(t) = Output due to Experiment,
n(t) = Noise Source at Input,
n'(t) = Output due to Noise at Input,
m (t) = Noise Source at Output,
u (t) = x(t) + n(t) = Actual Input,
v (t) = y(t) + n'(t) + m(t) = Actual Output.

Capital letters denote the Fourier Transform of the functions described.

Fig. 3.6. Illustration of Idealized and Actual Linear Systems.

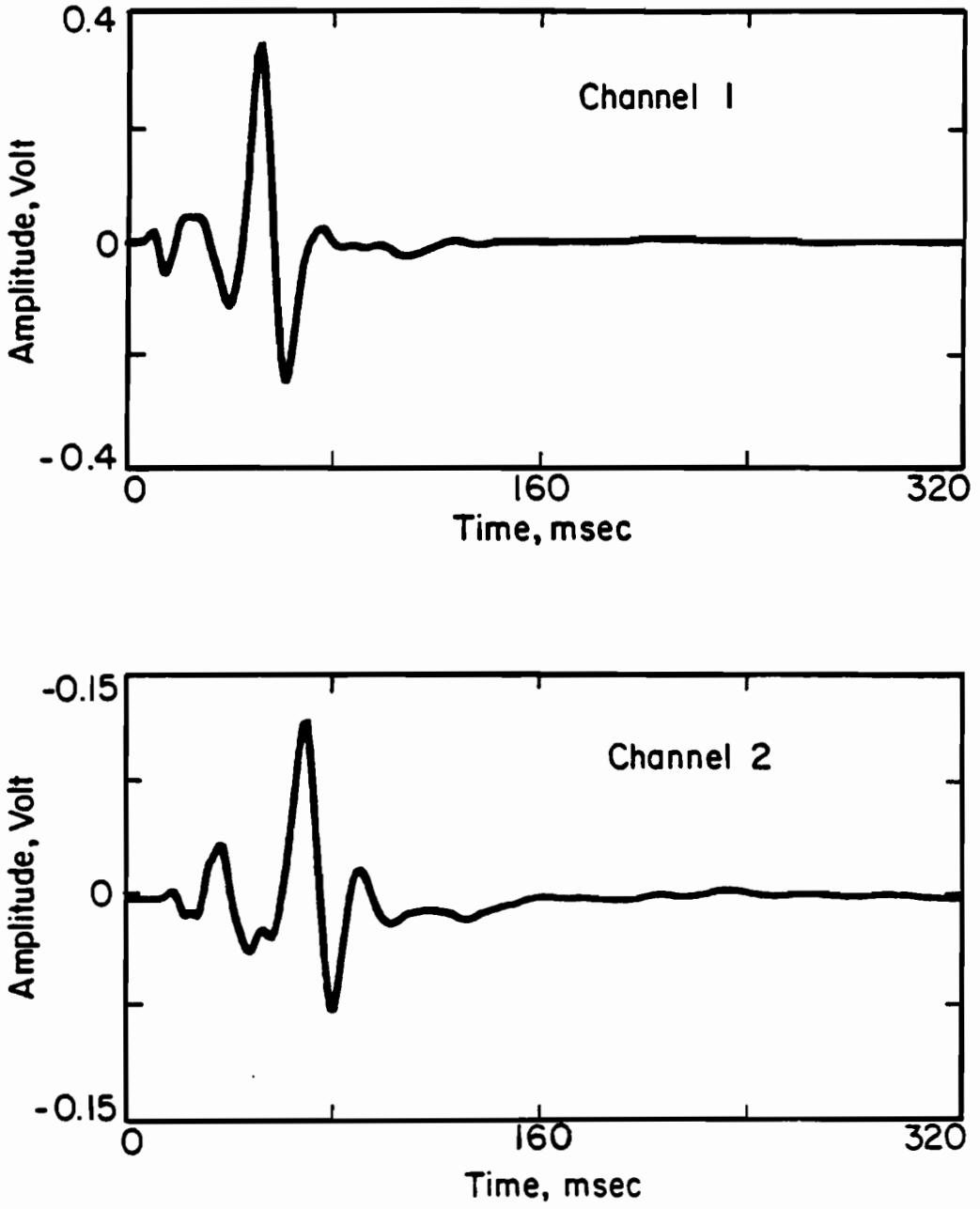

Fig. 3.7. Typical Set of Time Records from a Test on a Soil Site.

3.3.1 Linear Spectrum

The linear spectrum is simply the Fourier transform of a signal. Mathematically, it can be presented as:

$$S_x(f) = \int_{-\infty}^{+\infty} x(t)\ \exp(-j2\pi nt)dt \tag{3.17}$$

where $S_x(f)$ and $x(t)$ are the linear spectrum and actual time records, respectively. The linear spectrum consists of real and imaginary components (shown in Fig. 3.8) or interchangeably a magnitude and a phase (as shown in Fig. 3.9).

In SASW testing, the linear spectra are the initial functions evaluated in the field. These functions are then used to obtain the other spectral functions discussed next.

3.3.2 Auto Power Spectrum

The auto power spectrum is defined as:

$$G_{xx}(f) = S_x(f) \cdot S_x^*(f) \tag{3.18}$$

where $G_{xx}(f)$ is the auto power spectrum and $S_x^*(f)$ the complex conjugate of the linear spectrum, $S_x(f)$. The magnitude of the cross power spectrum is equal to the magnitude of linear spectrum squared. However, as the linear spectrum is multiplied by its complex conjugate, $G_{xx}(f)$ is a real valued function.

An excellent and rapid means of enhancing the quality of data collected in the field is the averaging of several records. (The writers have found that three to five averages typically gives a good representation of the frequency components.) In addition, the advantage of using $G_{xx}(f)$ over $S_x(f)$ in averaging is that no synchronized triggering is needed to evaluate $G_{xx}(f)$ when signaled averaged; whereas, a sophisticated triggering system is required for determining averaged values of $S_x(f)$. However, each function yields the same information.

The auto power spectrum is often used to identify the dominant frequencies (sometimes called natural frequencies) of a system.

Auto power spectra for the two channels of time domain data in Fig. 3.7 are presented in Fig. 3.10. One can see that the higher frequencies (600 to

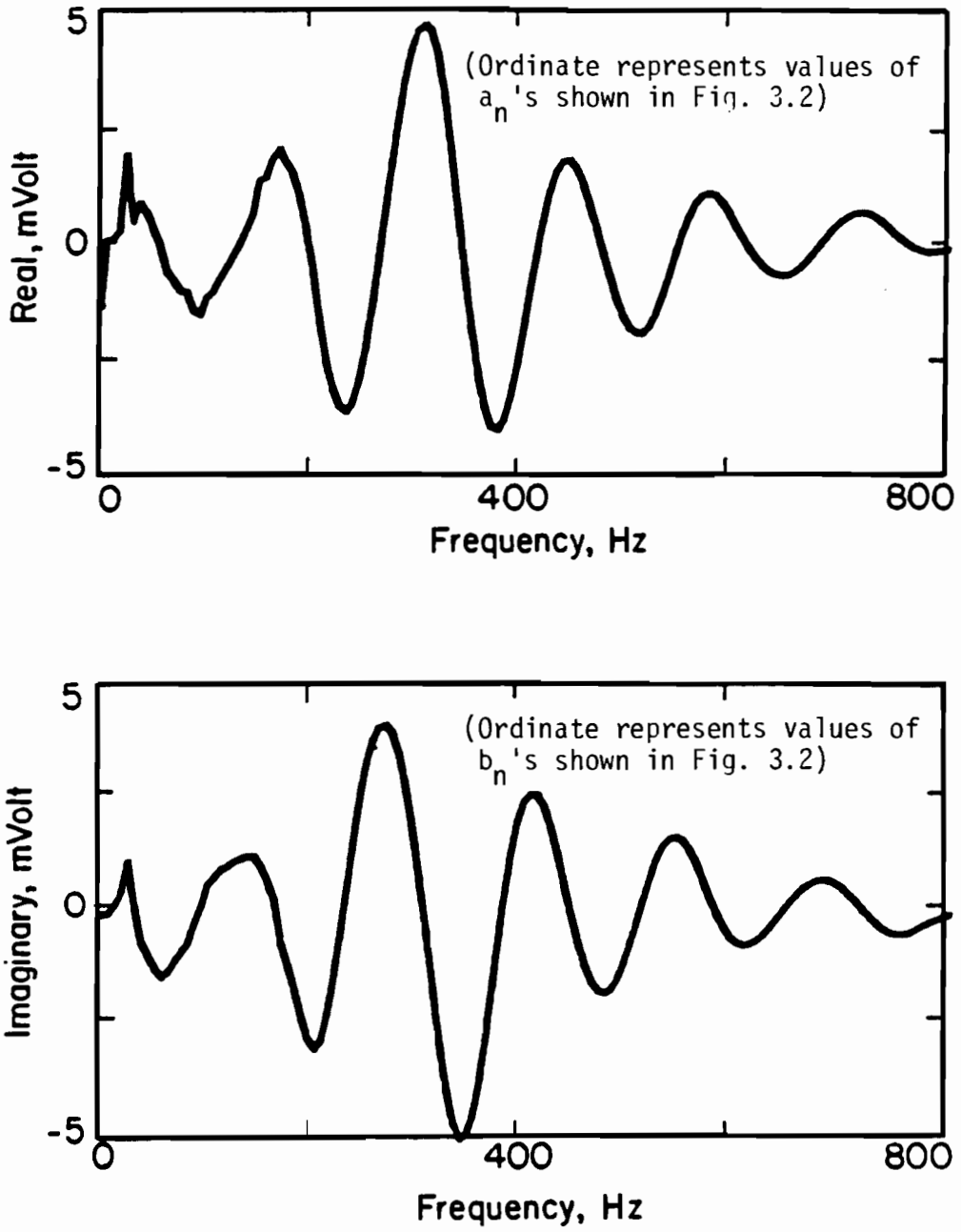

Fig. 3.8. Real and Imaginary Components of Linear Spectrum of Channel 1 Determined from Averaging Five Travel-Time Records Like the Ones Shown in Fig. 3.7.

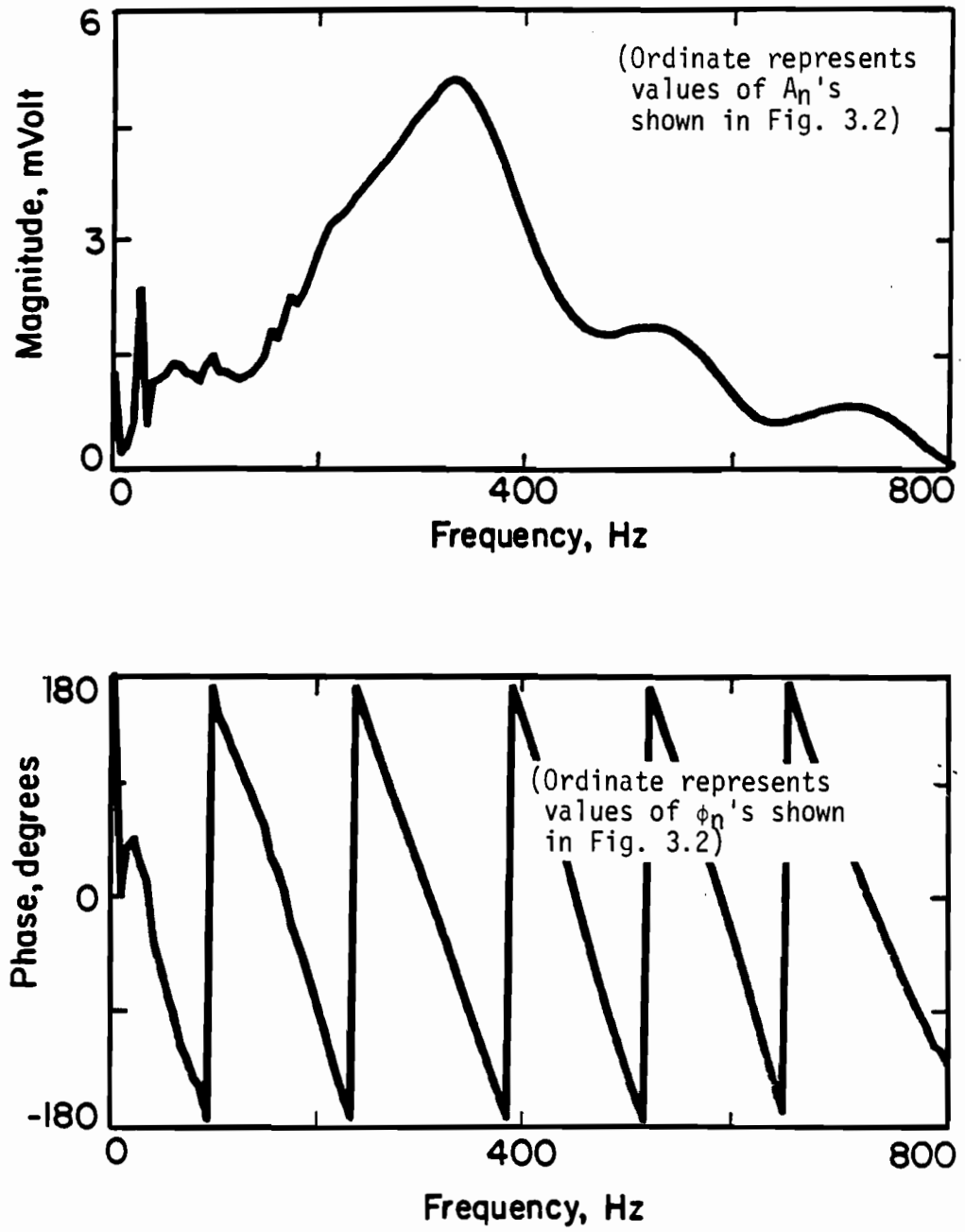

Fig. 3.9. Magnitude and Phase Components of Linear Spectrum of Channel 1 Determined from Averaging Five Travel-Time Records Like the Ones Shown in Fig. 3.7.

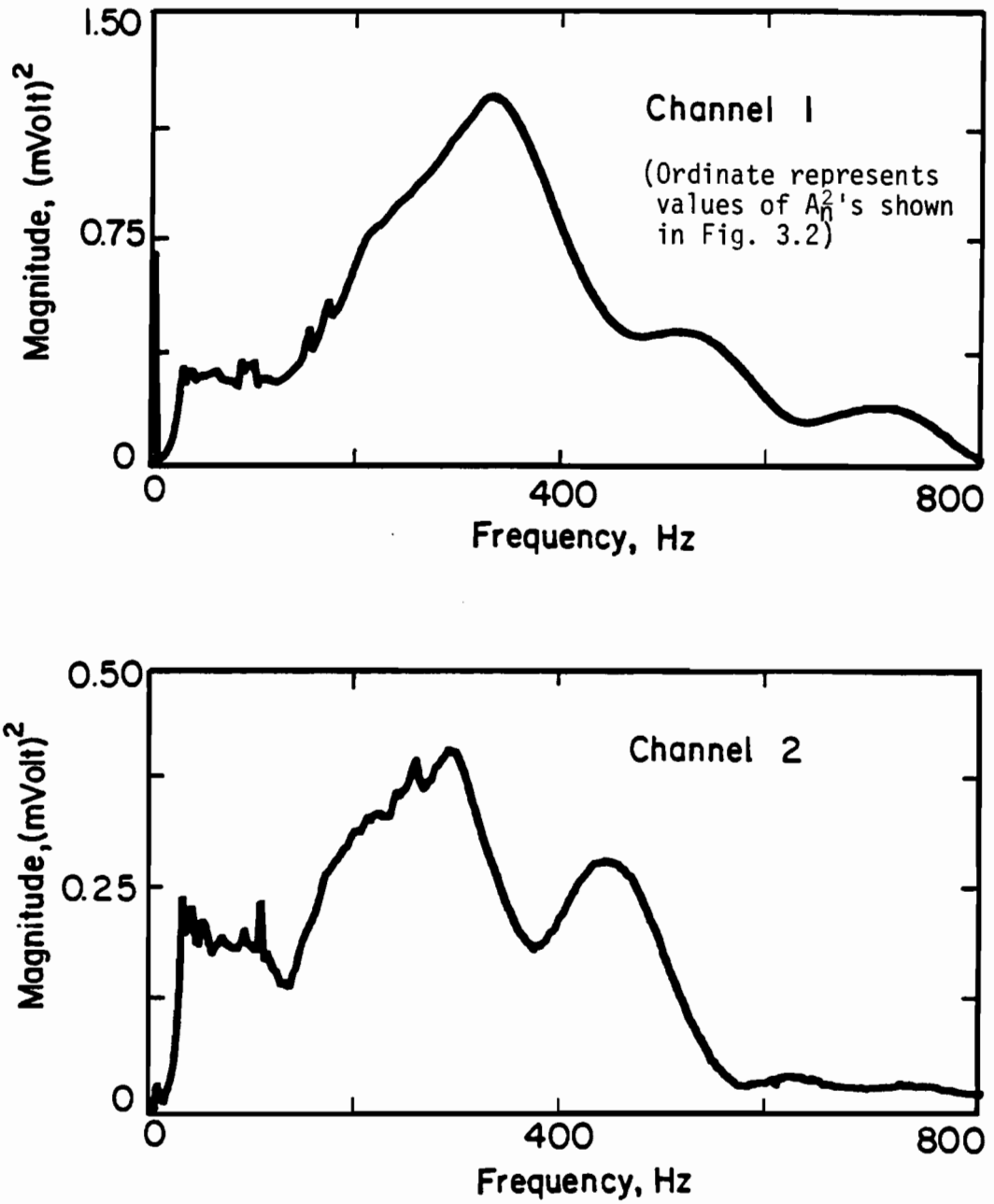

Fig. 3.10. Auto Power Spectra Determined from Averaging Five Time-Domain Records Like the Ones Shown in Fig. 3.7.

800 Hz) have attenuated faster than lower frequencies. This point just shows that the earth acts as a low-pass filter. In general, the waves have attenuated by a factor of about three at the lower frequencies.

3.3.3 Cross Power Spectrum

The cross power spectrum, $G_{yx}(f)$, is defined by:

$$G_{yx}(f) = S_y(f) \cdot S_x^*(f) \tag{3.19}$$

where, $S_y(f)$ is the linear spectrum of the output and $S_x^*(f)$ is the complex conjugate of the linear spectrum of the input. This function is a complex function and can be presented with real and imaginary components, or as shown in Fig. 3.11, with magnitude and phase. The magnitude corresponds to the mutual power between the input and output signals. The phase is indicative of the relative phase between the two signals due to any time delay or propagation delay. As the phase is a relative phase, synchronized triggering is not necessary.

Practically speaking, the phase of cross power spectrum is used to determine the travel times of surface waves at different frequencies. At each frequency, the associated phase is determined. A phase shift of 360 degrees corresponds to a travel time equal to one period. (The period, T, is the reciprocal of frequency, f.) Therefore, the ratio of phase shift over 360 degrees is equal to the ratio of travel time, t, over period, i.e.:

$$\frac{\phi}{360} = \frac{t}{T} \tag{3.20}$$

$$t = \frac{\phi}{360} \cdot T = \frac{\phi}{360} \cdot \frac{1}{f} \tag{3.21}$$

This process is described in detail in Nazarian and Stokoe, (1985).

3.3.4 Transfer Function

The ratio of the linear spectra of output over input is termed the transfer function, H(f), or frequency response function and is defined as:

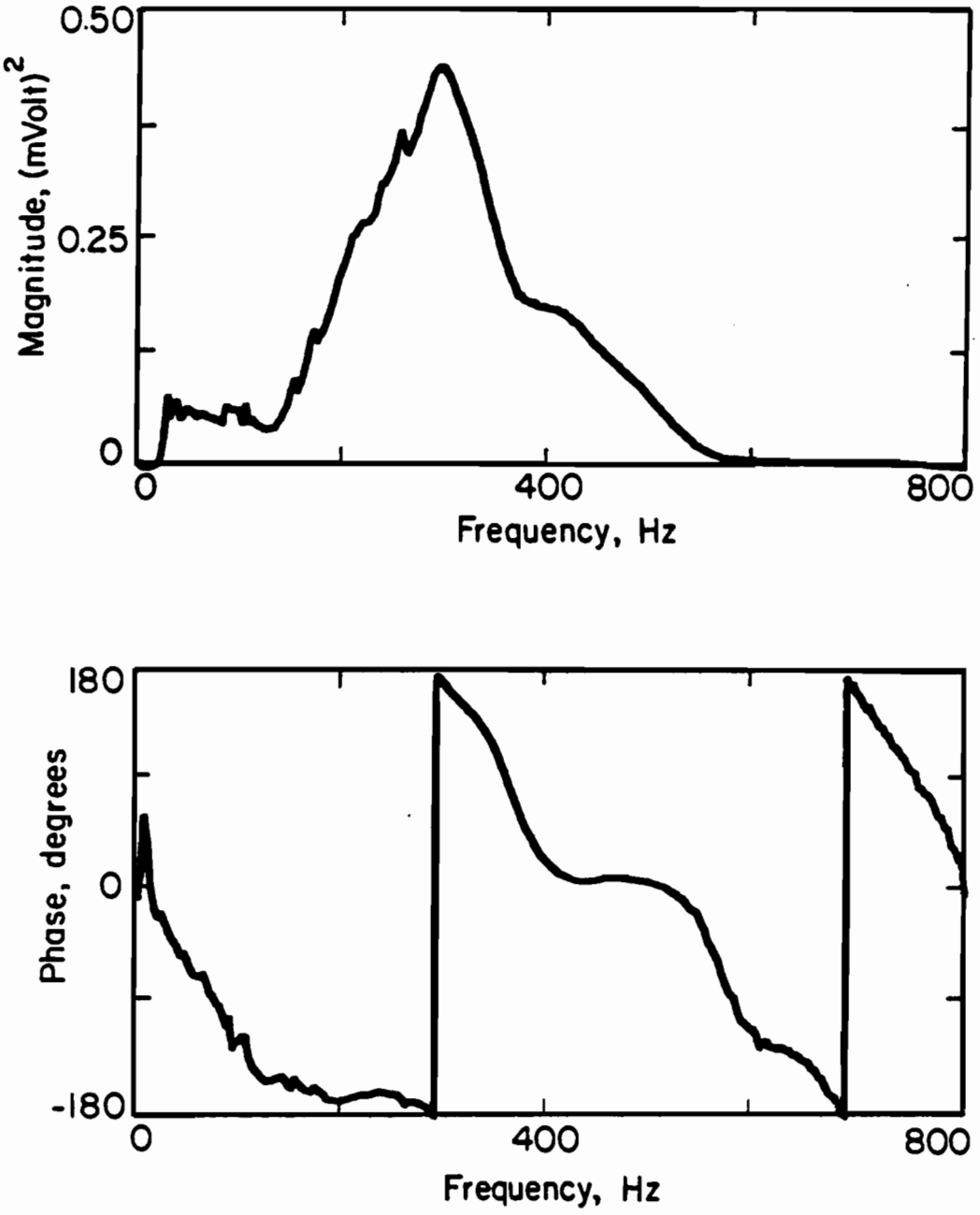

Fig. 3.11. Magnitude and Phase of Cross Power Spectrum Determined from Averaging Five Travel-Time Records Like the Ones Shown in Fig. 3.7.

$$H(f) = S_y(f)/S_x(f) \tag{3.22}$$

If the numerator and denominator are multiplied by the complex conjugate of the linear spectrum of the input signal so that:

$$H(f) = \frac{S_y(f) \cdot S_x^*(f)}{S_x(f) \cdot S_x^*(f)} \tag{3.23}$$

the numerator and denominator represent the cross power spectrum and auto power spectrum of the input, respectively, i.e.:

$$H(f) = \frac{G_{yx}(f)}{G_{xx}(f)} \tag{3.24}$$

These functions [$G_{yx}(f)$ and $G_{xx}(f)$]are usually determined before the transfer function is determined. As such, it is preferable to calculate H(f) from Eq. 3.24. The transfer function is a complex number at each frequency. The magnitude is equal to the magnitude of the cross power spectrum normalized by the magnitude of the auto power spectrum of the input. The phase is identical to that of the cross power spectrum as the auto power spectrum in the denominator is a real-valued function. Therefore, the phase information of the transfer function can be used (just as done with the cross power spectrum) to calculate the travel times of surface waves. The magnitude and phase information of the transfer function are illustrated in Fig. 3.12.

The transfer function is used to identify natural frequencies and damping properties of a linear system.

3.3.5 Coherence Function

The coherence function is the ratio of the output power caused by the measured input to the total measured output. Mathematically, the coherence function, $\gamma^2(f)$, is defined as:

$$\gamma^2(f) = \frac{G_{yx}(f) \cdot G_{yx}^*(f)}{G_{xx}(f) \cdot G_{yy}(f)} \tag{3.25}$$

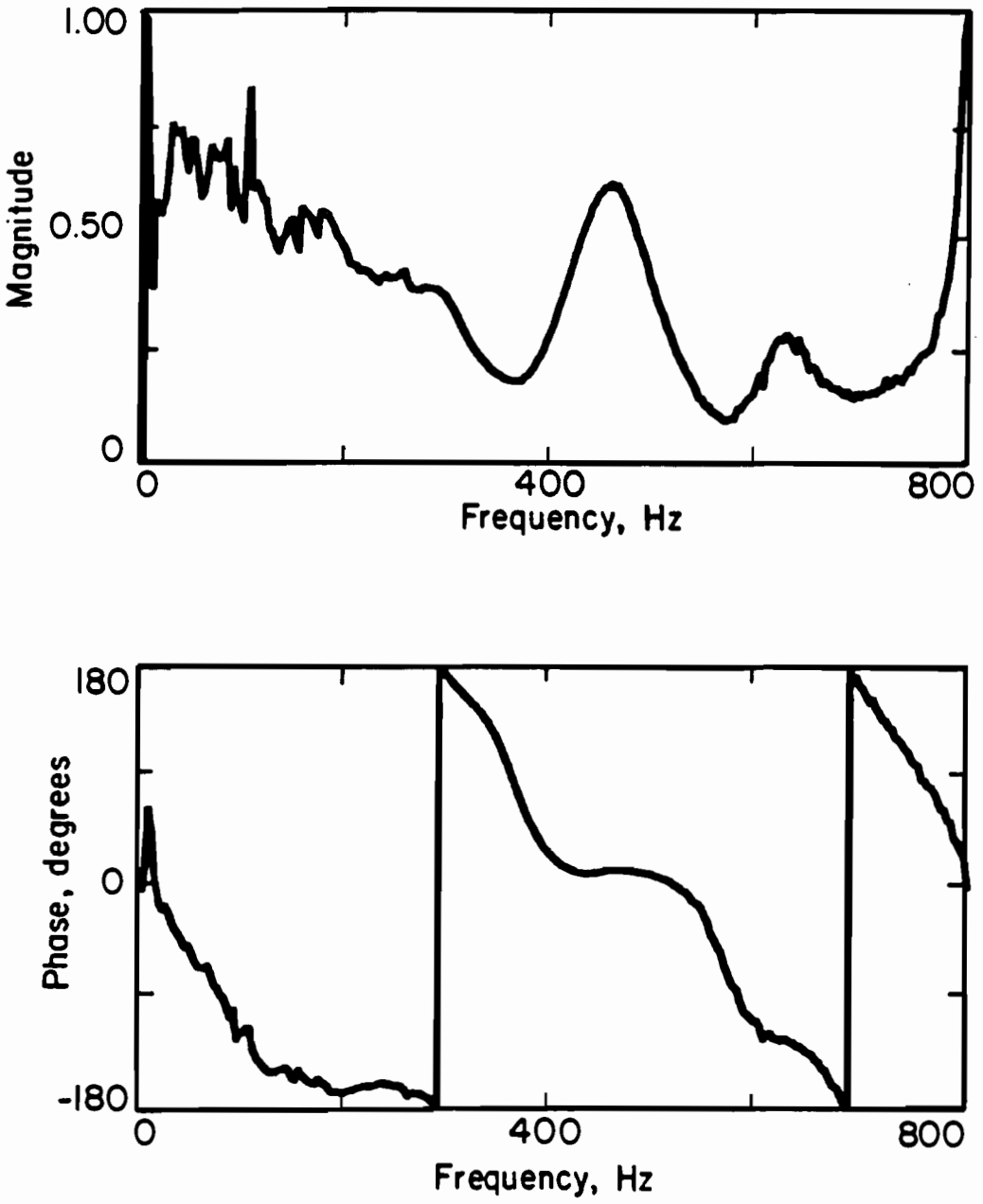

Fig. 3.12. Magnitude and Phase of Transfer Function Determined from Averaging Five Travel-Time Records Like the Ones Shown in Fig. 3.7.

If the system is ideal, as shown in Fig. 3.6a, the coherence will be equal to unity for all frequencies. But if some noise is present, the coherence may differ from unity. The coherence function is related to signal-to-noise ratio, (S/N), by:

$$(S/N) = \gamma^2(f)/[1 - \gamma^2(f)] \tag{3.26}$$

The coherence function is a good tool for assessing the quality of the observed signals. The coherence function should be used on averaged signals as for one set of input and output the coherence function is equal to one. The coherence function for five averages of the signals such as those shown in Fig. 3.7 is presented in Fig. 3.13. (All functions in Figs. 3.8 through 3.13 are from five averages.) A coherence value close to one indicates good correlation between the input and the output signals. However, a low coherence may not necessarily suggest bad correlation between the signals. Some reasons for low coherence besides the presence of noise are nonlinearity of the system, low resolution of the frequency bandwidth, and multiple input signals in the system.

3.4 SUMMARY

In this chapter, analyses in the frequency domain are presented as these analyses are instrumental in this study. The Fourier transform, discrete finite transform (DFT) and fast Fourier transform (FFT) are discussed. Spectral functions including linear spectrum, auto and cross power spectra, transfer function and coherence function are defined. An illustrative example is presented for each function determined from five averages of time-domain records like the one shown in Fig. 3.7.

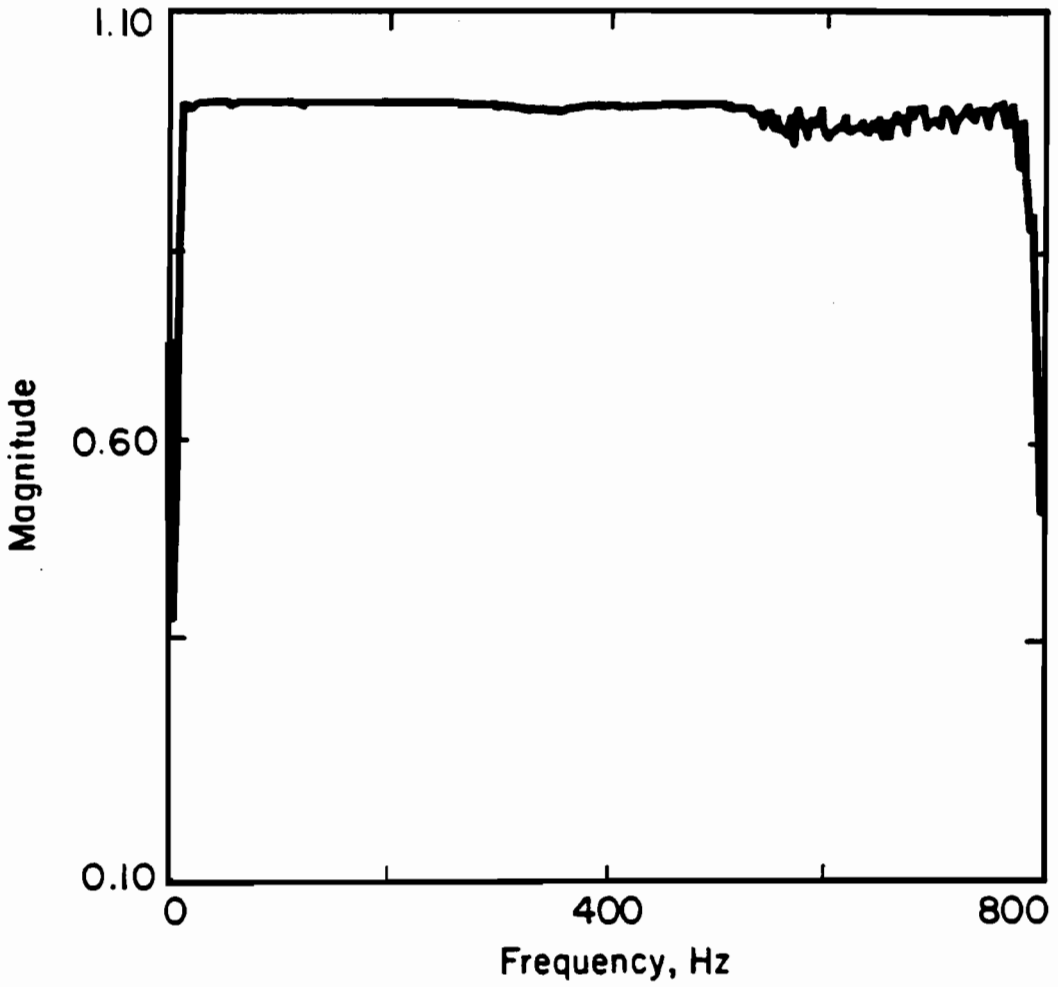

Fig. 3.13. Coherence Function Determined from Averaging the Spectral Functions from Five Travel-Time Records Like the Ones Shwon in Fig. 3.7.

CHAPTER FOUR. IN SITU EVALUATION OF PAVEMENTS

4.1 INTRODUCTION

It is a widely held belief that the most accurate means of determining in situ properties of different layers in a pavement system is by field testing. The general premise of this belief has certainly been proven true at geotechnical sites by numerous studies in earthquake engineering. On the other hand, laboratory testing is essential in understanding the influence of various parameters on the behavior of materials such as pavement materials. However, the exact numerical values of properties determined by laboratory tests must be carefully used and can be substantially in error due to problems such as non-representative samples, improper stress state during testing, and mechanical disturbance from sampling. As such, it is prudent to use field testing should be used to evaluate material properties whenever possible.

There are two basic approaches used today to evaluate the properties of pavement systems in the field. The first approach is to employ high intensity loads in an attempt to evaluate the nonlinear behavior of pavements. Elastic theory is then used to backcalculate the modulus profiles of the pavement system. The advantage of this approach is that an equivalent nonlinear modulus of the pavement may be determined. However, if these moduli are used to determine the stresses and strains in the pavement system, substantial errors may occur because the modulus profile is approximated with only three or four equivalent moduli and, hence, may only be appropriate for calculating surface displacements under loads similar to those used to evaluate the equivalent moduli.

The second approach is to determine elastic moduli in situ and to perform laboratory tests on representative samples to define the decrease of modulus with strain (and to some extent with stress). Then, by incorporating these two (laboratory and field) results, the actual nonlinear bheavior of the pavement system is determined. Over thirty years of research in earthquake engineering have shown that the second approach is very realistic; especially if one uses normalized moduli as shown in Figs. 2.6 and 2.7.

The Falling Weight Deflectometer device is a good example of the first testing approach, and the SASW testing method falls in the second category.

In this chapter, the most common nondestructive testing techniques used to evaluate the in situ properties of pavements are reviewed. In addition, several in situ seismic tests, which have been used mainly in geotechnical engineering but which have application to pavements, are included. A historical review of the use of surface waves (Rayleigh waves) in pavement evaluation then concludes the chapter.

4.2 TYPICAL NONDESTRUCTIVE TESTING OF PAVEMENTS

Nondestructive testing of pavements is normally done by making surface measurements of the response of a pavement structure to an external force. The response is generally in terms of measurement of surface deflections at several points. Elastic theory coupled with a layered medium is then employed to back-calculate the elastic properties of different layers by matching measured deflections with those calculated from a static load on the layered system.

Lytton et al (1975) studied different nondestructive methods in some detail. The major differences between different methods is the way the load is imparted to the pavement and the number and position of points at which deflections are measured. The characteristics of some deflection measuring devices are presented in Table 4.1. The methods that are based upon application of static loads consist of the Plate loading test, Benkelman beam, traveling deflectometer, Lacroix deflectograph, and curvature meter (Haas and Hudson, 1978). Vibratory nondestructive methods apply a steady state load to the pavement surface after applying some static seating load. The main devices in this category are the dynaflect, road rator, Waterways Experiment Station (WES) vibrator, and Federal Highway Administration (FHWA) thumper. Devices that use an impact as the source are the falling weight deflectometer, California (CAL) impulse testing, and Washington State University impulse testing.

The most dominant devices in nondestructive testing of pavements are the Dynaflect and falling weight deflectometer (FWD). A schematic of a dynaflect device is shown in Fig. 4.1. A peak-to-peak dynamic force of 1000 lb (4500 N)

TABLE 4.1. CHARACTERISTICS OF COMMON NONDESTRUCTIVE TESTING DEVICES USED ON PAVEMENT (FROM EAGLESON ET AL, 1981).

Device	Static Load 16f	Dynamic Load 16f	Loading Concept	Load Frequency, Hz	Number of Deflection Sensors*	Spacing,+ in.
(1)	(2)	(3)	(4)	(5)	(6)	(7)
Benkelman Beam	Variable Single Axle Load	—	Static	—	1	—
Dynaflect	1000	1000	Counter-rotating Weights	8	5	12
Road Rator	1500-7000	1000-8000	Electro-hydraulic Vibrator	10-80	4	12
Falling Weight Deflectometer	Variable	1500 to 24000	Drop Weight	Wide Range**	5 to 7	12

* Sensors are velocity transducers except for Benkelman Beam which a dial gauge is used.
** Duration of about 25 msec.
\+ Between adjacent receivers.

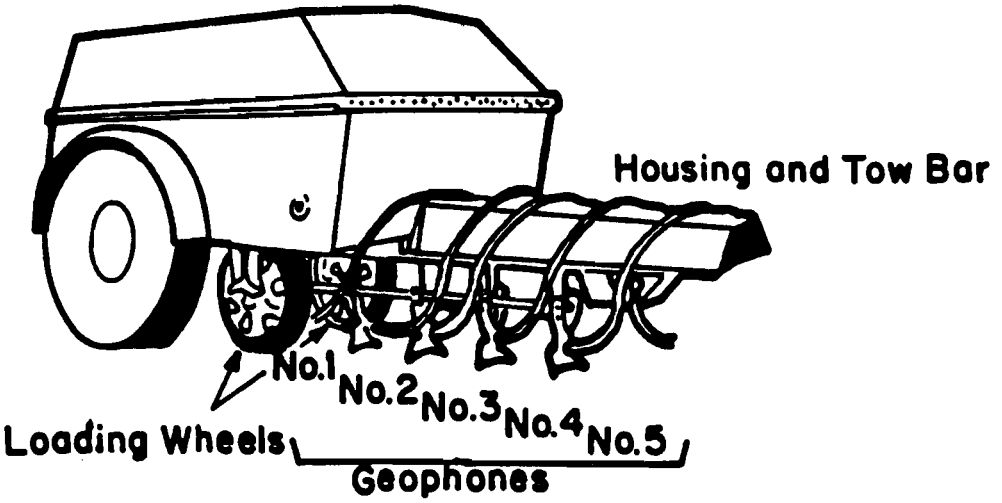

a. The Dynaflect System in Operating Position.

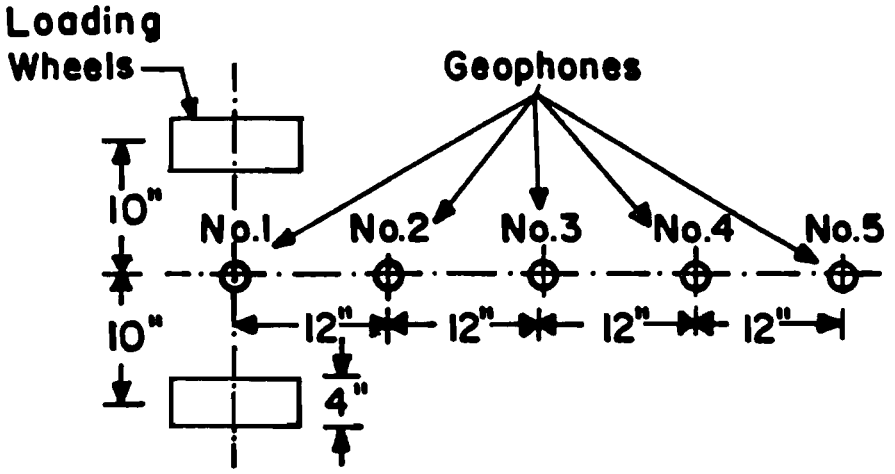

b. Configuration of Load Wheels and Geophones.

Fig. 4.1. Configuration of Dynaflect Load Wheels and Geophones in Operating Position (from Uddin, et al, 1983).

is generated by two counter-rotating eccentric masses at a frequency of 8 Hz. This force is transmitted to the pavement by two, 4-in. (10-cm) wide wheels. Five equally spaced geophones are used to measure deflections of the pavement system due to the load as shown in Fig. 4.1.

The falling weight deflectometer (FWD) is quite similar to the dynaflect device. The main differences are basically in the number of receivers, as seven geophones are used, and the load. A schematic of FWD is shown in Fig. 4.2. The load is developed by dropping a weight on a plate set on the pavement surface. The energy of the impact can be varied by changing the drop height or drop weight. The peak loading force varies from 1.5 to 24 kips (6.6 to 106 kN). The duration of impulse is around 25 to 30 msec, which simulates the duration of a load imposed by a moving wheel at 40 mph (64 km/h).

In both the Dynaflect and FWD, placement of the receivers and deployment of the loads can be done from a towing vehicle. However, the testing process for the FWD is more sophisticated and is controlled by a desk-top computer.

In the analysis of the load-deflection measurements, the pavement is modelled as a multilayered linear elastic system, and each layer is characterized by Young's modulus and Poisson's ratio. A computer program based upon linear elastic theory with static loading is then used to predict the deflections at the measurement points. Computed and measured deflections are compared and necessary adjustments in the value of the elastic modulus of each layer are made until measured and computed deflections compare well. This process is called "deflection-basin fitting".

The major assumptions in the deflection-basin fitting approach are:

1. the dynamic load can be replaced by an equal static load,
2. measured dynamic deflections are assumed equal to theoretical static deflections, and
3. the subgrade has constant stiffness and is extended to infinity or to a rigid layer underlying the subgrade at some depth.

The main advantages of these two methods are mobility and rapid testing in the field. However, these methods do not yield a unique solution as several combinations of moduli can be determined to produce a theoretical basin which matches the experimental deflection basin. This nonuniqueness becomes more pronounced as the number of layers assumed in the theoretical

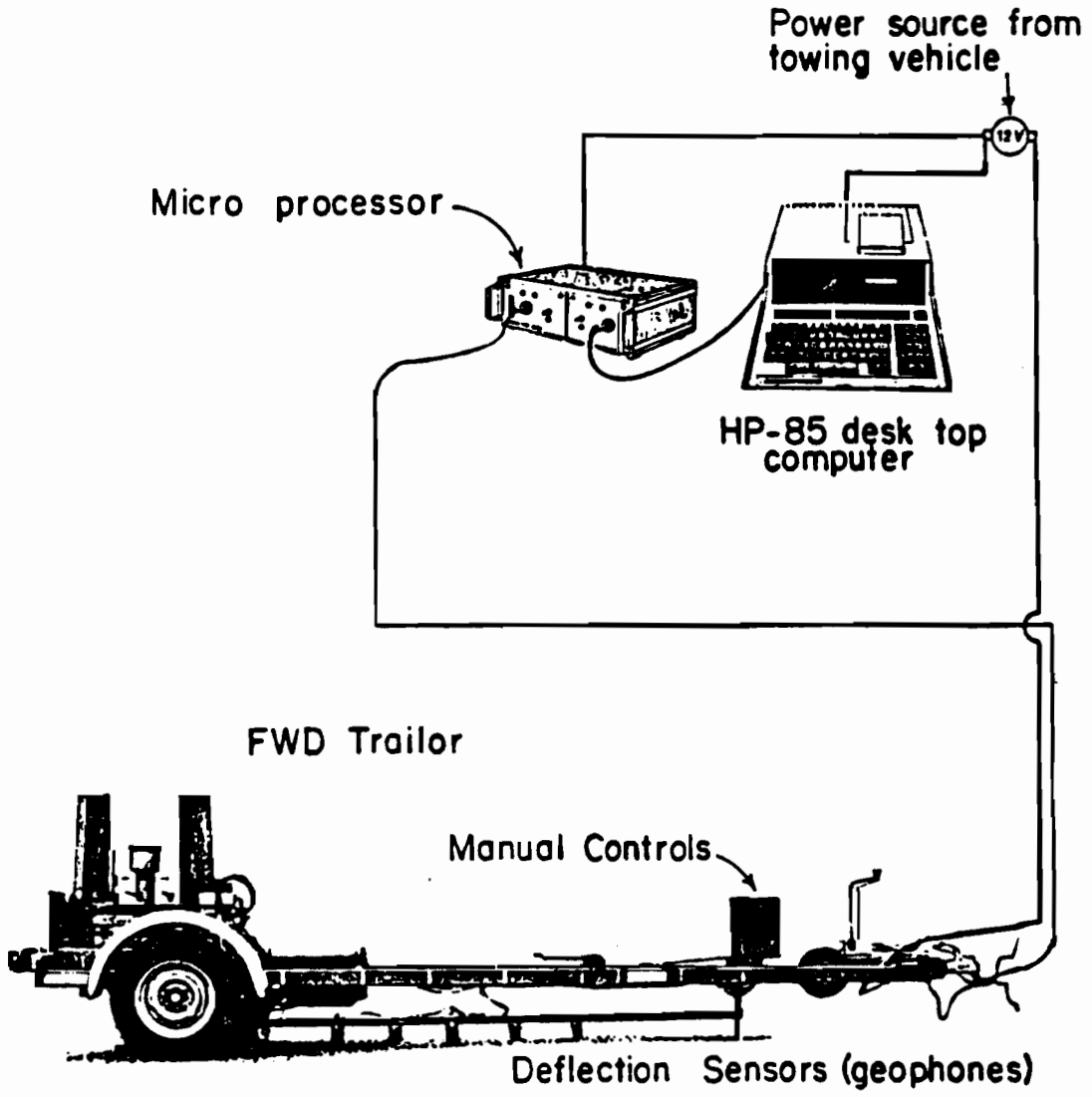

a. FWD in Operating Position

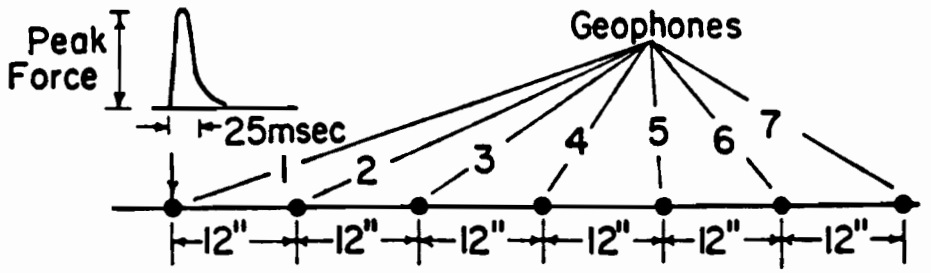

b. Geophones Configuration

Fig. 4.2. Schematic of Falling Deflectometer Device (from Uddin, 1984).

profiles is increased. As such, the number of layers are normally limited to three or four and the thickness of each layer must be assumed.

A recent study on the effects of different parameters involved in basin-fitting by Shao et al (1986) has shown that the dynamic nature of the load and the presence of bedrock at shallow depths may cause significant errors in basin-fitting. A second study by Nazarian and Stokoe (1986b) has shown that, with the receiver set-up used in both the Dynaflect and FWD, the algorithms used in basin-fitting is not sensitive to the properties of top thin layers in the pavement. As a result, continued work on the data analysis algorithms used by the FWD and dynaflect are underway on Project 1123.

4.3 SEISMIC FIELD METHODS

Seismic field methods have become a standard means of in situ evaluation of low-strain moduli of soils in geotechnical engineering. These methods are based on wave propagation in elastic media as discussed in Chapter Two. The methods normally involve applying a transient or steady-state excitation at one point in the medium and detecting the response at two or more locations. Wave velocities are determined from the recorded responses, and moduli are calculated using Eqs. 2.5 through 2.10.

In situ measurement of soil properties by wave propagation techniques can be summarized in the following six steps:

1. set up receivers at known distances from the source,
2. generate an impulse with the source,
3. measure travel time of wavefront from source to receivers,
4. calculate wave velocity (distance divided by time),
5. calculate elastic soil properties, and then
6. repeat steps 1 to 5 for different source/receiver locations.

In situ seismic methods can be categorized into two main groups; borehole methods and surface methods. Each group is discussed in the following sections.

4.3.1 Borehole Methods

In these methods, one or more boreholes are utilized as illustrated in Fig. 4.3, and compression (P) and shear (S) wave velocities are measured at

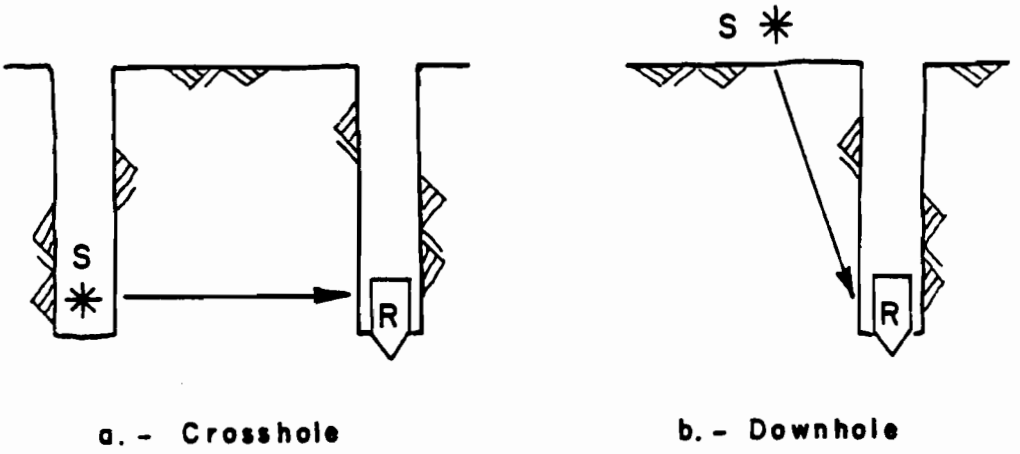

Fig. 4.3. Schematic Representation of Borehole Seismic Methods (from Hoar, 1982).

different depths in the soil deposit. The most common borehole methods are the crosshole and downhole. In the crosshole method, at least two boreholes are required. On the other hand, the downhole method can be performed with a single borehole. As a result, the cost efficiency offered by the downhole method often results in its selection at geotechnical sites when the choice is between these two borehole methods.

The ray paths of the seismic waves in boreholes tests are generally assumed to be directly between the source and receiver as illustrated in Fig. 4.3. The variation in soil properties with depth is then determined by changing the location of the source and/or receivers and repeating the test.

In pavement studies, borehole methods are infrequently used due to the fact that these techniques are time consuming and specialized personnel are required. However, to verify independently the results of SASW tests, crosshole tests have been used in studies performed by the writers. Therefore, a detailed description of the crosshole test as applied to pavements is presented in Section 4.4.

The downhole test can be briefly described as follows. Generally, a wooden plank source is placed on the ground surface and receivers are placed in the borehole (Patel, 1981). Usually only S-waves are measured because the casing typically adversely affects the P-wave results (at soil sites). Properties of materials in the near-vertical direction are predominantly measured. Advantages of the downhole test are placement of the source on the surface, minimum refraction problems and the need for only one borehole. However, as the depth increases, the path length of the wave increases, and the quality of the signals decreases. Downhole tests have not been used in pavement evaluation to the writers' knowledge but are widely used in geotechnical engineering. Downhole testing could, however, be applied to pavement sites.

4.3.2 Surface Methods

In these methods both the source and receivers are located on the surface. Thus, there is an economical advantage in these methods relative to borehole seismic methods in that no boreholes are required. Common surface methods are:

1. refraction,
2. reflection,
3. steady-state surface waves, and
4. spectral analysis of surface waves.

The simplified schemes of each of these tests are shown in Fig. 4.4.

The surface refraction method (Redpath, 1973) consists of measuring the travel times of body waves from a surface source to a linear array of receivers on the surface. The fastest path of the seismic waves depends upon the velocity distribution in the substructure, which is inferred from the time of first arrivals at each receiver. The main disadvantage of this method (which is a critical limitation in pavement evaluation) is that low-velocity layers beneath a high-velocity layer are not detected.

The surface reflection method (Borm, 1978) is very similar to the surface refraction method. The only difference is that measurement of waves reflected from different strata, rather than waves refracted along the interfaces of the layers, is the main objective. An important point in the test method is that the reflected ray is never the first arrival in the records monitored by the receivers. This point is the main drawback of the surface reflection method in engineering applications as interpretation of the time records becomes rather complicated. The other disadvantage of this method is that multiple reflections from one layer may obscure detection of the primary reflected waves from other layers. As a result, this method is mainly used in prospecting for oil at significant depths.

A sinusoidal wave generator is used as the source in the steady-state surface wave method, and the wavelengths of waves with different frequencies are evaluated by means of moving one receiver relative to another so that identical points on the wave form can be detected on the recording device. To obtain a better estimate of the wavelength associated with a given frequency, the receiver is located at several points, and the number of cycles (wavelengths) for each receiver spacing is determined and plotted against the distance from the source (Richart et al, 1970). An example of this process is shown in Fig. 4.5. A straight line is then fit through the data points at each frequency. The slope of each line is the reciprocal of the wavelength associated with each frequency. Knowing the frequency of excitation, f, and the wavelength, L_{ph}, the phase velocity, V_{ph}, can be determined by:

$$V_{ph} = f \cdot L_{ph} \tag{4.1}$$

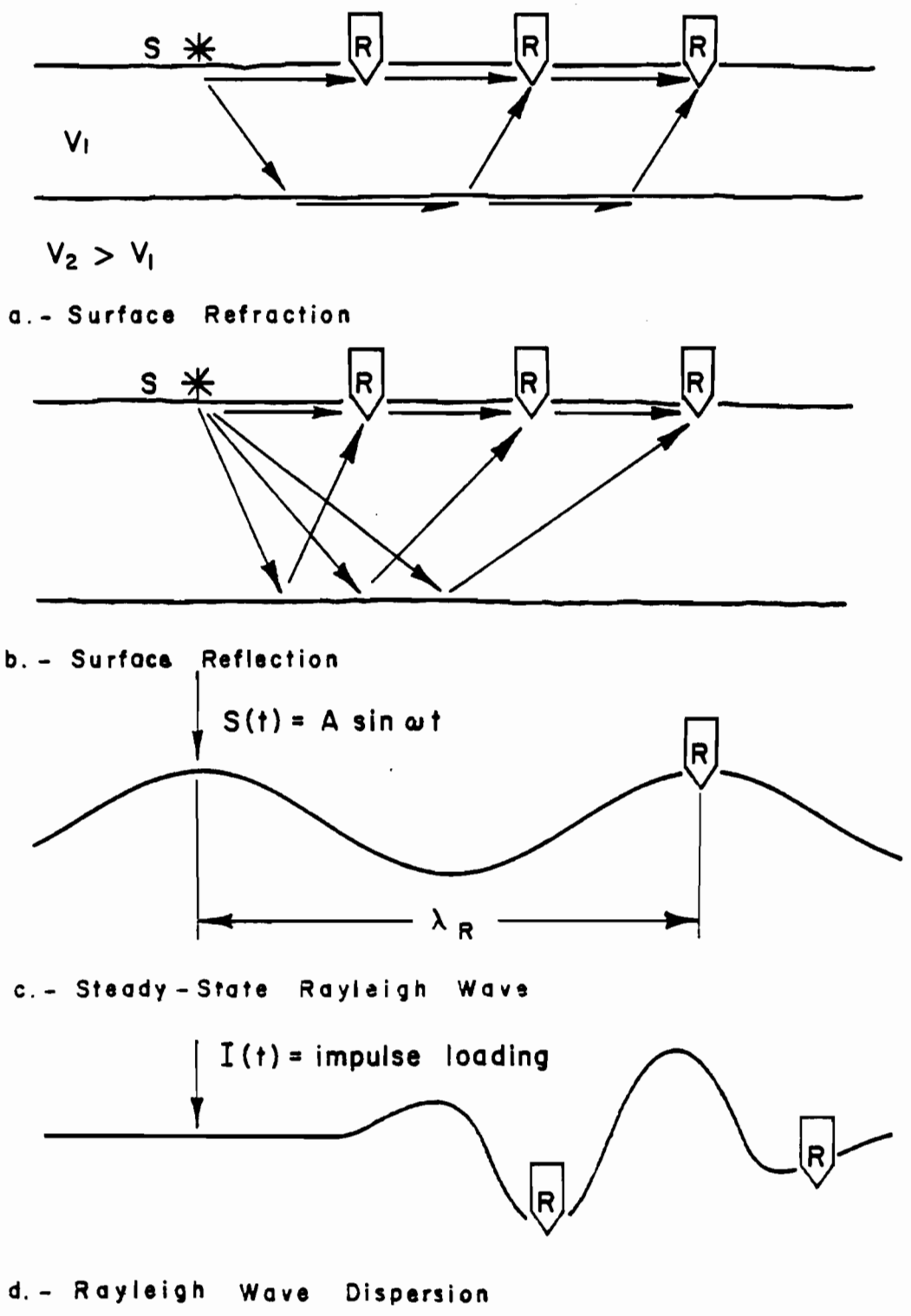

Fig. 4.4. Schematic Representation of Surface Seismic Methods (from Hoar, 1982).

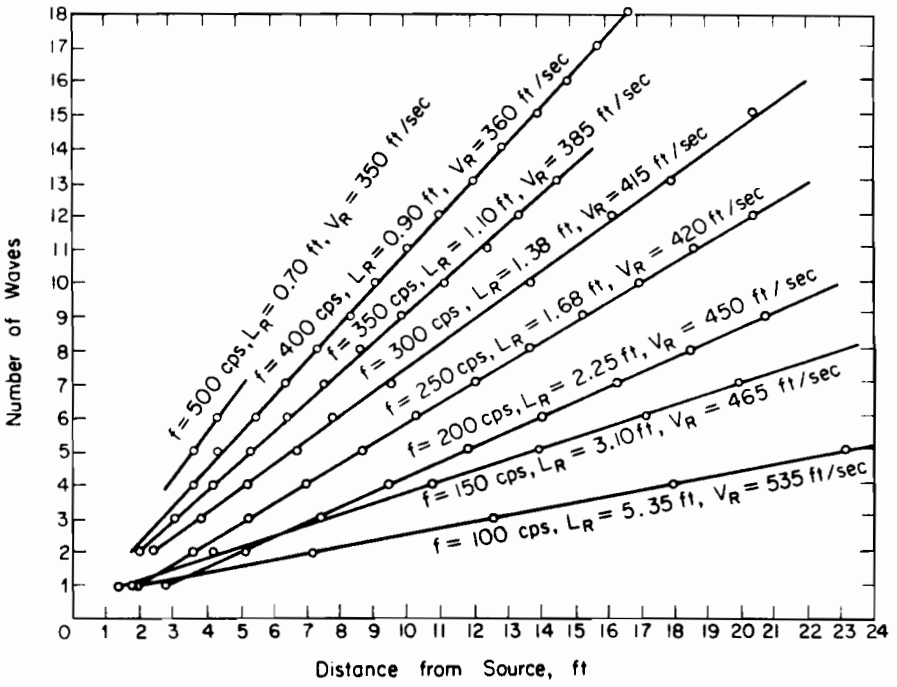

Fig. 4.5. Determination of Average Wavelength of Surface Waves from Steady-State Test (from Richart, et al, 1970).

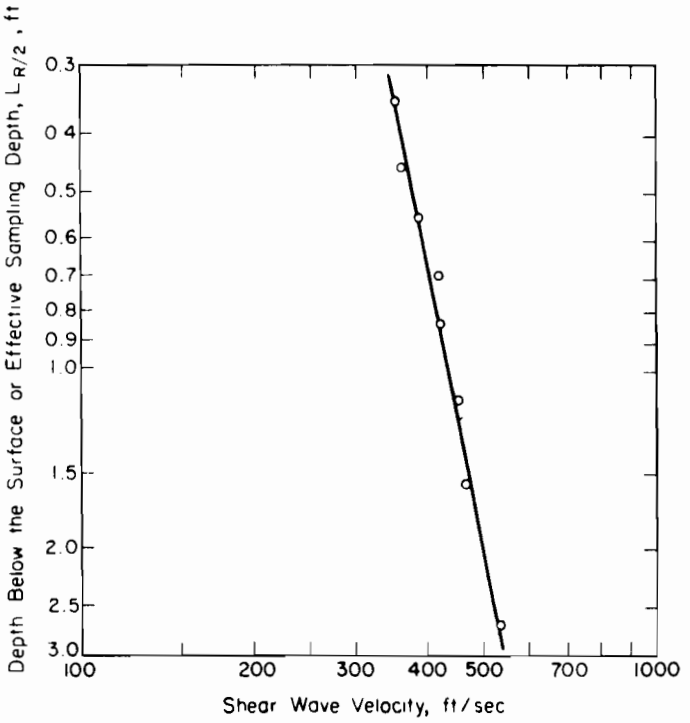

Fig. 4.6. Shear Wave Velocity Profile from Measurements Presented in Fig. 4.5.

The effective depth of sampling is assumed to be 1/2 to 1/3 of the wavelength, and the shear wave velocity is assumed to be in the range of one to 1.1 times the phase velocity.

As an example, the shear wave velocity profile obtained from the steady-state test shown in Fig. 4.5 is included in Fig. 4.6. Richart, et al (1970) assumed that the effective depth of sampling is equal to 1/3 of the wavelength and that the shear and phase velocities are equal.

Conceptually, the method involving spectral analysis of surface waves (SASW) is identical to the steady-state method. One of the main differences is the excitation source, which is transient in the SASW method. One benefit of a transient impact is that it can excite a wide range of frequencies with each impact. Thus, it is possible to record many different frequencies with one impact. A detailed discussion of the practical aspects of this method is presented in Nazarian and Stokoe (1985) while the historical development is presented in Section 4.5.

The other major difference between the SASW test and the original surface wave test is development of the inversion process. The inversion process is a rigorous means of determining the modulus and thickness of each layer from the dispersion curve as opposed to the approximate method used by Richart et al (1970). Theoretical aspects of the inversion process are discussed in Chapter Five.

4.4 CROSSHOLE SEISMIC TESTING OF PAVEMENTS

4.4.1 Testing Procedure

A schematic of the testing procedure on pavement sites is shown in Fig. 4.7. In this procedure, each borehole is advanced to the appropriate depth using solid-stem augers. At each testing depth, the drilling operation is stopped, the source is firmly placed at the borehole bottom, and then it is pushed approximately 6 in. (15 cm) into the material if possible. The receivers are placed at the same depth in the receiver boreholes and are firmly pushed into the material to ensure good coupling between the receivers and surrounding material. A vertical transient impulse is then applied to the source. This impulse generates P- and S-waves which are detected by receivers in the other holes as they pass by.

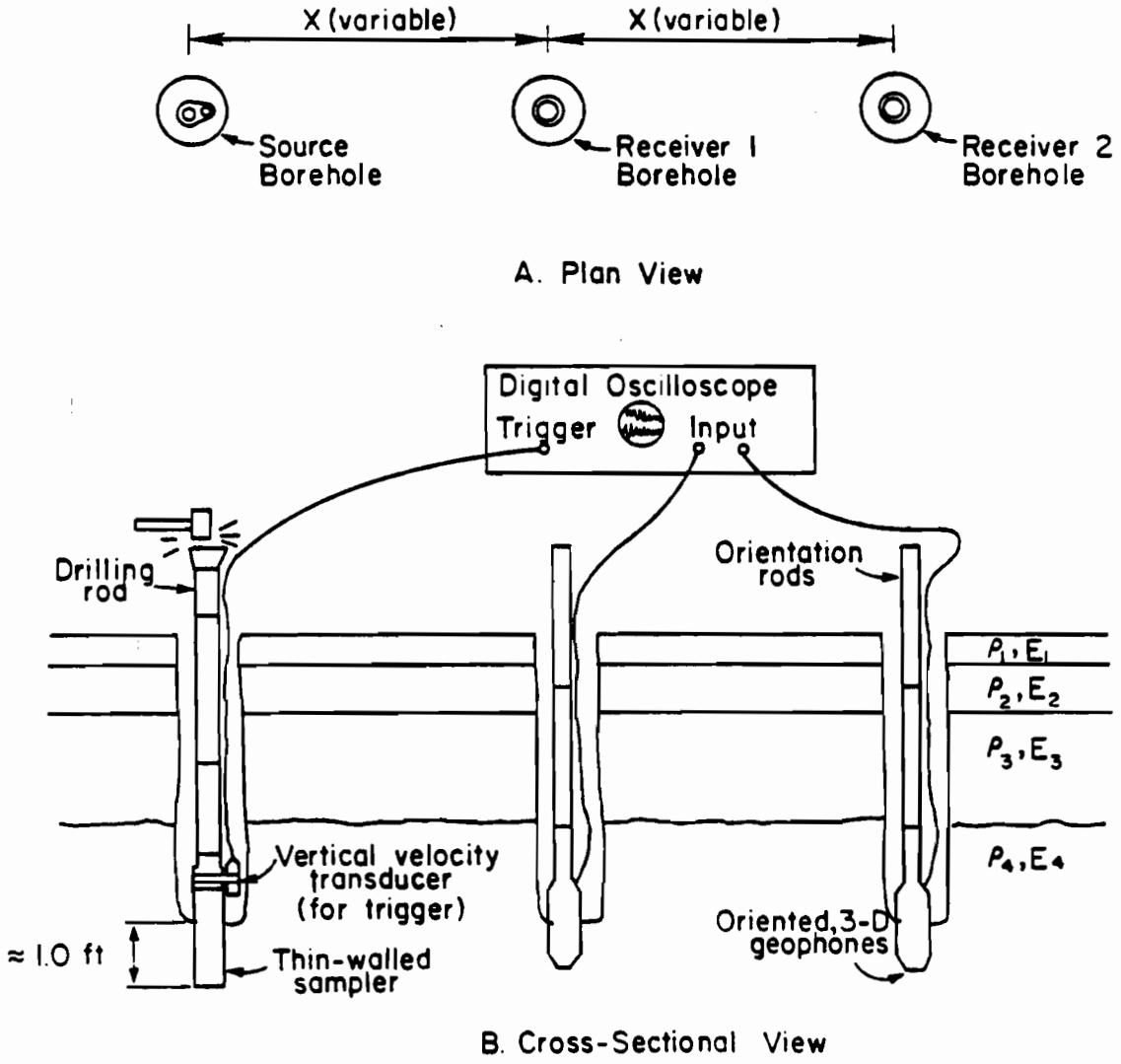

Fig. 4.7. Schematic of Crosshole Testing Technique at Pavement Sites.

The source consists of a sampling tube attached to a rod. A vertical velocity transducer secured to the rod just above the sampling tube serves as the trigger for the recording device. This trigger activates the recording device at essentially the instant body waves are created in the material at the bottom of the source.

The receivers consist of three-dimensional velocity transducers in which three receivers are oriented in three perpendicular directions (i.e., vertical and two perpendicular horizontal directions). The receivers are placed on the borehole bottom and then properly oriented with orientation rods which extend from the receivers to the surface. The receivers and transducer located on the source are connected to the recording device (a digital oscilloscope) through a switching box. By means of the switching box, the geophones with proper orientation for the wave motion to be measured are easily selected.

The vertical impulse to the rod is applied by an ordinary hammer. A vertical impulse transmitted through a medium generates P- and SV-waves which can be detected by radial horizontal and vertical geophones, respectively. Records of receiver outputs are saved on magnetic diskettes for future reference and in-house data reduction.

4.4.2 Data Reduction

Typical travel time records from the crosshole tests are shown in Fig. 4.8. The record in Fig. 4.8a consists of the output from the source receiver (upper trace) and the output from the vertical receiver in the first receiver borehole (lower trace). The record in Fig. 4.8b consists of the outputs from vertical receivers in the first and second receiver boreholes (upper and lower traces, respectively).

The upper trace in Fig. 4.8b is composed of three basic parts. The first part, the left side, is the initial smooth portion of the trace. This results from the fact that the impulse has started the trace moving across the oscilloscope screen, but no energy has yet arrived at the transducer in the first receiver borehole. The second part consists of the time between the first arrival, denoted by P, and the second arrival, denoted by S, which consists of waves of lower amplitude and higher frequency relative to the remainder of the trace. This portion of the trace is considered to represent energy transmitted by the P-wave. The third part of the trace consists of

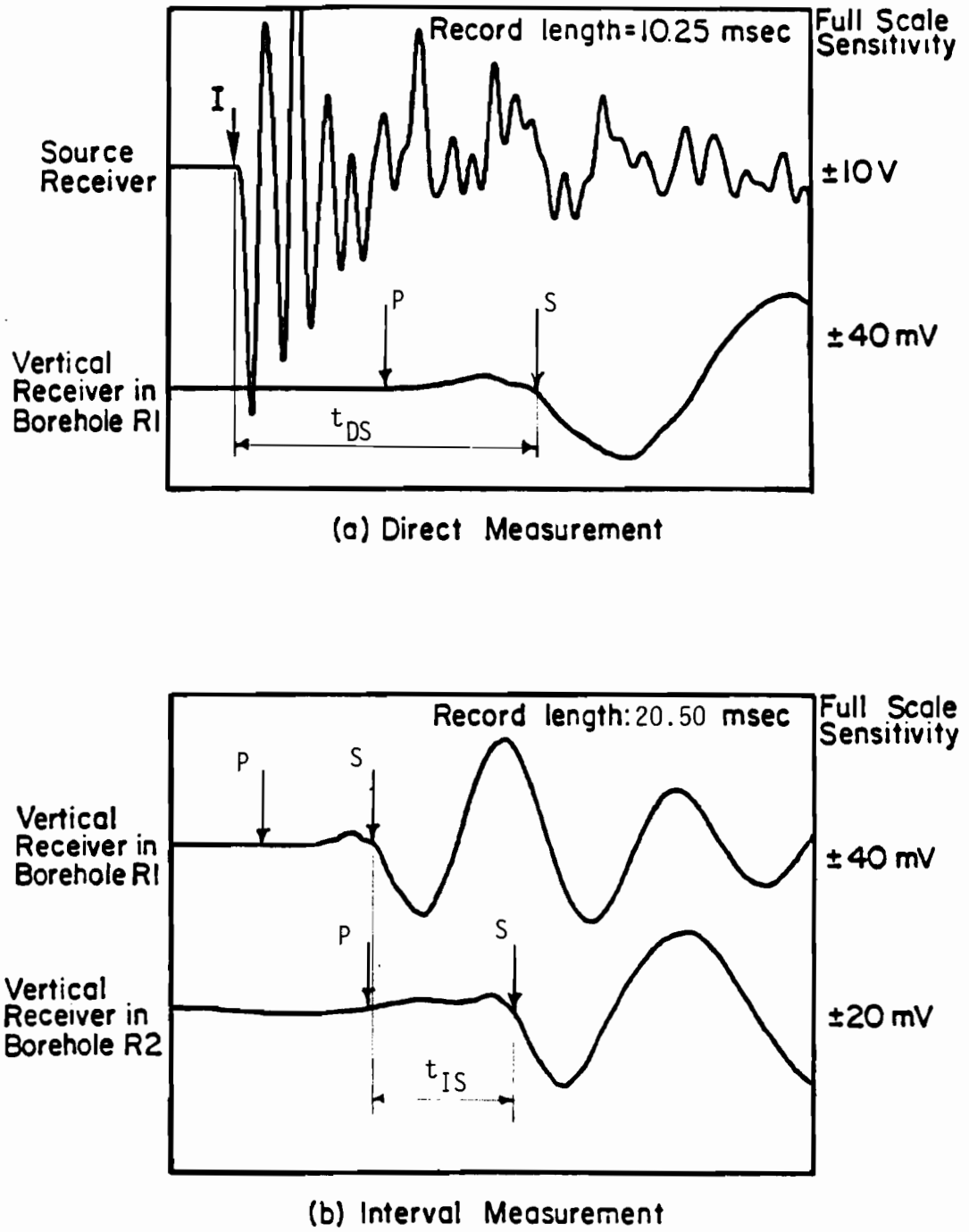

Fig. 4.8. Typical Crosshole Records for Determination of Shear Wave Travel Times.

waves of higher amplitude and lower frequency due, at least initially, to the arrival of the shear wave. The shear wave arrivals are identified as the beginning of the first large-amplitude energy excursion (Stokoe and Woods, 1972) and are marked as S in the figure.

Determination of the direct shear wave travel time from the source to receiver 1 is the time from the initiation of the impulse (marked as I in the upper trace of Fig. 4.8a) until the initial shear wave arrival at borehole R1. This time is denoted as t_{DS} in Fig. 4.8a. Determination of the interval shear wave travel time is illustrated in Fig. 4.8b. This is the time for the shear wave to propagate between the two receiver boreholes and is denoted as t_{IS} in the figure. Interval travel times minimize many of the variables which can affect these measurements (Stokoe and Hoar, 1978).

Other travel time records similar to the one shown in Fig. 4.8 but with radial horizontal receivers are also obtained at all depths to improve the accuracy and resolution with which P-wave travel times could be determined. One set of these records is shown in Fig. 4.9. Direct and interval travel times of the P-waves are shown as t_{DP} and t_{IP}, respectively.

4.5 HISTORICAL DEVELOPMENT OF SURFACE WAVE TECHNIQUE

Existence of surface waves was first discussed by Rayleigh (1887), and the first simple theoretical seismograph illustrating the existence of body and Rayleigh waves was presented by Lamb (1904). These simplified models were the corner stone for tremendous advancements in identifying and interpreting seismic records. For instance, surface waves, usually generated by earthquakes or explosions, have been used for geophysical prospecting and identifying the proper ties of the crust and mantle of the earth. The contribution of the geophysicists over the last 100 years to the advancement of determination of properties of materials in situ is so extensive that it cannot be covered in this section. However, application of the theoretical and experimental achievements of geophysicists in material characterization tailored for use in civil engineering projects is discussed.

The first known use of surface waves to determine soil properties for engineering purposes was credited to the German Society of Soil Mechanics before World War II (DEGEBO, 1938). The primary interest of that study was to

investigate the response of a foundation to steady-state vibration. A rotating-mass oscillator was used as a source to excite foundations in the range of frequencies between 10 and 60 Hz. Due to the lack of sensitive receivers in that period, excessive loads had to be imposed on the soil to generate adequate signals. As a result, nonlinear behavior was generated in the soil and somewhat unsuccessful application of the method occurred (primarily because the nonlinear behavior was not taken into account).

Bergstrom and Linderholm carried out similar tests in Sweden in 1946. This work was done on a fairly uniform soil which resulted in the surface waves exhibiting little dispersion in the study range of 14 to 32 Hz. They compared Young's moduli determined from surface wave and plate bearing tests in an attempt to correlate the modulus of subgrade reaction with Young's modulus. Plates with different diameters were used in the plate bearing tests. They found that the moduli of subgrade reaction from the large-diameter plates correlated well with the dynamic moduli from the surface wave tests. However, results from the smaller-diameter plates did not yield any appreciable relationship between the subgrade and dynamic moduli.

Van der Poel (1951) and Nijboer and Van der Poel (1953) investigated a flexible pavement system in Holland using surface waves. The range of frequencies in their tests was 10 to 60 Hz which corresponded to waves predominantly propagating in the subgrade soil.

Heukelom and Klomp (1962) used steady-state vibrators to perform surface wave tests on pavements. Mechanical and electrodynamic vibrators were used to generate low frequency (4 to 60 Hz) and high frequency (greater than 60 Hz) waves in their tests. The effect of drainage of the subgrade after a flood was investigated. The S-wave velocity profiles from their investigation are shown in Fig. 4.10. The material profile of the site, which was located on a runway, was not described; however, the layering in the profile is shown graphically in the figure. The ordinate which is titled as the approximate depth in Fig. 4.10, corresponds to one-half of the wavelength at each frequency. The abscissa is equal to the phase velocity determined at each frequency. In other words, they assumed an effective depth of sampling equal to 1/2 of the wavelength and a shear wave velocity equal to the phase velocity at each frequency.

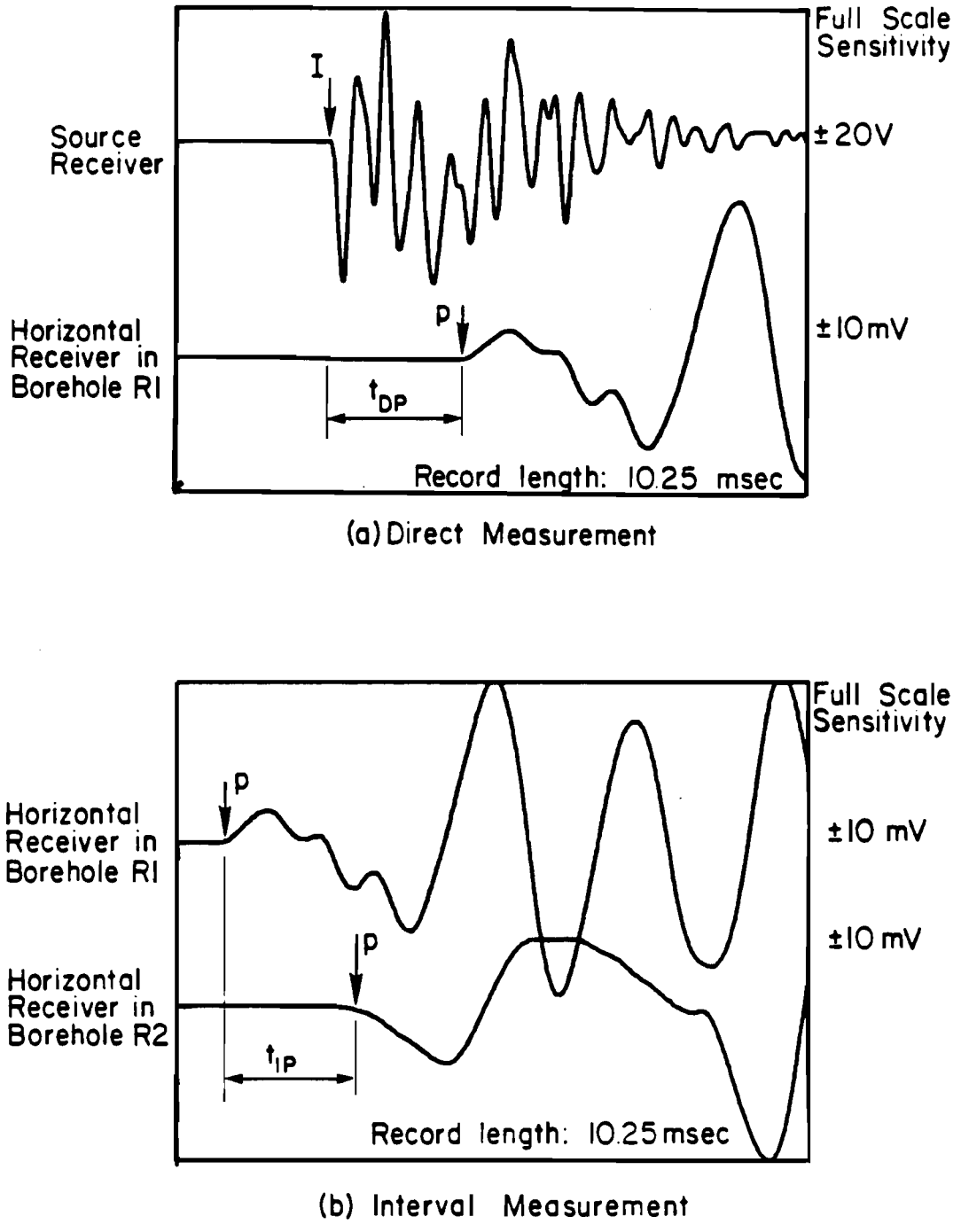

Fig. 4.9. Typical Crosshole Records for Determination of Compression Wave Travel Times.

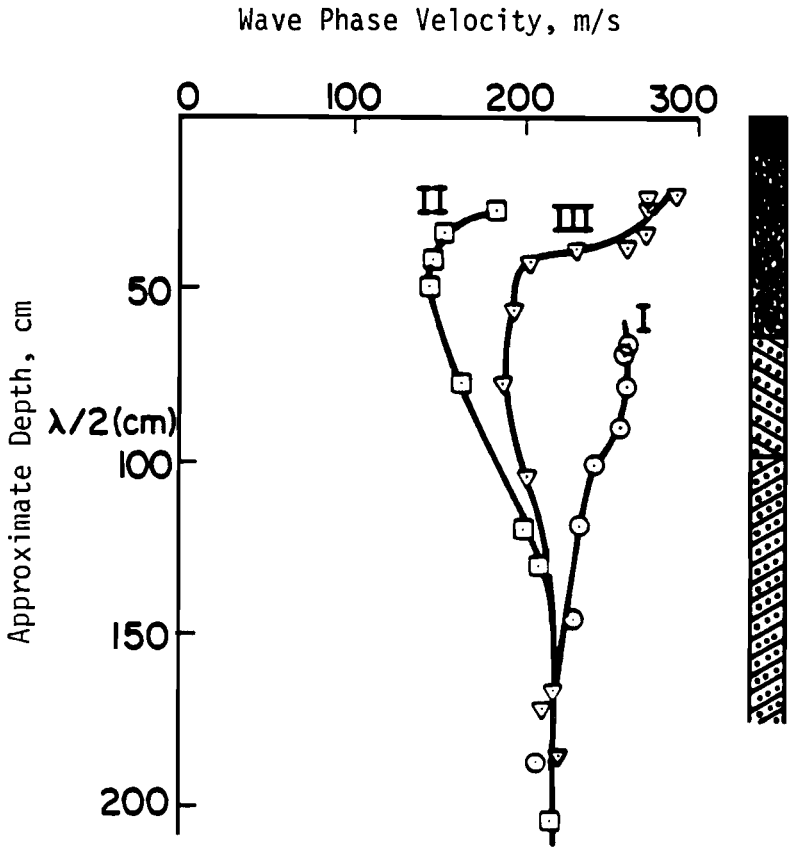

Fig. 4.10. Wave Phase Velocity as a Function of Approximate Depth, Showing the Softening of a Base Course by Water (II) and its Gradual Recovery on Draining (III), (from Heukelom and Klomp, 1962). Case I Represents Testing When the Base Course was Only Partially Built.

The curve in Fig. 4.10 denoted as I is the V_s profile determined by Heukelom and Klomp from tests performed when the base course was "half-way finished". The second and third curves (marked as II and III, respectively,) are from tests carried out after the finishing of the base and after the wearing course had been placed. Apparently, due the seasonal precipitation, the site was flooded, and the near-surface material became substantially softer (curve II, in Fig. 4.10). From the third test (curve III), they concluded, that as the water content of the material decreased, the stiffness increased. Unfortunately, they could not excite high enough frequencies to sample the pavement layers under investigation. (Note: The writers research shows that Heukelom and Klomp would have had to excite frequencies in the range of 3000 to 10,000 Hz to evaluate the upper pavement layer.)

The U.S. Army Engineer Waterways Experiment Station (WES) has used steady-state vibrations to determine elastic properties of in situ soils over the past 20 to 25 years. Ballard (1964), Fry (1965), Maxwell and Fry (1967), Ballard and Casagrande (1967), Cunny and Fry (1973), and Ballard and Chang (1973), among others, investigated numerous sites with the surface wave technique. The tests were carried out according to specifications set by WES which are described in detail by Maxwell and Fry (1965). The sources were either electromagnetic vibrators (for generating high frequencies) or mechanical vibrators using counter-rotating eccentric masses to generate low frequencies (up to 60 Hz). The WES procedure for obtaining the shear wave velocity profile from phase-velocity/wavelength data is identical to that of Heukelom and Klomp (1962), just discussed.

As an example of the WES procedure, the shear wave velocity profile from a site located in Buckboard Mesa, Nevada investigated by Fry (1965) is shown in Fig. 4.11. The site consists of a layer of residual soil that gradually turns into dense basalt. The approximate depths correspond to one-half of the wavelengths, and the shear wave velocities are assumed to be identical to propagation velocities measured in situ. Cunny and Fry (1973) compared in situ elastic moduli from surface waves tests with moduli obtained by resonant column tests at 14 sites. Cunny and Fry concluded that the laboratory-determined shear and Young's moduli were generally within 50 percent of the in situ moduli. They seemed to conclude that the WES procedure for handling surface wave data was acceptable. Woods and Richart (1967)

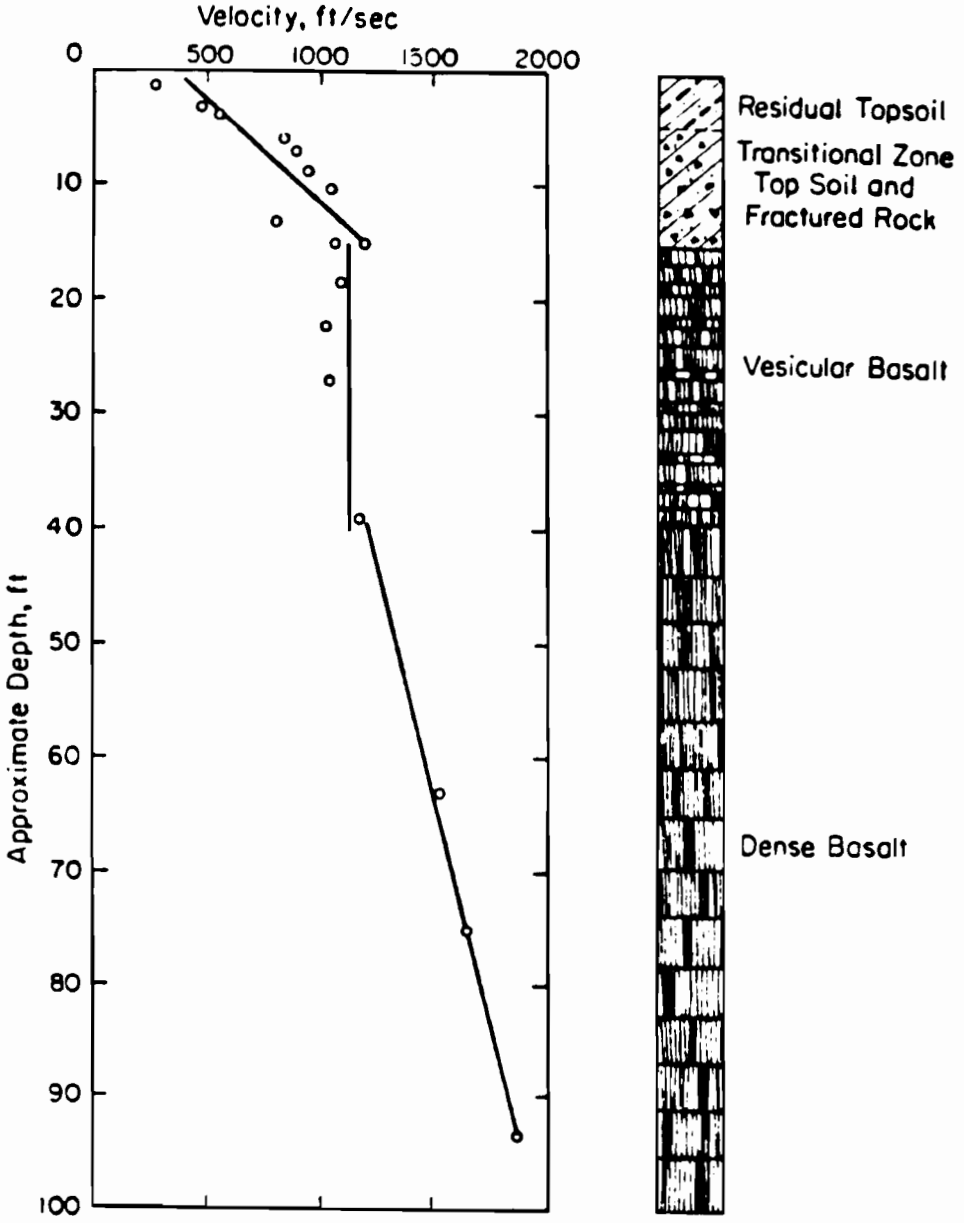

Fig. 4.11. Profile of Shear Wave Velocity vs. Depth in Rock Determined Using the WES Procedure (after Fry, 1965).

performed a series of surface wave tests in conjunction with a testing program set up to study the effect of trenches in screening elastic waves. They followed the procedure proposed by WES and also tacitly assumed the procedure was acceptable.

The greatest recent contribution in theoretical and practical aspects of surface wave testing on pavements was by Jones (1958). He proposed an analytical procedure to compute the moduli of different layers in a pavement system. An example of his investigation on a pavement section consisting of a 9-in. (23-cm) thick (nominally) concrete layer over subgrade is shown in Fig. 4.12. He assumed that the subgrade was a liquid layer and treated the concrete slab as a plate. From his study he reported the thickness of the concrete as 9.5 in. (24 cm). Upon coring, the concrete thickness was found to be quite close to 9.5 in. (24 cm).

Four groups of investigators have employed the spectral analysis of surface waves principles, mentioned in Section 4.2.2, to collect data in situ. Williams (1981) used a vibrator connected to broad-band noise generator (as opposed to a sine wave-generator) and a hammer as a source. These two sources, and sources similar to them, have the ability to generate waves over a wide range of frequencies. If the waves generated by these sources are captured on an appropriate recording device, Fourier transformed, and spectral analyses performed on them, the testing time can be reduced quite significantly (see Nazarian and Stokoe, 1985). Williams' interest was solely limited to constructing the experimental dispersion curves, and he did not report any shear wave velocity profile.

Heisey, et al (1982) used hammer blows to generate transient signals to construct the dispersion curves. He used a spectral analyzer as the recording device which accelerated the in-house data reduction several fold over Williams' approach (a tape recorder). Based upon tests on several soil and pavement sites, Heisey suggested an effective depth of sampling equal to 1/3 of the wavelength for each frequency. He also divided the surface wave velocities measured in the field by a factor approximately equal to 0.90 to obtain shear wave velocities.

Neilson and Baird (1975, and 1977) and Baird (1982) from the New Mexico Engineering Research Institute constructed a van to collect surface wave data conveniently. This van consists of a system operators area and a support

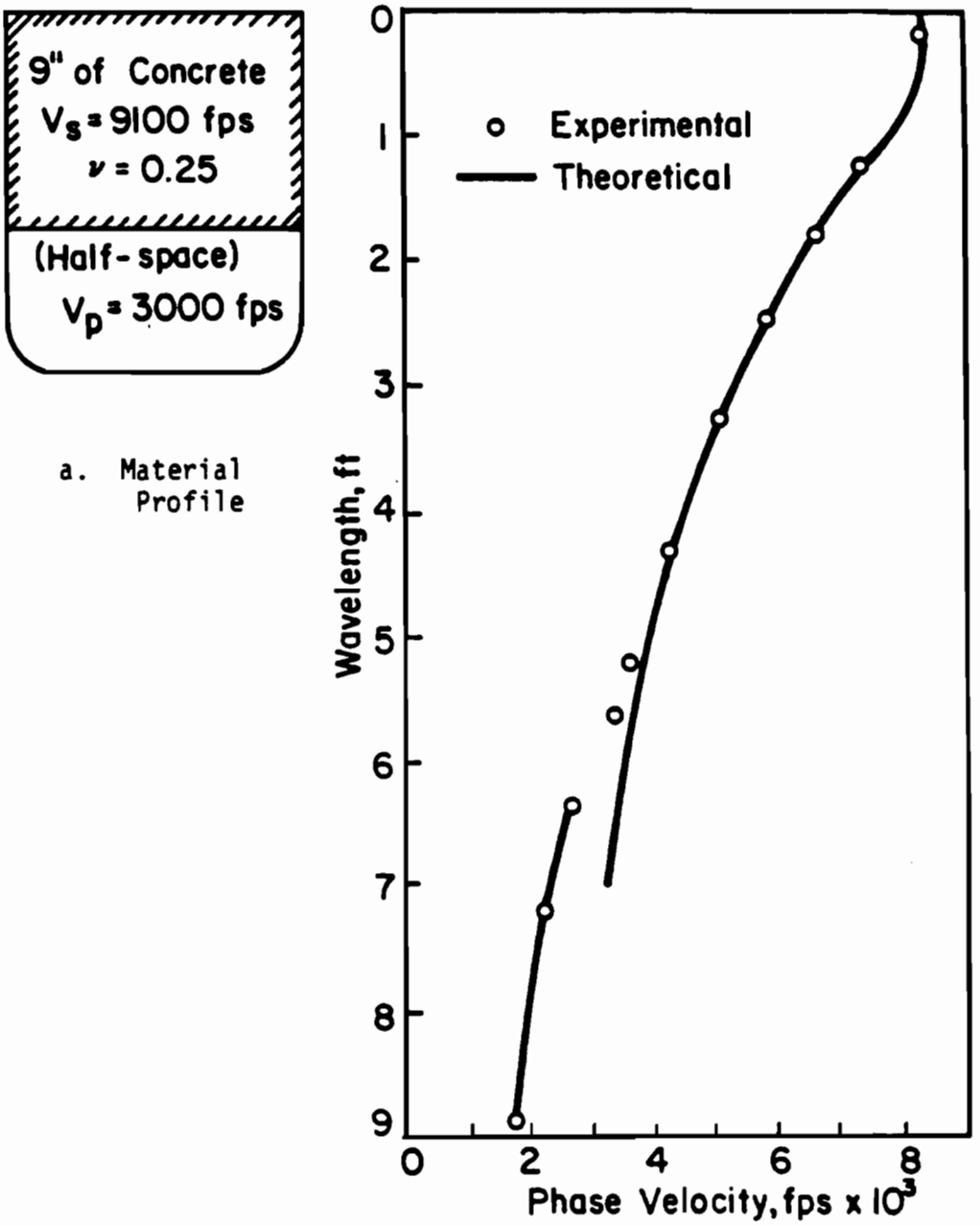

a. Material Profile

b. Dispersion Curves

Fig. 4.12. Comparison of Theoretical and Experimental Dispersion Curves for a Concrete Layer Over Soil (from Jones, 1958).

equipment area. A data acquisition system along with a system to control the deployment of an impact system are located in the system operators area. The support equipment area houses a 215-lb (950-N) programmable drop weight and two generators. The height of the drop and the weight of the loading system can be changed. The drop weight impacts a 12-in. (30-cm) diameter plate. The impulses are simultaneously monitored with as many as eight accelerometers. The data reduction is rather arbitrary and requires empirical correction factors to obtain moduli of the different layers. In other words, no rigorous inversion process was developed in this program.

A series of investigations was performed by Baker and Stevens (1983). A hydrohammer (soil compactor) was used as the seismic source. The travel time records were recorded on a 16-channel digital tape recorder. Data reduction is based upon constructing and matching of a synthetic travel time record (seismogram) with the experimental one obtained in the field.

In summary, in all the investigations reported above, in situ testing procedures may differ; however, invariably the goal is to determine the relationship between the propagation velocity of surface waves and wavelengths, called a dispersion curve. The next step is then to obtain a shear wave velocity-depth relationship based upon the dispersion information. In all the studies [except Jones (1958), and Baker and Stevens (1983)] the dispersive characteristic of surface waves was neglected, and after the dispersion curve was constructed, some approximate procedure was used to assess the shear wave velocity profile. In other words, the V_s profile was obtained by simply changing the scale of the axes of the dispersion curve. Generally, use of this process will not accurately predict the shear wave velocities. The reasons for this inaccuracy and an alternative process for determining the shear wave velocity profile from a given dispersion curve are presented in Chapter Five.

4.6 SUMMARY

In situ seismic methods used in determining dynamic stiffnesses of soil deposits and pavement systems are discussed in this chapter. Downhole and crosshole tests are the most popular methods used in geotechnical engineering projects. To date, crosshole testing is more desirable for pavement systems

as it yields more accurate and repeatable results once any refraction problems are taken into account. In the pavements area, the Dynaflect and the falling weight deflectometer are the most commonly used in situ testing techniques. These techniques are rapid in the field but have undesirable drawbacks in data reduction due to possible nonuniqueness of the solutions.

The historical development and employment of the surface wave method is also presented. Basic field testing with the method has evolved from steady-state vibrators and tape recorders to transient impacts and waveform analyzers as the availability to take sophisticated electronics into the field has increased. However, data reduction in most geotechnical engineering cases is based on arbitrary criteria which are generally in error. The data reduction problem is discussed in the next chapter and a improved solution (inversion) is proposed. This improved solution has been implemented in an interactive computer program, INVERT1, which is discussed in Report No. 1123-1 (Nazarian and Stokoe, 1986c).

CHAPTER FIVE. DISPERSIVE CHARACTERISTIC OF SURFACE WAVES

5.1 INTRODUCTION

In a homogeneous, isotropic, elastic, half-space, the velocities of surface waves do not vary with frequency. However, since the properties of pavement systems exhibit variations with depth (are not homogeneous vertically), surface wave velocities vary with frequency. This frequency dependency of wave velocity in a heterogeneous medium is termed dispersion, and surface waves are thus said to be dispersive. A plot of wave velocity versus frequency (or wavelength) is called a dispersion curve. It is this dispersive characteristic of surface waves that is the fundamental basis of the SASW method.

The dispersive characteristic of surface waves can be demonstrated by means of either phase or group velocity. Phase velocity is defined as the velocity with which a seismic disturbance of a single frequency propagates in the medium. Group velocity, on the other hand, is the velocity of groups of frequencies in a seismogram in a dispersive medium. Definition of phase and group velocities is based upon the principle of stationary phase which indicates that significant arrivals in the seismogram occur when the phase is stationary with respect to frequency. The phase is stationary several wavelengths away from the source and near the maximum or minimum of the wavelet. In a medium in which the velocity varies with frequency, the wave train changes shape as it propagates, and, therefore, group velocity differs from phase velocity, especially when the wave propagates over a long distance.

Phase and group velocities are related by:

$$V_g = V_{ph} + k \frac{dV_{ph}}{dk} \tag{5.1}$$

with

$$k = \omega / V_{ph} \tag{5.2}$$

where:

V_g = group velocity,
V_{ph} = phase velocity,
k = wave number, and
ω = rotational frequency.

As an example, the time records of waves propagating in a medium at different distances from the source are shown in Fig. 5.1. The lines corresponding to phase and group velocities are also shown in this figure. Phase velocity is found by a best fit line through the troughs or peaks at the zeros of the wavelets. However, group velocity is obtained by drawing a straight line (best fit line) connecting the maximum or minimum envelopes. In Fig. 5.1, the troughs are used for determining phase velocity. In practice, phase velocity is often determined first as a function of frequency, and group velocity is calculated using Eq. 5.1. In this study, only phase velocities are considered. Group velocities are disregarded herein because phase velocities contain all the information required to calculate elastic moduli of the pavements. It should also be mentioned that throughout this chapter apparent Rayleigh wave velocity and phase velocity are used interchangeably and are considered synonymous.

The study of dispersion of waves in a horizontally-layered half-space relies upon derivation of the so-called dispersion function (i.e., the relationship between phase velocity and frequency). Thomson (1950) introduced the first matrix solution of this problem. However, his work contained an error in the sense that continuity of strains was assumed at layer interfaces as opposed to displacements. Haskell (1953) reworked Thomson's procedure imposing continuity of displacements at layer interfaces and thus developed the first successful matrix solution of Rayleigh wave motion in a layered system.

In the classical approach, the dispersion function and wavelengths (or frequencies) are obtained by vanishing a determinant whose elements are functions of mass densities and elastic moduli of the layers as well as phase velocities and frequencies. The Haskell-Thomson technique builds up the (surface wave) dispersion function as the product of layer matrices which relate the displacement components as well as the stress components acting on the interface to those associated with the next interface. The product of

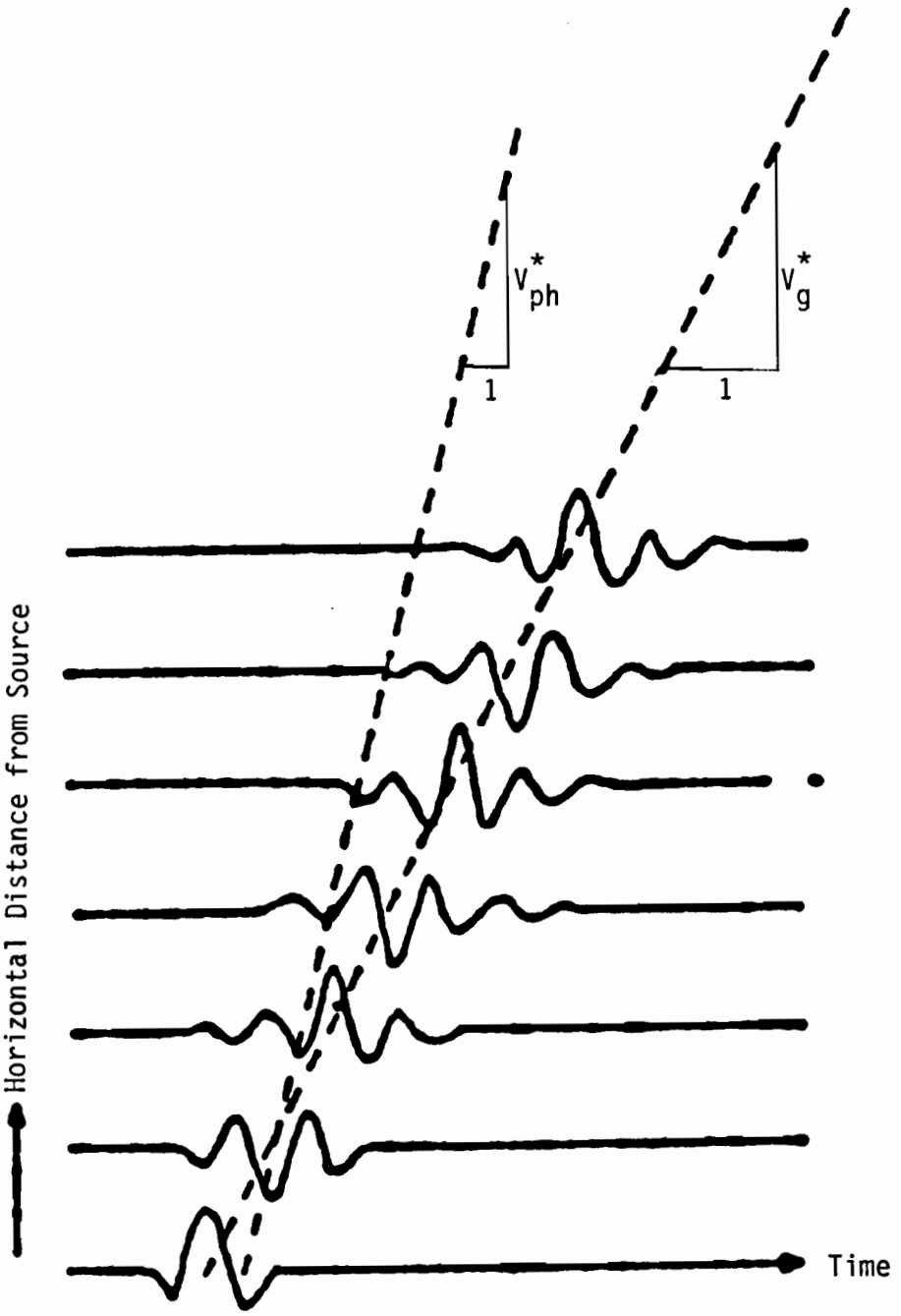

Fig. 5.1. Illustration of Phase Velocity and Group Velocity (from Sheriff, 1982).

these layer matrices then relates the stress and displacement components of motion at the deepest interface to those at the free surface.

The Haskell-Thomson solution exhibits numerical difficulties at high frequencies. These difficulties are caused by the computation of squares of exponential terms leading to loss of significant figures in the components of certain matrix products. Knopoff (1964), Dunkin (1965), Thrower (1965), Schwab and Knopoff (1970), and Watson (1970) suggest methods to solve this problem. The works of Dunkin, Thrower, and Watson are all extensions of the original Haskell-Thomson matrix formulation. Knopoff's technique begins with the immediate construction of the dispersion function by means of determinants, and then analyzes or decomposes these determinants into a product of interface matrices which are from submatrices of the determinants. Each of these interface submatrices relates the components of motion in the layer on one side of the interface to those in the layer on the other side.

In this chapter the Haskell-Thomson technique along with its numerical difficulties at high frequencies are first discussed. Dunkin's approach to circumvent these numerical difficulties is also presented as this approach is employed in the inversion process discussed in Nazarian and Stokoe (1985) and Nazarian and Stokoe (1986c). Thrower's approach is quite similar to Dunkin's solution which is described in this chapter. However, Thrower suggested some slight modifications to determine the solution to propagation of surface waves in a layered system which becomes softer with depth. As Thrower's solution is very similar to Dunkin's solution, his work is not repeated herein. The final section of this chapter includes a study of factors affecting the dispersion function.

5.2 HASKELL-THOMSON APPROACH

Many problems in geophysics involve propagation of elastic surface waves in a layered half-space. Usually the half-space is divided into homogeneous and isotropic solid layers as shown in Fig. 5.2. In the nth layer, displacements u_n and w_n in directions x and z, respectively, and σ_{zn} and τ_{xzn}, normal and shear stresses on horizontal planes, respectively, can be expressed in terms of two potentials:

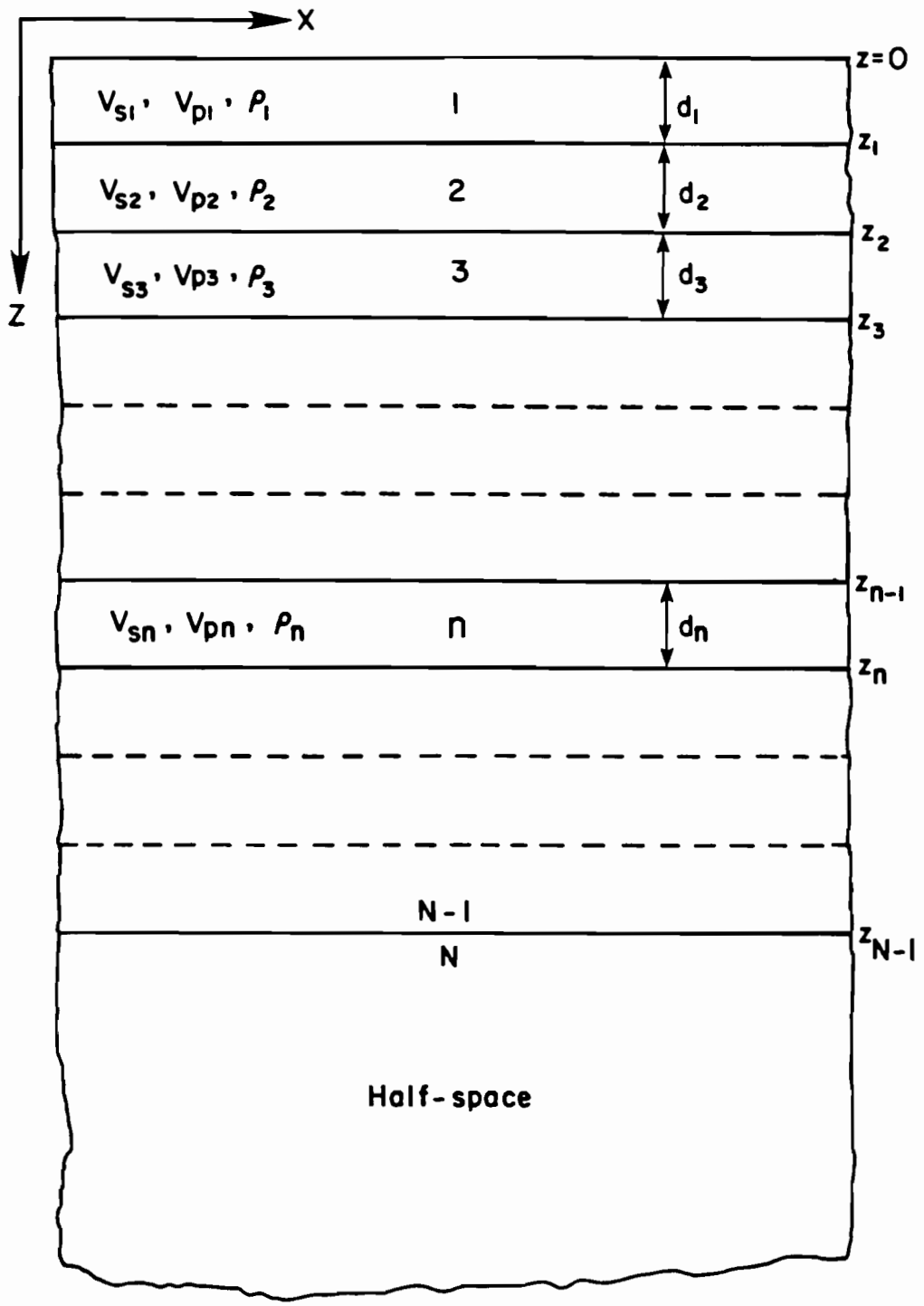

Fig. 5.2. Idealized Model of a Heterogeneous Medium.

ϕ_n = a scalar potential corresponding to compression waves, and

$\vec{\psi}_n$ = a vector potential corresponding to shear waves.

As mentioned before, it was assumed that the condition of plane strain exists. As a result of this assumption, it can be shown that the x- and z-components of the vector potential $\vec{\psi}_n$ are equal to zero. For simplicity, the y-component of the vector potential (i.e. potential corresponding to shear in the x-z plane) will be called ψ_n, hereafter. These potentials are obtained for each layer as solutions of the equations:

$$\nabla^2\phi_n = \frac{1}{V_{pn}^2}\frac{\partial^2\phi_n}{\partial t^2} \tag{5.3}$$

$$\nabla^2\ \psi_n = \frac{1}{V_{sn}^2}\frac{\partial^2\psi_n}{\partial t^2} \tag{5.4}$$

where the operator ∇^2 is the Laplacian operator and is defined as:

$$\nabla^2 = \frac{\partial^2}{\partial x^2} + \frac{\partial^2}{\partial y^2} + \frac{\partial^2}{\partial z^2} \tag{5.5}$$

Once again, due to assumption of plane strain, it can be shown that the derivative of the potentials with respect to y is equal to zero so that Eq. 5.5 can be written as:

$$\nabla^2 = \frac{\partial^2}{\partial x^2} + \frac{\partial^2}{\partial z^2} \tag{5.6}$$

For a harmonic wave, the potentials ϕ_n and ψ_n can be Fourier transformed with respect to time and x so that the result can be written as:

$$\Phi_n = \phi_n \exp[-i(\omega t - kx)] \tag{5.7}$$

$$\Psi_n = \psi_n \exp[-i(\omega t - kx)] \tag{5.8}$$

where,

$i = \sqrt{-1}$,

Φ_n = amplitude of potential ϕ_n,

Ψ_n = amplitude of potential ψ_n, and

k = wave number of phase velocity as defined in Eq. 5.2.

By substituting Eqs. 5.7 and 5.8 into Eq. 5.3 and 5.4, the amplitudes Φ_n and Ψ_n satisfy the equations:

$$\frac{d^2\Phi_n}{dz^2} = r_n^2 \Phi_n \tag{5.9}$$

$$\frac{d^2\Psi_n}{dz^2} = s_n^2 \Psi_n \tag{5.10}$$

where:

$$r_n^2 = k^2 - k_{pn}^2 \tag{5.11}$$

$$s_n^2 = k^2 - k_{sn}^2 \tag{5.12}$$

in which $k_{pn} = \omega/V_{pn}$ and $k_{sn} = \omega/V_{sn}$ are defined as wave numbers for compression and shear waves in the nth layer, respectively.

The solutions of Eqs. 5.9 and 5.10 can be written as:

$$\Phi_n = U_{pn} \exp[ir_n(z-z_{n-1})] + D_{pn} \exp[-ir_n(z-z_{n-1})] \tag{5.13}$$

$$\Psi_n = U_{sn} \exp[is_n(z-z_{n-1})] + D_{sn} \exp[-is_n(z-z_{n-1})] \tag{5.14}$$

In Eqs. 5.13 and 5.14, z is depth to the surface which is bound between z_{n-1} and z_n (top and bottom of layer n, respectively). Parameters U_{pn} and U_{sn} are coefficients of terms corresponding to upgoing P- and S-waves, respectively. Similarly, D_{pn} and D_{sn} correspond to coefficients of terms associated with downward propagating P- and S-waves in the nth layer. It is convenient to rewrite Eqs. 5.13 and 5.14 as:

$$\Phi_n = \Phi_{up}(z) + \Phi_{dn}(z) \tag{5.15}$$

$$\Psi_n = \Psi_{up}(z) + \Psi_{dn}(z) \tag{5.16}$$

where:

$$\Phi_{up}(z) = U_{pn} \exp[ir_n(z-z_{n-1})] \tag{5.17}$$

$$\Phi_{dn}(z) = D_{pn} \exp[-ir_n(z-z_{n-1})] \tag{5.18}$$

$$\Psi_{up}(z) = U_{sn} \exp[is_n(z-z_{n-1})] \tag{5.19}$$

$$\Psi_{dn}(z) = D_{sn} \exp[-is_n(z-z_{n-1})] \tag{5.20}$$

Let the vector $\overline{\Phi}_n(z)$ be defined as:

$$\overline{\Phi}_n(z) = [\Phi_{up}(z), \Psi_{up}(z), \Phi_{dn}(z), \Psi_{dn}(z)]^T \tag{5.21}$$

The displacements un and wn from elastic theory are equal to:

$$u_n = \frac{\partial \Phi_n}{\partial z} + \frac{\partial \Psi_n}{\partial x} \tag{5.22}$$

$$w_n = \frac{\partial \Phi_n}{\partial z} + \frac{\partial \Psi_n}{\partial x} \tag{5.23}$$

and the stresses σ_{zn} and τ_{xzn} are equal to (for simplicity σ_{zn} and τ_{xzn} are replaced by σn and τ_n):

$$\sigma_n = (\lambda_n + 2G_n)\left(\frac{\partial u_n}{\partial x} + \frac{\partial w_n}{\partial z}\right) - 2G_n \frac{\partial u_n}{\partial x} \tag{5.24}$$

$$\tau_n = G_n \left(\frac{\partial u_n}{\partial z} + \frac{\partial w_n}{\partial x}\right) \tag{5.25}$$

where:

λ_n = Lame's constant of the nth layer, and
G_n = shear modulus of the nth layer.

In terms of potentials Φ_n and Ψ_n, the stresses can be expressed as (using Eqs. 5.22 and 5.23):

$$\sigma_n = \lambda_n \nabla^2 \Phi_n + 2G_n \left(\frac{\partial^2 \Phi_n}{\partial z^2} - \frac{\partial^2 \Psi_n}{\partial z \partial z}\right) \tag{5.26}$$

$$\tau_n = G_n \left(2 \frac{\partial^2 \Phi}{\partial z \partial x} - \frac{\partial^2 \Psi}{\partial x^2} + \frac{\partial^2 \Psi}{\partial z^2}\right) \tag{5.27}$$

Once again as a matter of convenience, another vector, $\bar{S}_n(z)$, is introduced so that:

$$\bar{S}_n(z) = [u_n(z),\ w_n(z),\ \sigma_n(z),\ \tau_n(z)]^T \tag{5.28}$$

At any point in layer n, Dn and Sn are related by:

$$\bar{S}_n(z) = T_n \bar{\Phi}(z) \tag{5.29a}$$

or

$$\bar{\Phi}_n(z) = T_n^{-1} \cdot \bar{S}_n(z) \tag{5.29b}$$

Matrix T_n is a 4x4 matrix defined as:

$$T_n = \begin{bmatrix} ik & -s_n & ik & s_n \\ r_n & ik & -r_n & ik \\ a_n & b_n & a_n & -b_n \\ c_n & -a_n & -c_n & -a_n \end{bmatrix} \tag{5.30}$$

with

$$a_n = G_n(k_n^2 - s_n^2) \tag{5.31}$$

$$b_n = 2iG_n k_n s_n \tag{5.32}$$

$$c_n = 2iG_n k_n r_n \tag{5.33}$$

in which k_n, r_n and s_n are defined in Eqs. 5.2, 5.11 and 5.12, respectively; and G_n is the shear modulus of layer n.

Furthermore, the potentials at the top and bottom of the nth layer are related by:

$$\bar{\Phi}_n(z_n) = E_n \bar{\Phi}_n(z_{n-1}) \tag{5.34}$$

where:

$$E_n = \begin{bmatrix} \exp(ir_n d_n) & 0 & 0 & 0 \\ 0 & \exp(is_n d_n) & 0 & 0 \\ 0 & 0 & \exp(-ir_n d_n) & 0 \\ 0 & 0 & 0 & \exp(-is_n d_n) \end{bmatrix} \tag{5.35}$$

and $d_n = z_n - z_{n-1}$ (thickness of layer n). Since the stresses and displacements in the two layers at the nth layer interface (i.e., top of layer n+1 and bottom of layer n) should be equal, one can write:

$$\bar{S}_{n+1}(z_n) = \bar{S}_n(z_n) \tag{5.36}$$

If Eq. 5.29a is substituted in Eq. 5.36,the result will be:

$$\bar{S}_{n+1}(z_n) = T_n \bar{\Phi}_n(z_n) \tag{5.37}$$

Parameter $\bar{\Phi}_n(z_n)$ is then substituted by the right hand side of Eq. 5.34, so that:

$$\bar{S}_{n+1}(z_n) = T_n E_n \bar{\Phi}_n(z_{n-1}) \tag{5.38}$$

Once again Eq. 5.29b is utilized to rewrite Eq. 5.38 in the form of:

$$\bar{S}_{n+1}(z_n) = (T_n E_n T_n^{-1}) \bar{S}_n(z_{n-1}) \tag{5.39}$$

If a matrix Q_n is defined as:

$$Q_n = T_n E_n T_n^{-1} \tag{5.40}$$

then Eq. 5.39 can be written as:

$$\bar{S}_{n+1}(z_n) = Q_n \bar{S}_n(z_{n-1}) \tag{5.41}$$

Matrix Q_n has two functions. First, Q_n allows continuity of stresses and displacements at an interface, and second it defines the stresses and displacements at each point in the layer. Equation 5.41 can be utilized to relate the displacements and stresses at the ground surface to those at the deepest interface by:

$$\bar{S}_N(z_{N-1}) = Q_{N-1} \cdot Q_{N-2} \cdots\cdots Q_2 \cdot Q_1 \, \bar{S}_1(o) \tag{5.42}$$

or

$$\bar{S}_N(z_{N-1}) = R' \bar{S}_1(0) \tag{5.43}$$

where:

$$R' = \prod_{i=1}^{N-1} Q_i \tag{5.44}$$

In Eq. 5.44, $\overline{\prod}$ denotes the product of all the Q matrices in Eq. 5.42. By substituting Eq. 5.29b into Eq. 5.44 , one can write:

$$\bar{\Phi}_N(z_{N-1})(T_N^{-1}R')\bar{S}_1(0) \tag{5.45}$$

or

$$\bar{\Phi}_N(z_{N-1}) = R\,\bar{S}_1(0) \tag{5.46}$$

where:

$$R = T_N^{-1}\,R' = T_N^{-1}\prod_{i=1}^{N-1} Q_i \tag{5.47}$$

If the surface of half-space is free of tractions, $\bar{S}_1(0)$ is given by:

$$\bar{S}_1(0) = [u_1(0),\ w_1(0),\ \sigma_1(0),\ \tau_1(0)]^T$$

or (5.48)

$$\bar{S}_1(0) = [u_1(0),\ w_1(0),\ 0,\ 0\ ]^T$$

In addition, for an excitation on the surface of the half-space, waves in the last layer can only travel downwards (radiation condition) so that:

$$\bar{\Phi}_N(z_{N-1}) = [\Phi_{up}(z_{N-1}),\ \Psi_{up}(z_{N-1}),\ \Phi_{dn}(z_{N-1}),\ \Psi_{dn}(z_{N-1})]^T$$

$$= [\ 0,\ 0,\ \Phi_{dn}(z_{N-1}),\ \Psi_{dn}(z_{N-1})]^T \tag{5.49}$$

If Eqs. 5.48 and 5.49 are incorporated in Eq. 5.46, the result will be:

$$\left[\begin{array}{c} 0 \\ 0 \\ \hline \Phi_{dn}(z_{N-1}) \\ \Psi_{dn}(z_{N-1}) \end{array}\right] = \left[\begin{array}{cc:cc} r_{11} & r_{12} & r_{13} & r_{14} \\ r_{21} & r_{22} & r_{23} & r_{24} \\ \hdashline r_{31} & r_{32} & r_{33} & r_{34} \\ r_{41} & r_{42} & r_{43} & r_{44} \end{array}\right] \left[\begin{array}{c} u_1(0) \\ w_1(0) \\ \hdashline 0 \\ 0 \end{array}\right] \tag{5.50}$$

The matrix and two vectors in Eq. 5.50 can be partitioned into submatrices as indicated by the dotted lines, such that:

$$\begin{bmatrix} 0 \\ A \end{bmatrix} = \begin{bmatrix} R_{11} & R_{12} \\ R_{21} & R_{22} \end{bmatrix} \begin{bmatrix} B \\ 0 \end{bmatrix} \tag{5.51}$$

which leads to two equations.

It is much more convenient mathematically to solve the equation

$$R_{11} \cdot B + R_{12} \cdot 0 = 0 \tag{5.52}$$

or

$$R_{11} \cdot B = 0 \tag{5.53}$$

For a nontrivial solution

$$\det(R_{11}) = 0 \tag{5.54}$$

This equation, which is a function of frequency and phase velocity, is the desired solution to the problem of propagation of surface waves in a layered medium which is simply called the dispersion function.

If there are N layers in the medium, there will be 4N-2 boundary conditions to be satisfied; namely, continuity of two displacement components

and two stress components at each interface, and vanishing of stresses at the free surface. These 4N-2 equations contain 4N-2 unknowns. As such, the Haskell-Thomson matrix solution can be programmed easily for computer use.

5.3 PROBLEMS WITH THE HASKELL-THOMSON APPROACH

It was shown that the solution to the dispersion function requires finding the roots of the determinant of matrix R_{11} in the last section. At high frequencies some components of matrix R_{11} become large, causing a loss of significant figures in terms in the dispersion function which, in turn, make it impossible to obtain accurate values of the roots. The source of this discrepancy is discussed herein.

If Eq. 5.47 is expanded as shown below:

$$R = T_N^{-1} \cdot \prod_{i=1}^{N-1} Q_i = T_N^{-1} \cdot Q_{N-1} \cdot Q_{N-2} \cdots Q_N \cdots Q_2 \cdot Q_1 \qquad (5.55)$$

by substituting for Q_n from Eq. 5.40, the R-matrix can be written as:

$$R = T_N^{-1} \cdot Q_{N-1} \cdot Q_{N-2} \cdots (T_n E_n T_n^{-1}) \cdots Q_2 \cdot Q_1 \qquad (5.56a)$$

$$R = T_N^{-1} \cdot Q_{N-1} \cdot Q_{N-2} \cdots Q_{n+1} T_n) E_n (T_n^{-1} \cdot Q_{n-1} \cdots Q_2 \cdot Q_1) \qquad (5.56b)$$

or

$$R = Z E_n W \qquad (5.57)$$

where:

$$Z = T_N^{-1} \cdot Q_{N-1} \cdot Q_{N-2} \cdots Q_{N+1} \cdot T_n$$

$$W = T_N^{-1} \cdot Q_{n-1} \cdots Q_2 \cdot Q_1$$

Then by using Eq. 5.35, each element of matrix R, r_{ij}, is a linear combination of the exponentials of layer n, i.e.,

$$R_{ij} = a_i \exp(ir_n d_n) + a_2 \exp(is_n d_n) + a_3 \exp(-ir_n d_n) + a_4 \exp(-is_n d_n) \quad (5.58)$$

Parameters a_1, a_2, a_3, and a_4 are known parameters computed from multiplication of the three matrices Z, En, and W. Therefore, in computing the determinant of submatrix R_{11}, these terms will contain squares of exponentials; for instance terms of $\exp(ir_n d_n)$,

$$\det(R_{11}) = r_{11}\, r_{12} - r_{21}\, r_{12} \exp(2ir_n d_n) + \ldots \quad (5.59)$$

If for a given frequency and phase velocity, the determinant of R_{11} is computed, and if the value of r_n becomes large and positive, the first term on the right hand side of Eq. 5.56 will be dominant and will cause a loss in the significant figures retained in $\det(R_{11})$ with regard to the other terms. However, these terms will cancel out eventually. Therefore, if somehow these terms can be omitted before calculating the determinant of matrix R_{11}, the problem can be avoided. This is the approach advocated by Dunkin and discussed next.

5.4 DUNKIN APPROACH

To reformulate the Haskell-Thomson formulation to allow the use of high frequencies in the solution of the dispersion function, Dunkin (1965) took advantage of two theorems. Theorem one indicates that if there are n matrices of order of 2 or greater, the second order subdeterminants of the product of these matrices (being multiplied) are equal to the products of the subdeterminant of each matrix where the summed pair of indices are only distinct pairs of distinct indices. To clarify this theorem, consider n matrices A_1 to A_n and a matrix P such that:

$$P = A_1 \cdot A_2 \cdot A_3 \ldots . A_n \quad (5.60)$$

If $P\begin{vmatrix} ij \\ kl \end{vmatrix}$ is a second order subdeterminant of matrix P, i.e.:

$$p\begin{vmatrix} ij \\ kl \end{vmatrix} = p_{ik} \cdot p_{jl} - p_{il} \cdot p_{jk} \quad (5.61)$$

then:

$$p\begin{vmatrix} ij \\ kl \end{vmatrix} = a_1\begin{vmatrix} ij \\ mn \end{vmatrix} \cdot a_2\begin{vmatrix} mn \\ op \end{vmatrix} \cdots a_{n-1}\begin{vmatrix} st \\ uv \end{vmatrix} \cdot a_n\begin{vmatrix} uv \\ kl \end{vmatrix} \tag{5.61}$$

where $a\begin{vmatrix} mn \\ op \end{vmatrix}$ is the second order subdeterminant of matrix Al constructed from elements a_{mo}, a_{mp}, a_{no}, and a_{np}. Also this theorem indicates that one can choose mn to be 12, 13, 14, etc., but one never includes both 12 and 21, for example.

The second theoreom is that subdeterminants of the Q matrices defined in Eq. 5.40 do not contain products of like exponentials. By inspecting Eq 5.35, E_n is a diagonal matrix with:

$$e\begin{vmatrix} ij \\ kl \end{vmatrix} = 0 \quad \text{for } ij \neq kl \tag{5.63}$$

By employing theoreom one to Eq. 5.40, it can be shown that:

$$q_n\begin{vmatrix} ij \\ kl \end{vmatrix} = t_n\begin{vmatrix} ij \\ ab \end{vmatrix} \cdot e_n\begin{vmatrix} ab \\ cd \end{vmatrix} \cdot \tilde{t}_n\begin{vmatrix} cd \\ kl \end{vmatrix} \tag{5.64}$$

where $\tilde{t}_n$ and t_n are the second order subdeterminants of T_{n-1} and T_n, respectively. Consequently, by using Eq. 5.63, Eq. 5.64 can be rearranged to:

$$q_n\begin{vmatrix} ij \\ kl \end{vmatrix} = t_n\begin{vmatrix} ij \\ ab \end{vmatrix} \cdot \tilde{t}_n\begin{vmatrix} ab \\ kl \end{vmatrix} \cdot e_n\begin{vmatrix} ab \\ ab \end{vmatrix} \tag{5.65}$$

The importance of the two theorems becomes apparent when they are applied to Eq. 5.53. Using the first theoreom, Eq. 5.54 can be written as:

$$\det(R_{11}) = r\begin{vmatrix} 12 \\ 12 \end{vmatrix} = \tilde{t}_N\begin{vmatrix} 12 \\ ab \end{vmatrix} \cdot q_{N-1}\begin{vmatrix} ab \\ cd \end{vmatrix} \cdots q_1\begin{vmatrix} ef \\ 12 \end{vmatrix} \tag{5.66}$$

which is a linear expression in the second order subdeterminants of any Q_n matrix. By the second theoreom, this expression does not contain any products of like exponentials. Therefore, if the expressions for the subdeterminants of the Q_n are used as the basis of calculation (as opposed to elements of Q_n) the numerical cancellation of like exponentials, such as $\exp(2r_n d_n)$ discussed in the last section, is not necessary since such terms have already been omitted. Therefore, by direct calculation of the submatrices instead of direct multiplication of the elements of the matrices, the numerical difficulties discussed in Section 5.3 for high frequencies are solved.

5.5 PARAMETRIC STUDY OF DISPERSIVE CHARACTERISTIC

In Section 5.2 the dispersion function was calculated. This function is a relationship between frequency and phase velocity. Now, if different frequencies are assumed and the phase velocity associated with each frequency is calculated and plotted, the outcome will be a curve called a dispersion curve. The shape of a dispersion curve is affected by three independent properties of the material composing each layer for a given profile which are:

1. shear wave velocity,
2. Poisson's ratio, and
3. mass density.

However, other combinations of these parameters can be assumed; such as replacing shear wave velocity by shear modulus or using compression wave velocity instead of Poisson's ratio. In the remainder of this chapter, the effect of each of these factors is discussed. These parameters can be studied more effectively by means of simple cases of two- or three-layered systems. As such, each parameter is discussed by means of selecting simple cases, and then the results are generalized for more complex conditions.

Another parameter which affects the dispersion curve is the thickness of each layer. As layer thicknesses change, the shape of the dispersion curve changes accordingly. This matter is studied as well.

Solution to the dispersion function yields many roots at each frequency. The smallest root is called the solution to the fundamental mode, and others are termed the solution to higher modes. The dispersion curves presented herein correspond to roots of the fundamental mode and curves representing higher modes are disregarded.

5.5.1 Effect of Shear Wave Velocity

In an elastic medium, surface waves are dispersive only if a velocity contrast exists in the layering. To illustrate this point, consider a layer of soil overlying bedrock. Assume that the shear wave velocity of the soil layer is 1/3 of the shear wave velocity of the bedrock. The dispersion curve for this profile is shown by the solid line in Fig. 5.3. In the figure, wavelengths are normalized relative to the height of the soil layer, and phase velocities are normalized relative to the shear wave velocity of the soil

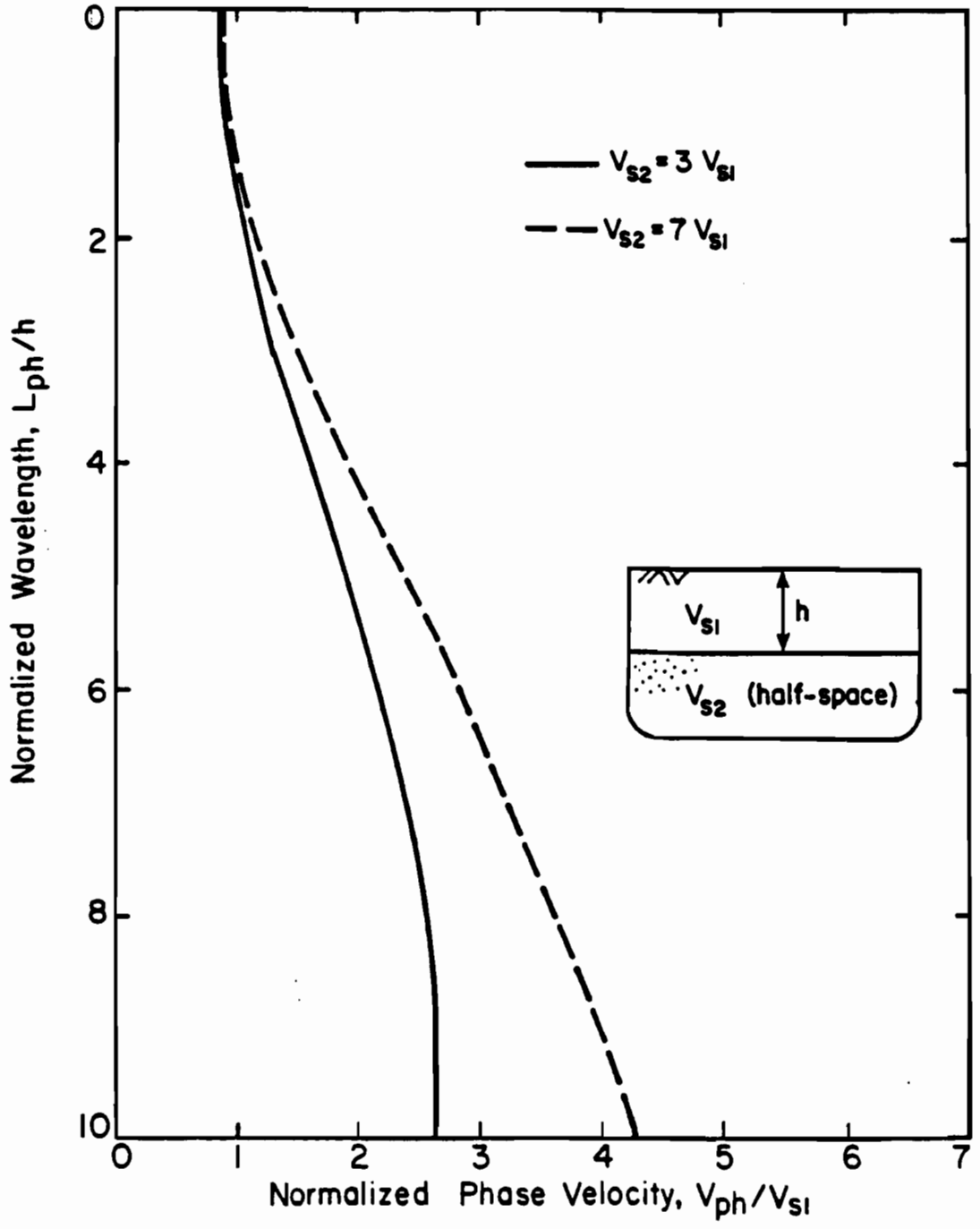

Fig. 5.3. Theoretical Dispersion Curves for a Layer Underlain by a Stiff Elastic Half-Space.

layer. At short wavelengths, the phase velocities are close to the R-wave velocity of the top layer. In other words, for waves with short wavelengths (relative to the height of the layer) the half-space has very little effect on the dispersion curve. Hence, for these short wavelengths, the top layer acts like a half-space by itself.

The other extreme involves long wavelengths (say eight to ten times the thickness of the top layer and longer). In this case phase velocities are quite close to the R-wave velocity of the rock which means that the top layer does not have an appreciable affect on the dispersion curve. However, between these two extremes there is a transition zone in which the phase velocity is greater than the R-wave velocity of the top layer and less than the R-wave velocity of the half-space.

The extent of this transition zone in the intermediate wavelengths depends on the velocity contrast between the layers. This point is illustrated by the dashed line in Fig. 5.3 which represents the dispersion curve for the same layering used in the example above except that the shear wave velocity of the half-space is seven times greater than that of the top layer. For the first case (1:3), the transition zone is from about a normalized wavelength of one to eight, and the phase velocity is approximately equal to R-wave velocity of the half-space at a wavelength of ten. In the second case (1:7), in which the half-space is about 50 times stiffer than the soil layer, at a normalized wavelength of ten, phase velocity is only on the order of 70 percent of the R-wave velocity of the half-space. In this case, at short wavelengths phase velocities are about the same as the first case (1:3); however, phase velocities become close to the R-wave velocity of the half-space at much longer wavelengths (about a normalized wavelength of 20).

The same trend is true in the case of a high-velocity layer, say concrete, underlain by a softer half-space (soil). Dispersion curves corresponding to the the same layering as used in the first example (Fig. 5.3), except that now the ratios of the shear wave velocities of the layers are reversed, are shown in Fig. 5.4. In the first case the velocity ratio is equal to seven (dashed line). This velocity contrast corresponds to a ratio of elastic moduli of approximately 50 for equal mass densities and Poisson's ratios. The dispersion curve consists of two branches. The branch marked as I is similar to the dispersion curve for the flexural mode of a plate (see

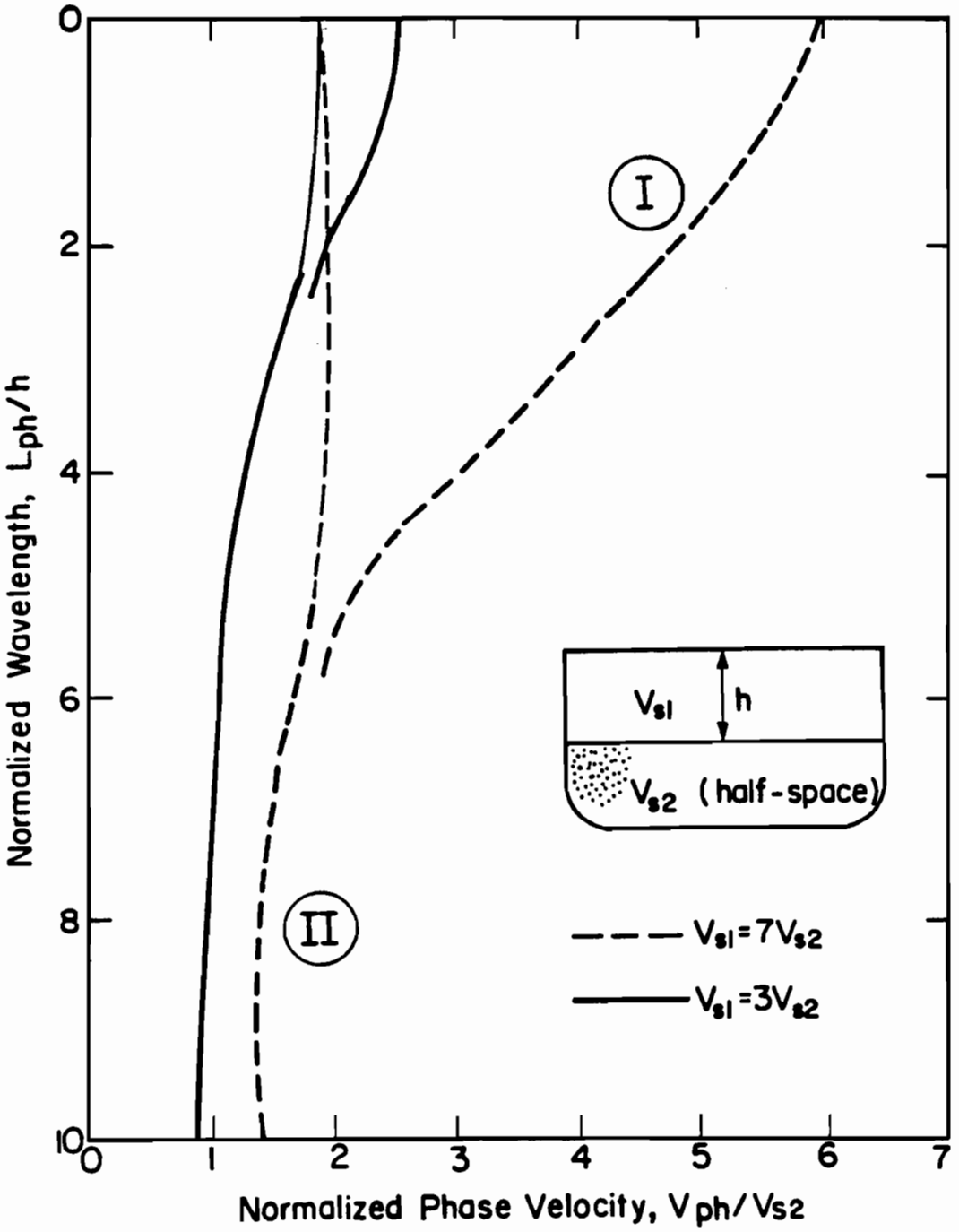

Fig. 5.4. Theoretical Dispersion Curves for a Stiff Layer Underlain by an Elastic Half-Space.

Section 5.6) modified due to presence of a half-space beneath it. The second branch (marked as II) which is asymptote to the compression wave velocity of the lower layer (in this case equal to a normalized velocity of 2 as the Poisson's ratio of the lower layer is 0.33) corresponds to another mode of vibration termed an interfacial mode of vibration (Ewing et al, 1957). In a medium with this type of layering the roots of the determinant are complex (see Section 5.6). At high frequencies, the imaginary components of the complex roots for branch II (shown with a thin dashed line) are so high relative to the real part that the wave will attenuate and the vibration will not propagate; hence, this portion is absent in the experimental dispersion curve. It can also be seen that, even at a normalized wavelength of ten, the normalized velocity is approximately 1.5 times the velocity of the half-space. At short wavelengths, up to a normalized wavelength of about 0.5, phase velocities (on branch I) are close to the R-wave velocity of the concrete layer.

Also shown in Fig. 5.4 is a dispersion curve for a velocity ratio of three. In this case, the phase velocity is equal to the shear wave velocity of the half-space at a normalized wavelength of about six. The two branches of the dispersion curve are also demonstrated in this case.

5.5.2 Effect of Poisson's Ratio

In Chapter Two it is shown that in a homogeneous half-space the effect of Poisson's ratio on the ratio of R- to S-wave velocities is not significant. In this section it will be demonstrated that the effect of Poisson's ratio on the dispersion curve is also small.

The dispersion curves for a two-layered system consisting of a layer of soft material underlain by a stiffer half-space are shown in Fig. 5.5. The contrast in shear wave velocities was kept small so that the curves could be plotted on the same graph with an expanded scale in order that differences could be easily distinguished. The ratio of shear wave velocity of the half-space to V_s of the top layer is 1.5. It can be seen that over a range of Poisson's ratios of 0.15 to 0.49, normalized velocities at a given wavelength vary by no more than ten percent. Furthermore, if Poisson's ratios of the layers are assumed to be equal to 0.33 but the actual Poisson's ratio is 0.49, an error of only about four percent will occur. Therefore, it is obvious that

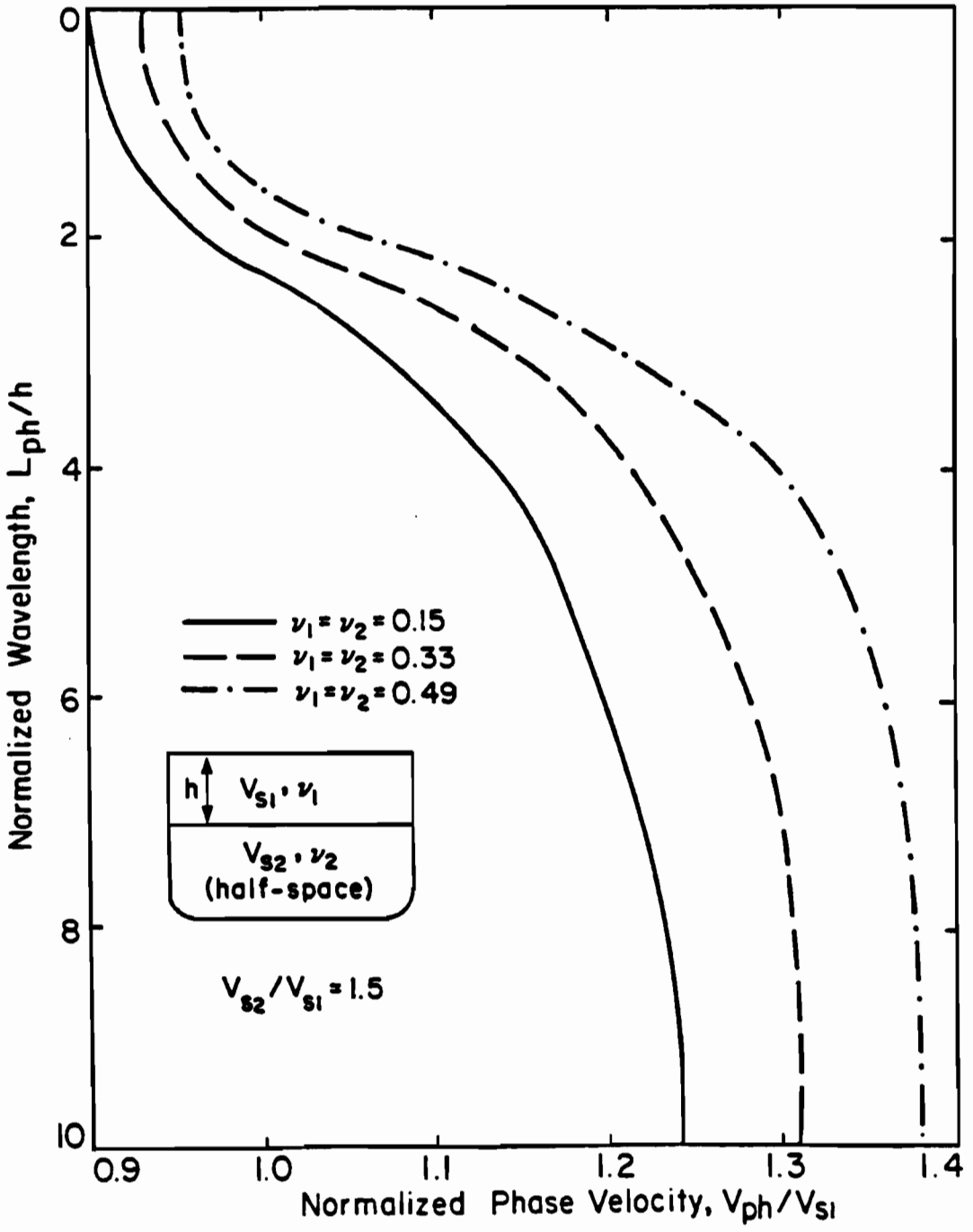

Fig. 5.5. Effect of Poisson's Ratio on Dispersion Curve.

for practical applications one can select reasonable values for Poisson's ratio of the material in a pavement system without introducing significant errors in the construction of the dispersion curve.

5.5.3 Effect of Mass Density

The effect of varying mass densities on the dispersion curve is on the order of the effect of varying Poisson's ratios. The absolute values of mass densities of different layers do not affect the shape of the dispersion curve, but the contrast in mass densities causes some changes in the curve. As an example of this effect, consider the dispersion curves for a layer of softer material underlain by a stiffer half-space (ratio of the shear velocities of 1.5) shown in Fig. 5.6. Two extreme cases are used. In the first case, the mass densities of the two layers are equal. In the second case, it was assumed that the half-space has a mass density 1.5 times greater than that of the top layer. The dispersion curves, as shown in Fig. 5.6, do not deviate much, with the maximum difference on the order of six percent.

5.5.4 Effect of Layer Thicknesses

For a given profile if the thicknesses of all layers are changed by a constant factor, the shape of the dispersion curve is not altered, but the curve is scaled proportional to the constant factor. This point is illustrated in Fig. 5.7 where the dispersion curves for several three-layered systems are shown. The two top layers each have a thickness of h/2 so that depth to the half-space is equal to h.

In the first case, the S-wave velocity of the second layer was assumed equal to that of the half-space. This assumption resulted in a two-layered system with the thickness of the top layer equal to h/2. The dispersion curve for this system is shown by the solid line in Fig. 5.7. The wavelengths in the figure are normalized relative to h (not h/2).

In the second case, the S-wave velocity of the intermediate layer (second layer) was changed to equal the S-wave velocity of the first layer. The profile in this case is identical to the profile of the first case, except that the thickness of the top layer is now equal to h (twice as thick as the first case). The dispersion curve for this profile is shown by the dashed line in Fig. 5.7.

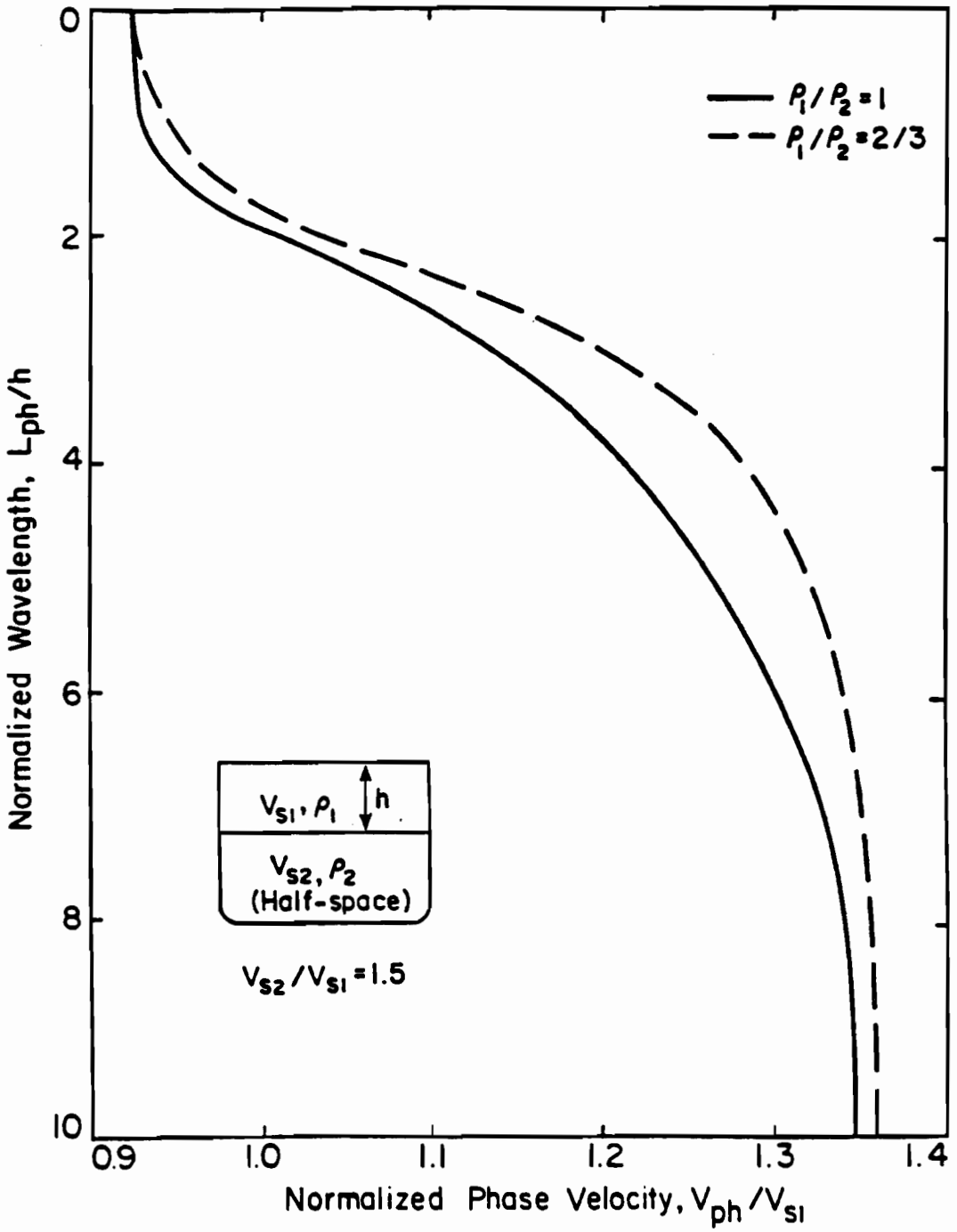

Fig. 5.6. Effect of Mass Density on Dispersion Curve.

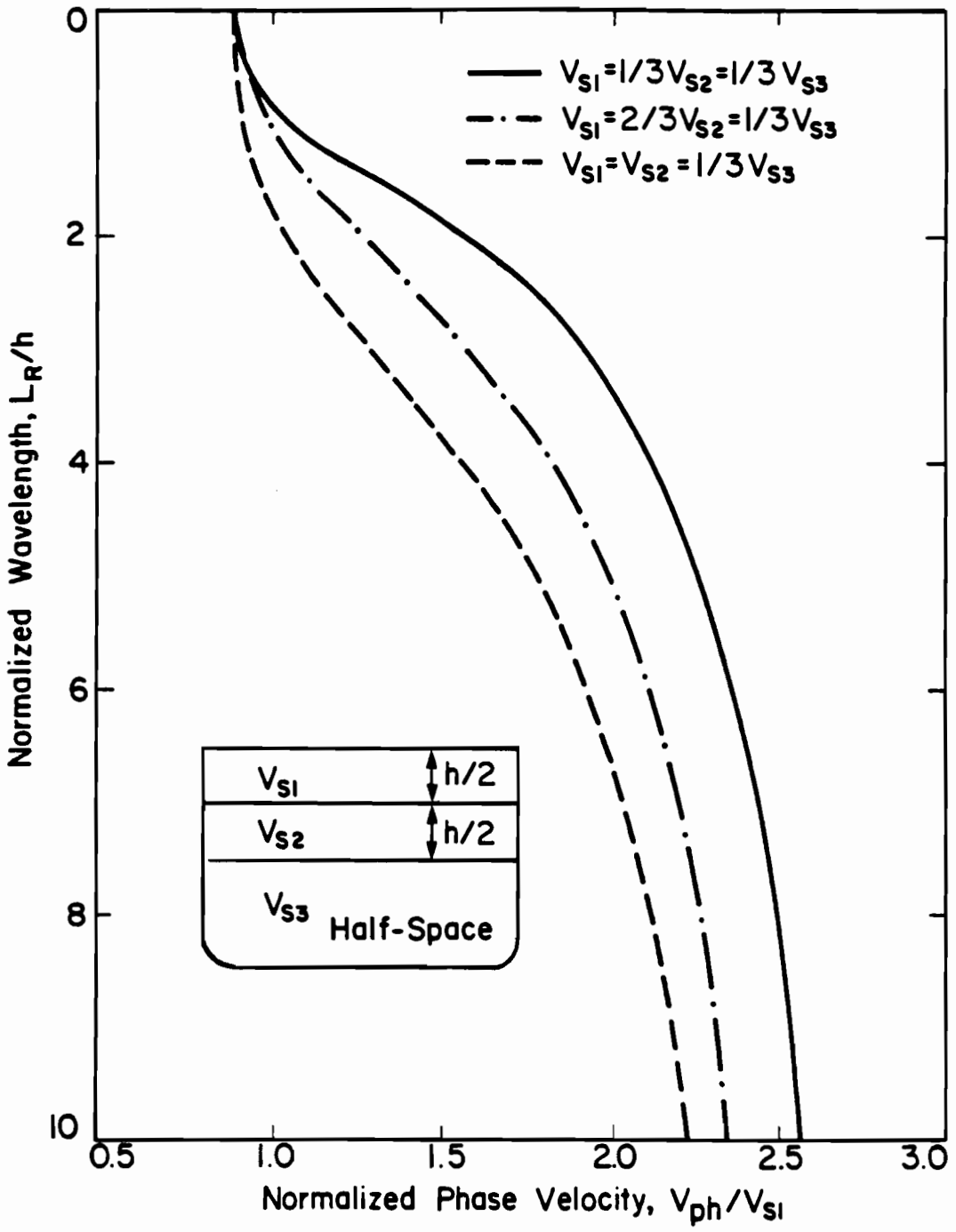

Fig. 5.7. Effect of Layer Thickness on Dispersion Curve.

The shape of the two curves are quite similar. However, the curve from the first case (with a depth to the half-space of h/2) approaches the low-frequency asymptote, which is equal to the R-wave velocity of the half-space, at much shorter wavelengths. If the curve in this case had been normalized relative to h/2 (as oppose to h), the curves from the first and the second cases would have been identical.

The third curve shown in Fig 5.6 corresponds to a case where the S-wave velocity of the second layer, V_{s2}, has an intermediate value, between V_{s1} and V_{s3}. It can be seen that as the stiffness of the intermediate layer increases the dispersion curve is shifted towards higher phase velocities.

It should be mentioned that the curves in Figs. 5.2 and 5.6 for the case, where layering and shear wave velocities are identical (1:3 case), differ because different Poisson's ratios were used. It should also be mentioned that it is not necessary to know layer thicknesses when inverting the measured dispersion curve. This section was included simply to show the effect of layer thickness on the dispersion curve.

5.6 DISCUSSION ON PROPAGATION OF SURFACE WAVES

The values of r^2 and s^2 (defined in Eqs. 5.11 and 5.12) in the half-space, for say a two-layer system, play an important role with regard to the type of wave propagated. Different characteristics of motion can be expected depending upon values of r^2 and s^2. If r and s are real (i.e., r^2 and s^2 are positive), which means that the S- and P-wave velocities are greater than the phase velocity, the roots of the dispersion equation are real and correspond to normal propagation modes of the surface waves. In this situation the waves propagate without attenuation as no material damping is incorporated in elastic theory.

If r^2, s^2, or both become negative, r or s will become imaginary which will result in roots of the dispersion function which are imaginary and analogous to leaky modes (Aki and Richards, 1980). In leaky modes the amplitudes of waves decay rapidly with distance from the source, and a substantial amount of energy is transmitted to the adjacent layer.

In soil sites the stiffness of different layers gradually increases with depth so that normal modes of propagation of Rayleigh waves are anticipated.

For a pavement, on the contrary, the stiffness of the near-surface material is much higher than the underlying soil, and normal modes of propagation can be expected only in the subgrade. Therefore, for data on pavements some other type of wave propagation should be considered. To elaborate more on this subject, consider the case of a layered plate. In this case the dispersion equation will be quite similar to the case discussed in Section 5.2, except that the boundary conditions will differ at the bottom of the plate as this boundary will be a free surface (as oppose to a half-space in the last discussion). In this case, the stress components (i.e., σ_N and τ_N) should vanish, instead of the parameters that are associated with the upgoing waves (i.e., U_{pN} and U_{sN})in the half-space. The mathematical approach is identical to that of a layered medium up to Eq. 5.42. For a plate, the stresses and displacements at the bottom of the last layer should be related to the stresses and displacements of the surface which gives:

$$\bar{S}_N(z_N) = R'\bar{S}_1(0) \tag{5.67}$$

where

$$R^{\cdot} = \prod_{i=1}^{N} Q_i \tag{5.68}$$

If Eq. 5.67 is expanded and subdivided into submatrices, as shown in Eqs. 5.50 through 5.53, the dispersion function will be obtained. This function is equal to:

$$\det(R_{12}) = 0 \tag{5.69}$$

The solution to the dispersion equation in this case leads to two modes of vibration, symmetric and antisymmetric (also called longitudinal and flexural modes, respectively). The case of a single-layered plate is considered as an example. The symmetric and antisymmetric modes from this medium are shown in Fig. 5.8. At high frequencies, phase velocities are close to the R-wave velocity in both modes. As the frequency decreases (as wavelength becomes longer), the phase velocities of the symmetric modes of propagation increase until they become asymptotic to the compression wave

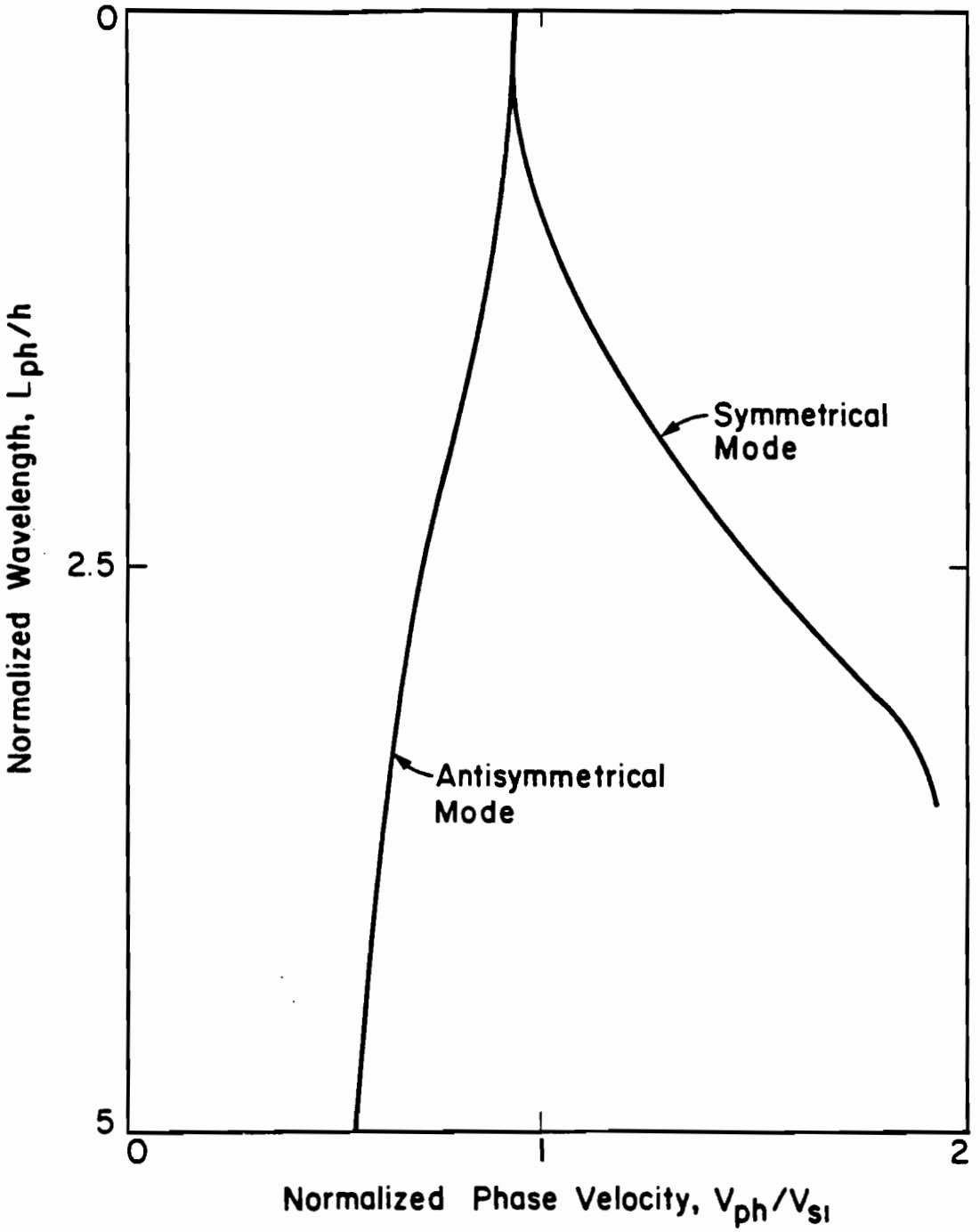

Fig. 5.8. Schematic of Difference Modes of Propagation of Surface Waves in a Plate.

velocity of the plate. On the contrary, in the antisymmetric modes, phase velocities decrease with decreasing frequencies to a minimum of zero. Meeker and Meitzler (1964) have a detailed discussion on the characteristics of different modes, and the reader is referred to that paper for more information.

As the phase velocities from experimental tests on pavements decrease with decreasing wavelengths, modes similar to antisymmetric modes of propagation in a plate can describe these systems more appropriately. To analyze experimental data from systems with velocities greater than the subgrade material, Thrower (1965) has shown that the assumption of a plate on a half-space can be used adequately to model a pavement system.

5.7 SUMMARY

In this chapter, the Haskell-Thomson procedure for determining the dispersion function (Eq. 5.54) is discussed. It is shown that at high frequencies this procedure encounters numerical problems. The Dunkin extension of the Haskell-Thomson formulation for solution of the dispersion function at high frequencies is briefly presented. Finally, factors affecting the dispersion function are examined. The main parameters affecting this function are shear wave velocity, mass density and Poisson's ratio of the material composing each layer. It is demonstrated that the effect of the last two parameters is not significant and, in practical cases, is less than five percent. Also the effect of intermediate layers is discussed. As the velocities of the intermediate layers increase, the dispersion curve is shifted towards higher phase velocities. The chapter is concluded with a discussion of types of propagation expected to occur in a pavement system.

CHAPTER SIX. CONCLUSIONS

In this report the theoretical aspects of the SASW method are reviewed. It is shown that all steps taken to collect wave velocities in the field and to reduce the field data are based on sound theoretical principles and a minimal number of simplifying assumptions are used.

The theory of elastic wave propagation is utilized to determine the propagation velocity of surface waves. An introduction to wave propagation theory is included. To perform the in situ tests more rapidly, spectral analysis and Fourier transform principles are utilized. An overview of spectral analyses and the usefulness of each function are described.

To determine meaningful modulus profiles as well as the thicknesses of different layers, an algorithm required for determining modulus profiles from velocity of propagation of surface waves from different wavelengths has been developed. The general process for which the algorithm is employed is called inversion herein. The theory behind this algorithm is described in a logical and simplified manner in Chapter 5.

Overall, it is shown that all steps of the SASW method are based on sound theory, and the manner in which the test is performed and the data are reduced is consistent with the theoretical basis.

REFERENCES

1. Aki, K., and Richards, P.G. (1980), Quantitative Seismology, Theory and Methods, Vol. 1, W.H. Freeman and Company, San Francisco, 557 pp.

2. Anderson, D.G., and Woods, R.D. (1975), "Comparison of Field and Laboratory Shear Moduli," Proceedings, Conference on In Situ Measurement of Soil Properties, ASCE, Vol. I, Raleigh, North Carolina, pp. 69-92.

3. Baird, G.T. (1982), "Wave Propagation Method of Pavement Evaluation," New Mexico Engineering Research Institute, University of New Mexico, Albuquerque, New Mexico.

4. Ballard, R.F., Jr. (1964), "Determination of Soil Shear Moduli at Depths by In Situ Vibratory Techniques," Miscellaneous Paper No. 4-691, U.S. Army Engineer Waterways Experiment Station, Vicksburg, Mississippi.

5. Ballard, R.F., Jr., and Casagrande, D.R. (1967), "Dynamic Foundation Investigations, TAA-2A Radar Site, Cape Kennedy, Florida," Miscellaneous Paper 4-878, U.S. Army Engineer Waterways Experiment Station, Vicksburg, Mississippi.

6. Ballard, R.F., Jr., and Chang, F.K. (1973), "Rapid Subsurface Exploration; Review of Selected Geophysical Techniques," Miscellenaous Paper No. S-69-30, U.S. Army Engineer Waterways Experiment Station, Vicksburg, Mississippi.

7. Baker, T.G., and Stevens, J.L. (1983), "Shallow Shear Wave Velocity and Q Structures at the El Centro Strong-Motion Accelerograph Array," Geophysical Research Letters, Vol. 10, No. 9, pp. 853-856.

8. Bergstrom, S.G., and Linderholm, S. (1946), "Dynamisk Metod att Utrona Ultiga Marklagers Genomsnittliga Elasticitetsegens kaper," Handlinger NO. 7, Svenska Forsknings-Institutet for Cement och Betong Vid. Kungl. Tekniska, Hogskolan.

9. Bolt, B.A. (1976), Nuclear Explosions and Earthquakes, W.H. Freeman and Co., San Francisco, 309 pp.

10. Borm, G.W. (1978), "Methods from Exploration Seismology: Reflection, Refraction and Borehole Prospecting," Proceedings of the Conference on Dynamical Methods in Soil and Rock Mechanics, Karlsruhe, Germany, Vol. III, pp. 87-114.

11. Brigham, E.O. (1974), The Fast Fourier Transform, Prentice-Hall, Inc., Englewood Cliffs, New Jersey, 253 pp.

12. Chen, L.S. (1948), "An Investigation of Stress-Strain and Strength Characteristics of Cohesionless Soils by Triaxial Compression Tests," Proceedings, Second International Conference on Soil Mechanics and Foundation Engineering, Rotterdam, Vol. V.

13. Cunny, R.W., and Fry, Z.B. (1973), "Vibratory In Situ and Laboratory Soil Moduli Compared," Journal of the Soil Mechanics and Foundations Division, ASCE, Vol. 99, No. SM12, pp. 1055-1076.

14. DEGEBO (1938), "Deutsche Gesellschaft fur Bodenmechanik," Vol. 4, Springer, Berlin.

15. Dunkin, J.W. (1965), "Computation of Modal Solutions in Layered, Elastic Media at High Frequencies," Bulletin of Seismological Society of America, Vol. 55, No. 2, pp. 335-358.

16. Eagleson, B., Heisey, J.S., Hudson, W.R., Meyer, A.H., and Stokoe, K.H., II (1981), "Comparison of Falling Weight Deflectometer and Dynaflect for Pavement Evaluation," Report No. 256-1, Center for Transportation Research, University of Texas, Austin, Texas.

17. Ewing, W.H., Jardetzky, W.S., and Press, L.C.R. (1957), Elastic Waves in Layered Media, McGraw-Hill Book Company, New York, 380 pp.

18. Fry, Z.B. (1965), "Dynamic Soils Investigations Project Buggy, Buckboard Mesa Nevada Test Site, Mercury, Nevada," Miscellaneous Paper No. 4-666, U.S. Army Engineer Waterways Experiment Station, Vicksburg, Mississippi.

19. Haas, R., and Hudson, W.R. (1978), Pavement Management Systems, McGraw Hill Book Co., New York, New York, 456 pages.

20. Haskell, N.A. (1953), "The Dispersion of Surface Waves in Multilayered Media," Bulletin of Seismological Society of America, Vol. 43, No. 1, pp. 17-34.

21. Hardin, B.O. (1978), "The Nature of Stress-Strain Behavior in Soils," Proceedings, Conference on Earthquake Engineering and Soil Dynamics, ASCE, Pasadena, California, Vol. I.

22. Hardin, B.O., and Drnevich, V.P. (1972), "Shear Modulus and Damping in Soils: Measurement and Parameter Effects," Journal of the Soil Mechanics and Foundations Division, ASCE, Vol. 95, No. SM6, pp. 603-624.

23. Heisey, J.S., Stokoe, K.H., II, Hudson, W.R., and Meyer, A.H. (1982), "Determination of In Situ Shear Wave Velocities from Spectral Analysis of Surface Waves," Research Report 256-2, Center for Transportation Research, The University of Texas at Austin, 277 pp.

24. Heukelom, W., and Klomp, J.G. (1962), "Dynamic Testing as a Means of Controlling Pavements During and After Construction," Proceedings, International Conference on Structural Design of Asphalt Pavements, Ann Arbor, Michigan, pp. 495-510.

25. Hewellet Packard (1981), "The Fundamentals of Signal Analysis," Application Note 243, Hewellet Packard Co., USA, 57 pages.

26. Hoar, R.J. (1982), "Field Measurement of Seismic Wave Velocity and Attenuation for Dynamic Analyses," Ph.D. Dissertation, The University of Texas, Austin, Texas, 479 pages.

27. Jones, R. (1958), "In Situ Measurment of the Dynamic Properties of Soil by Vibration Methods," Geotechnique, Vol. III, No. 1.

28. Knopoff, L. (1964), "A Matrix Method for Elastic Wave Problems," Bulletin of Seismological Society of America, Vol. 54, No. 1, pp. 431-438.

29. Krizek, R.J. (1977), "Fabric Effects on Strength and Deformation of Kaolin Clay," Proceedings, Ninth International Conference on Soil Mechanics and Foundation Engineering, Tokyo, Japan, Vol. I.

30. Lamb, H. (1904), "On the Propagation of Tremors Over the Surface of an Elastic Solid," Philosophical Transactions of the Royal Society of London, Vol. A203, pp. 1-42.

31. Lytton, R.L., Moore, W.M., and Mahoney, J.P. (1975), "Pavement Evaluation: Phase I, Pavement Evaluation Equipment," Report No. FHWA-RD-75-78, Federal Highways Administration, Washington, D.C.

32. Maxwell, A.A., and Fry, F.B. (1967), "A Procedure for Determining Elastic Modul of In Situ Soils by Dynamic Techniques," Proceedings, International Symposium on Wave Propagation and Dynamic Properties of Earth Materials, Albuquerque, New Mexico, pp. 913-920.

33. Meeker, T.R., and Meitzler, A.H. (1964), Physical Acoustics, Vol.1, Part A, Academic Press, New York, New York, pp. 111-167.

34. Miller, G.F., and Pursey, H. (1955), "On the Partition of Energy Between Elastic Waves in a Semi-Infininte Solid," Proceedings, Royal Society of London, A, vol. 233, pp. 55-69.

35. Nazarian, S. (1984), "In Situ Determination of Elastic Moduli of Soil Deposits and Pavement Systems by Spectral-Analysis-of-Surface-Wave Method," Ph.D. Dissertation, The University of Texas at Austin, 446 pp.

36. Nazarian, S., Stokoe, K.H., II, and Hudson, W.R. (1983), "Use of Spectral Analysis of Surface Waves for Determination of Moduli and Thicknesses of Pavement Systems," Transportation Research Record, No. 945, Washington, D.C., pp. 38-45.

37. Nazarian, S., and Stokoe, K.H., II (1985), "In Situ Determination of Elastic Moduli of Pavement Systems by Spectral-Analysis-of-Surface - Waves Method (Practical Aspects," Research Report 368-1F, Center for Transportation Research, The University of Texas at Austin, 161 pp.

38. Nazarian, S., and Stokoe, K.H., II (1986a), "Analytical Study of the Sensitivity of the Falling Weight Deflectometer Device to Determining Moduli of Farm-to-Market Roads," Technical Memorandum No. IAC (86-87) 0936-3, Center for Transportation Research, The University of Texas at Austin, 28 pp.

39. Nazarian, S., and Stokoe, K.H., II (1986b), "Evaluation of the Sensitivity of the SASW Method in Determining Thicknesses of Layers in Pavement Systems," Technical Memorandum No. IAC (86-87) 0946-4, Center for Transportation Research, The University of Texas at Austin, 42 pp.

40. Nazarian, S., and Stokoe, K.H., II (1986c), "Users Guide for Interactive Program "INVERT" Used in INversion of Dispersion Curves," Research Report 1123-1, Center for Transportation Research, The University of Texas at Austin, (in press).

41. Neilson, J.R., and Baird, G.T. (1975), "Air Force System for Nondestructive Tsting of Pavements," Symposium on Nondestructive Testing and Evaluation of Airport Pavements, Vicksburg, Mississippi.

42. Neilson, J.P., and Baird, G.T. (1977), "Evaluation of an Impulse Testing Technique for Nondestructive Testing of Pavements," Research Report CEEDO-TR-77-46, Tyndall Air Force Base, Panama City, Florida.

43. Nijober, L.W., and Van der Poel, C. (1953), "A Study of Vibration Phenomena in Asphaltic Road Construction," Proceedings, Association of Asphaltic Pavement Technology, pp. 197-231.

44. Ogura, K. (1979), "Development of a Suspension Type S-Wave Log System," Technical Note TN-34, OYO corporation, Tokyo, Japan, 23 pp.

45. Patel, N.S. (1981), "Generation and Attenuation of Seismic Waves in Downhole Testing," M.S. Thesis, The University of Texas, Austin, Texas, 411 pp.

46. Rayleigh, L. (1887), "On Waves Propagated Along the Plane Surface of an Elastic Solid," Proceedings, London Mathematical Society, Vol. 17, pp. 4-11.

47. Redpath, B.B. (1973), "Seismic Refraction Exploration for Engineering Site Investigation," Report TRE-73-4, U.S. Army Engineer Waterways Experiment Station, Corps of Engineers, Vicksburg, Mississippi, 52 pp.

48. Richart, F.E., Jr., Hall, J.R., Jr., and Woods, R.D. (1970), Vibrations of Soils and Foundations, Prentice-Hall, Inc., Englewood Cliffs, New Jersey, 414 pp.

49. Schwab, F., and Knopoff, L. (1970), "Surface Wave Dispersion Computations," Bulletin of Seismological Society of America, Vol. 60, No. 2, pp. 321-344.

50. Shao, K-Y, Roesset, J.M., and Stokoe, K.H., II, (1986), "Dynamic Interpreation of Dynaflect and Falling Weight Deflectometer Tests on Pavement Systems," Research Report Number 437-1, Center for Transportation Research, The University of Texas, Austin, Texas, (in press).

51. Sheriff, R.E. (1982), Encyclopedia Dictionary of Exploration Geophysics, Society of Exploration Geophysicists Publication, Tulsa, 266 pp.

52. Stokoe, K.H., II, and Chen, A.T.F. (1980), "Effects on Site Response of Methods of Estimating In Situ Soil Behavior," Proceedings, Seventh World Conference on Earthquake Engineering, Turkey.

53. Stokoe, K.H., II, and Hoar, R.J. (1978), "Variables Affecting in Situ Seismic Measureements," Proceedings, Conference on Earthquake Engineering and Soil Dynamics, ASCE, Pasadena, California, Vol. II, pp 919-939.

54. Stokoe, K.H., II, and Lodde, P.F. (1978), "Dynamic Response of San Francisco Bay Mud," Proceedings, Conference on Earthquake Engineering and Soil Dynamics, ASCE, Pasadena, California, Vol. II, pp. 940-959.

55. Stokoe, K.H., II, and Woods, R.D. (1972), "In Situ Shear Wave Velocity by Cross-Hole Method," Journal of the Soil Mechanics and Foundations Division, ASCE, Vol. 98, No. SM5, pp. 443-460.

56. Thomson, W.T. (1950), "Transmission of Elastic Waves Through a Stratified solid Medium," Journal of Sound Vibration, Vol. 2, No. 3, pp. 210-226/

57. Thrower, E.N. (1965), "The Computation of the Dispersion of Elastic Waves in Layered Media," Journal of Sound Vibration, Vol. 2, No. 3, pp. 210-226.

58. Uddin, W., Nazarian, S., Hudson, W.R., Meyer, A.H., and Stokoe, K.H., II (1983), "Investigations into Dynaflect Deflections in Relation to Location/Temperature Parameters and In Situ Material Characterization of Rigid Pavements," Research Report 256-5, Center for Transportation Research, The University of Texas at Austin.

59. Van der Poel, C. (1951), "Dynamic Testing of Road Construction," Journal of Applied chemistry, Vol. 1, No. 7, pp. 281-290.

60. Van der Poel, C. (1954), "A General System Describing the Visco-Elastic Properties of Bitumens and Its Relation to Routine Test Data," Shell Bitumen Reprint No. 9, Shell Laboratories-Komink-likeke.

61. Watson, T.H. (1970), "A Note on Fast Computation of Rayleigh Wave Dispersion in the Layered Elastic Half-Space," Bulletin of Seismological Society of america, vol. 60, No. 1, pp. 161-166.

62. Williams, O. (1981), "Rayleigh Wave Velocity Measurements Using Broad Band Frequency Sources," Miscellaneous Paper EL-81-3, U.S. Army Engineer Waterways Experiment Station, Vicksburg, Mississippi, 31 pp.

63. Woods, R.D., and Richart, F.E., Jr. (1967), "Screening of Elastic Surface Waves by Trenches," Proceedings, International Symposium on Wave Propagation and Dynamic Properties of Earth Materials, Albuquerque, New Mexico, pp. 275-290.

64. Yoder, E.J., and Witczack, M.W. (1975), "Principles of Pavement Design, John Wiley & Sons, Inc., New York, New York, 2nd Edition, 711 pp.